Max-Planck-Institut
für Meteorologie

MAX PLANCK
GESELLSCHAFT

International Max Planck Research School
on Earth System Modelling

Using simple models to understand changes in the tropical mean atmosphere under warming

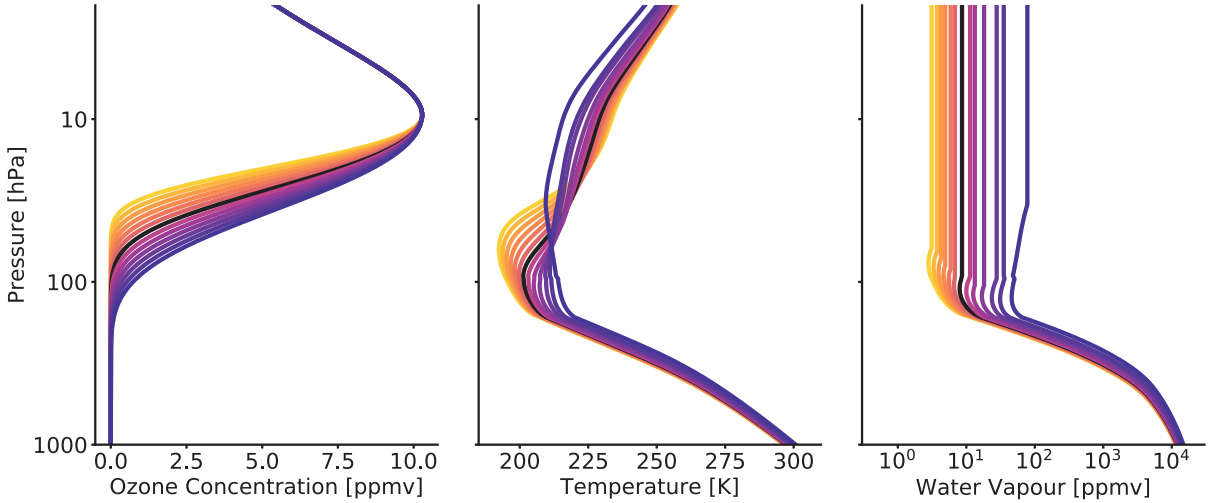

Sally Dacie

Hamburg 2020

Berichte zur Erdsystemforschung
Reports on Earth System Science

233
2020

Hinweis

Die Berichte zur Erdsystemforschung werden vom Max-Planck-Institut für Meteorologie in Hamburg in unregelmäßiger Abfolge herausgegeben.

Sie enthalten wissenschaftliche und technische Beiträge, inklusive Dissertationen.

Die Beiträge geben nicht notwendigerweise die Auffassung des Instituts wieder.

Die "Berichte zur Erdsystemforschung" führen die vorherigen Reihen "Reports" und "Examensarbeiten" weiter.

Notice

The Reports on Earth System Science are published by the Max Planck Institute for Meteorology in Hamburg. They appear in irregular intervals.

They contain scientific and technical contributions, including Ph. D. theses.

The Reports do not necessarily reflect the opinion of the Institute.

The "Reports on Earth System Science" continue the former "Reports" and "Examensarbeiten" of the Max Planck Institute.

Anschrift / Address

Max-Planck-Institut für Meteorologie
Bundesstrasse 53
20146 Hamburg
Deutschland

Tel./Phone: +49 (0)40 4 11 73 - 0
Fax: +49 (0)40 4 11 73 - 298

name.surname@mpimet.mpg.de
www.mpimet.mpg.de

Layout

Bettina Diallo and Norbert P. Noreiks
Communication

Copyright

Using simple models to understand changes in the tropical mean atmosphere under warming

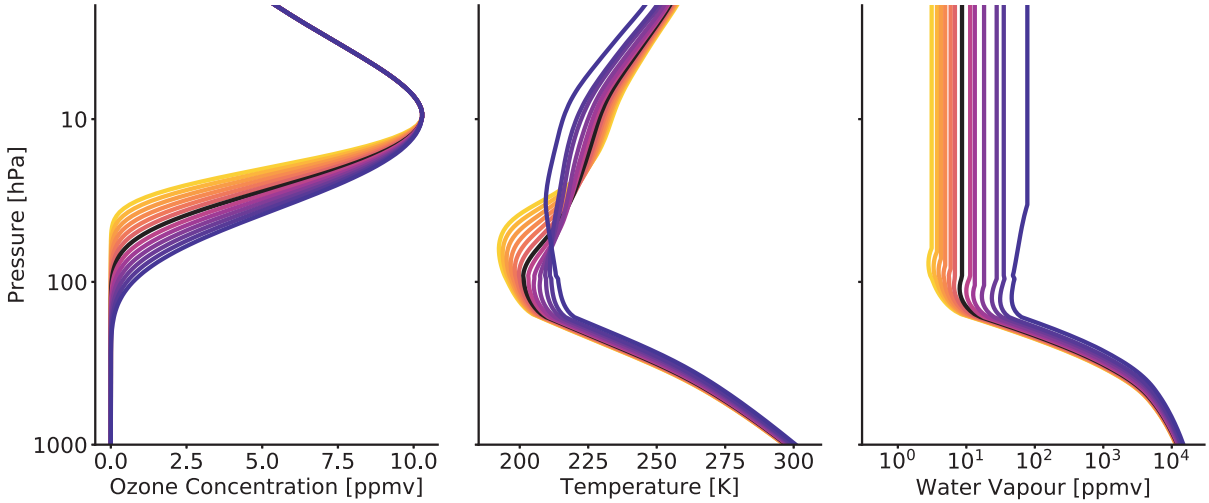

Sally Dacie

Hamburg 2020

Sally Dacie
aus Leicester, Großbritannien

Max-Planck-Institut für Meteorologie
The International Max Planck Research School on Earth System Modelling
(IMPRS-ESM)
Bundesstrasse 53
20146 Hamburg

Universität Hamburg
Geowissenschaften
Meteorologisches Institut
Bundesstr. 55
20146 Hamburg

Tag der Disputation: 16. Juni 2020

Folgende Gutachter empfehlen die Annahme der Dissertation:
Dr. Hauke Schmidt
Prof. Dr. Stefan A. Buehler

Vorsitzender des Promotionsausschusses:
Prof. Dr. Dirk Gajewski

Dekan der MIN-Fakultät:
Prof. Dr. Heinrich Graener

Berichte zur Erdsystemforschung / Max-Planck-Institut für Meteorologie 233
Reports on Earth System Science / Max Planck Institute for Meteorology 2020

ISSN 1614-1199

Acknowledgements

First and foremost, I would like to acknowledge my PhD advisors and advisory panel chair, Hauke Schmidt, Bjorn Stevens and Stefan Buhler, for giving my project direction and in particular for allowing me freedom to explore. I am very grateful to Lukas Kluft, with whom I have really enjoyed working and who has contributed a lot, designing the framework for konrad and helping me to realise my ideas in code. It has also be a pleasure to work with Ed Charlesworth, whose willingness to share his ozone model and his knowledge of atmospheric chemistry were very helpful. Many thanks also to Jiawei Bao and Diego Jiménez de la Cuesta Otero for nice conceptual discussions, Katherine Fodor for helping me to understand the theory behind the weak temperature gradient hypothesis and Sergey Kosukhin and Tobias Becker for finding time to help me whenever I asked. I would also like to thank Hauke Schultz, Qiong Yang and Qiang Fu for observational cloud data, Joy Merwin Monteiro from climt for his encouragement and advice, as well as Thomas Birner, Kerry Emanuel and Anna Shapiro for the inspiring discussions we had during their visits to MPI. Additionally, thanks to Didier Roche for giving me the opportunity to chair a session at EGU 2019 and to everyone who contributed, making our session both enjoyable and interesting. Thanks to Sebastian Müller, Hyunju Jung and Clarissa Kroll for keeping me company in the office, and Gustavo Hime and Sebastian Rast for sharing their opinions. Thanks to my previous colleagues, Lidia van Driel-Gesztelyi, Dave Long and David Pérez Suárez, whose attitudes to science, scientific writing and coding in science respectively continue to influence my work.

Additionally, I would like to acknowledge Antje Weitz, Connie Kampmann, Michaela Born, Christina Rickers and Angela Gruber for all their assistance with administrative tasks.

Finally, I would like to mention some of the people who have supported me during the last three years and helped make that time both enjoyable and memorable. Thanks to Seb and Rafaela for Friday evenings, Vimal and Priyanka for satisfying my cravings for Indian food, Johannes for organising nice activities, Dian for cake baking and table tennis, Alberto for board games and triathlon training, Bernhard for our unforgettable trip to the Great Wall, Hao-wei for taking me to the 17th floor to watch fireworks, Alon for his positivity, Roman for a piece of special chocolate cake, Martin for his interesting life stories and Jan and Jan from Salon for making me laugh. Thanks to my previous and current flatmates for making me feel at home; Benjamino, Raul, Pablo, Felix, Michael, James, Mario, Arthur, Andres, Ella, Marianna and Nico. And thanks to all of the friends outside of Hamburg and my family, who have visited me here or gone on holiday with me during the last few years, who have provided me with much needed breaks; Anna, Markus, Sam, Dawn, Rachael, Theresa, Fiona, Rikesh, Dan, Ellie, Laura, James, Mark, Monica, Chiara, Charlotte, my sister Ruth, my aunt Pam and my parents.

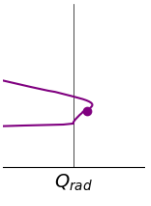

Abstract

In this work, we focus on a few aspects of tropical mean climate, namely the tropical tropopause layer (TTL) and surface temperatures, ozone, and precipitation, and in particular how these change under a CO_2 induced warming scenario. Our interest lies in understanding different processes and their interactions, rather than making accurate predictions. As such, we have contributed to the development of two simple numerical models, one for calculating temperature profiles and the other for ozone profiles, as well as creating an analytical model to study mean precipitation and circulation changes.

Our one-dimensional radiative-convective equilibrium model, konrad, allows us to determine how a variety of factors can affect TTL and surface temperatures. The TTL is of particular interest, because there are discrepancies between global climate models regarding its temperature structure and evolution under climate change. The TTL temperatures in our model are sensitive to CO_2 concentration, the ozone profile, the inclusion of a high cloud, the method of convective adjustment and the upwelling velocity, which is used to calculate a dynamical cooling rate in the stratosphere. Moreover, the temperature response of the TTL to changes in each of the above factors sometimes depends on the others. With regards to the surface, we are especially interested in the effect of changes in stratospheric ozone under a warming scenario. We perform experiments using our simple ozone scheme, Agatha, as well as idealised ozone profiles and ozone profiles from chemistry climate models. Using Agatha we find that the transport term makes a large contribution to the ozone concentrations in the lower stratosphere, but that chemical reactions in the middle and upper stratosphere also play a role. The surface temperature response to changes in ozone is strongly amplified by both stratospheric and tropospheric water vapour changes.

Finally, using output from konrad and a few simple assumptions such as water and energy balance, we try to explain why rainfall increases in a warming climate and predict how the tropical mean circulation changes to accommodate this. We find precipitation increases of 2.0 to 2.7 % per Kelvin increase in surface temperature, but only 1.4 to 2.0 % K^{-1} when the increase in surface temperature is caused by CO_2. By thinking of the atmosphere as two distinct regions, a saturated moist region of upward motion and a subsidence region, we derive mean circulation. Using this simplistic approach, in a warming climate we find a slowdown of the mean circulation and an increase in upwelling area. However, the upper troposphere is not well represented by our approach, suggesting that the conceptual picture generally accepted by the community needs to be revised.

Zusammenfassung

In dieser Dissertation liegt der Schwerpunkt auf mehreren Aspekten der tropischen Atmosphäre: der tropischen Tropopause (TTL), der Bodentemperatur, dem Ozon und dem Niederschlag und insbesondere der Veränderung dieser Aspekte bei CO_2 induzierter Erwärmung. Unser Ziel ist es nicht genaue Prognosen zu erstellen, sondern verschiedene Prozesse und ihr Zusammenspiel zu verstehen. Zu diesem Zweck haben wir zur Entwicklung zweier einfacher numerischer Modelle beigetragen, eines zur Berechnung von Temperaturprofilen, das andere für Ozonprofile. Weiterhin haben wir ein analytisches Modell zur Untersuchung von Nierderschlags- und Zirkulationsveränderungen erstellt.

Mit unserem eindimensionalen Strahlungs-Konvektions-Gleichgewicht Modell, konrad, sind wir in der Lage den Einfluss verschiedener Faktoren auf die TTL und die Bodentemperatur zu untersuchen. Die TTL ist interessant, da globale Klimamodelle in den Prognosen ihrer Temperatur und der durch den Klimawandel verursachten Veränderung dort nicht übereinstimmen. In konrad reagiert die TTL Temperatur auf die CO_2 Konzentration, die Ozonprofile, das Einbeziehen einer hohen Wolke, die Methode der konvektiven Anpassung und die Geschwindigkeit, die für die Berechnung einer dynamischen Abkühlung in der Stratosphäre benutzt wird. Darüber hinaus wird die Reaktion der TTL Temperatur auf Veränderungen einer der obengenannten Faktoren manchmal von anderen Faktoren beeinflusst. Bezüglich des Bodens interessieren wir uns insbesondere für die Auswirkung der durch die Erwärmung verursachten Veränderungen stratosphärischen Ozons. Wir führen Experimente mit verschiedenen Konfigurationen des Ozons durch: mit unserem einfachen Ozonmodel Agatha, mit idealisierten Ozonprofilen und mit Ozonprofilen aus Klimamodellen mit gekoppelter Atmosphärenchemie. Mit Agatha finden wir heraus, dass für die Ozonkonzentration in der unteren Stratosphäre vor allem Transportprozesse aber auch chemische Reaktionen in der mittleren und oberen Stratosphäre wichtig sind. Die Reaktion der Bodentemperatur auf Veränderungen des Ozons wird durch stratosphärische und troposphärische Wasserdampfveränderungen stark vergrößert.

Mit den Ergebnissen von konrad und einigen einfachen Annahmen versuchen wir zum einen zu erklären, warum Niederschlag in einem sich wärmenden Klima ansteigt und zum anderen vorherzusagen, wie die tropische mittlere Zirkulation sich daran anpasst. Wir finden einen Anstieg des Niederschlags von 2,0 bis 2,7 % pro Kelvin Erwärmung der Bodentemperatur. Falls die Erwärmung der Bodentemperatur durch CO_2 verursacht wird, reduziert sich der Anstieg auf 1,4 bis $2{,}0\,\%\,\mathrm{K}^{-1}$. Indem wir die Atmosphäre in zwei Gebiete aufteilen, ein gesättigtes feuchtes Gebiet, in dem sich die Luft aufwärts bewegt, und ein Gebiet, in dem die Luft absinkt, können wir Veränderungen der durchschnittlichen Zirkulation abschätzen. Mit dieser Vorgehensweise finden wir in einem wärmer werdenden Klima eine Verlangsamung der durchschnittlichen Zirkulation und eine Vergrößerung des Gebiets von aufsteigender Luft. Allerdings ist die obere Troposphäre nicht gut dargestellt, was darauf hinweist, dass das allgemein akzeptierte konzeptionelle Bild überarbeitet werden muss.

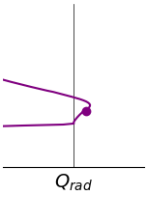

Contents

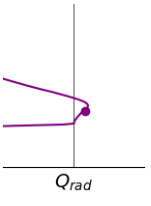

Chapter 1

The tropical atmosphere

1.1 Radiative convective equilibrium

Radiative convective equilibrium (RCE) provides a simple framework to study the tropical atmosphere. It describes the balance between net radiative cooling and convective heating and is a good approximation for the troposphere in the tropics, where other processes such as advection can be neglected. The net radiative cooling consists of longwave cooling produced by the emission of radiation by the atmosphere, longwave warming as some of this radiation and that emitted by the surface is absorbed by the atmosphere, and shortwave radiative heating as solar radiation is absorbed. The convective heating is provided both by the release of latent heat as saturated air parcels rise and cool and their water vapour condenses out, and by sensible heating. Above the troposphere there is a transition layer (the tropical tropopause layer, TTL, section 1.3.1) to radiative equilibrium in the stratosphere, where stable stratification prohibits convective activity. The large scale Brewer-Dobson circulation (section 1.3.2) plays a role in the stratosphere and affects the TTL structure.

For more than 50 years numerical RCE models have been used, which include mathematical representations of radiative transfer and convection and cover a wide range of complexity. The first one-dimensional (1D) convective-radiative model was developed and used by Manabe and Strickler (1964); Manabe and Wetherald (1967), and the latter publication is arguably the most important climate research paper to date (Forster, 2017). Their model used a maximum of 18 levels, a radiative scheme based on two absorption bands of H_2O, one band of CO_2 and one band of ozone, and a convective adjustment in the troposphere to a lapse rate of -6.5 K km^{-1}. New to the previous study of Manabe and Strickler (1964), Manabe and Wetherald (1967) coupled the tropospheric water vapour content to the temperature by using a fixed relative humidity profile. They studied changes in the equilibrium temperature profile caused by a doubling of CO_2 and found the surface temperature to increase by 2.3 K. This quantity is often referred to as the equilibrium climate sensitivity or ECS and its value is still strongly debated (Jiménez-de-la Cuesta and Mauritsen, 2019). In addition, Manabe and Wetherald (1967) were the first to note that an increase in CO_2 causes a decrease in temperature in the stratosphere. They also studied the effects of cloudiness, ozone profile and surface albedo on the temperature profile.

Since then, numerous researchers have made use of 1D RCE models to investigate various phenomena, including Hummel and Kuhn (1981c) comparing constant and pressure-dependent lapse rates, Hummel and Kuhn (1981b) predicting cloud altitudes and thicknesses as well as their feedbacks, Satoh and Hayashi (1992) on the effects of convective upflows and downflows, and Chae and Sherwood (2007) on the seasonal cycle of TTL temperatures. 3D RCE models have increased in popularity, allowing researchers to study convection in both parameterised and explicit setups, the organisation of convection (*e.g.* Becker et al., 2017), precipitation (*e.g.* Cronin et al., 2015) and convectively

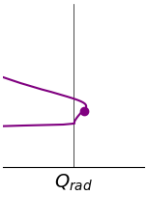

generated gravity waves (*e.g.* Müller et al., 2018). The first RCE model intercomparison project was proposed by Wing et al. (2018), encouraging more research and collaboration centered on RCE modelling in both 1D and 3D, and Warren et al. (2020) call for more studies to extend RCE models to radiative-convective-dynamical equilibrium (RCDE) models by adding a mean background tropical upwelling term, allowing a larger variety of climate states to be investigated.

Most of the work in this thesis is based around the development and use of a 1D RCE model to understand various aspects of tropical mean climate. The rest of the introduction to the thesis provides a description of some aspects of the tropical atmosphere, important either for the assumptions used in 1D RCE models, or to test the output from RCE simulations against our conceptual understanding.

1.2 The free troposphere

1.2.1 The moist adiabat

In the tropical troposphere, it is assumed that the temperature profile everywhere is set by regions of moist convection, according to the weak temperature gradient (Section 1.2.2). In this section, a derivation is given for the moist adiabatic lapse rate, which describes the change in temperature with height produced by regions of moist convection under a set of basic assumptions. The main assumption is that the regions of moist convection are comprised of parcels of saturated air that are moving upwards quickly, such that they are not affected by radiation. Another assumption is that diffusion (entrainment and turbulence) can be ignored.

To begin the derivation, we start with the energy balance of a rising saturated parcel, which, under these assumptions, is given by

$$0 = c_p \frac{\mathrm{d}T}{\mathrm{d}z} + L_v \frac{\mathrm{d}q^*}{\mathrm{d}z} + g \tag{1.1}$$

where the first term represents changes in energy related to temperature changes, the second changes in energy due to condensation and the third term is for the change in potential energy of the parcel as it rises. z is height, T is temperature, c_p is the heat capacity at constant pressure, L_v is the latent heat of vapourisation, g is Earth's gravity, and q^* is the saturation water vapour mass fraction:

$$q^* = \frac{m_v^*}{m} = \frac{\rho_v^*}{\rho} \tag{1.2}$$

where m is mass, ρ is density and variables with no subscript are for the air, while those with the subscript v are for water vapour and the asterisk indicates saturation.

Using the ideal gas law, $p = \rho\ R\ T$, for both air and for water vapour, we can rewrite equation 1.2 as

$$q^* = \frac{R\ p_v^*}{R_v\ p} \tag{1.3}$$

where p is the air pressure, p_v^* is the partial pressure due to water vapour at saturation, R is the specific gas constant of air and R_v that for water vapour. As long as p_v^* is small, R is well approximated by the specific gas constant of dry air and we assume that R and R_v are constant with height. Then, we can calculate the fractional change in q^* with height as

$$\frac{\mathrm{d}}{\mathrm{d}z}\log(q^*) = \frac{\mathrm{d}}{\mathrm{d}z}\log(p_v^*) - \frac{\mathrm{d}}{\mathrm{d}z}\log(p) \tag{1.4}$$

For the fractional change in p, we assume hydrostatic balance, $\mathrm{d}p = -\rho g \mathrm{d}z$, and the ideal gas law, to get that

$$\frac{\mathrm{d}}{\mathrm{d}z}\log(p) = -\frac{g}{R\,T} \tag{1.5}$$

The fractional change in p_v^* can be obtained by assuming the Clausius-Clapeyron relation, giving

$$\frac{\mathrm{d}}{\mathrm{d}z}\log(p_v^*) = -\frac{L_v}{R_v\,T^2}\frac{\mathrm{d}T}{\mathrm{d}z} \tag{1.6}$$

Substituting equations 1.5 and 1.6 into equation 1.4 gives

$$\frac{\mathrm{d}}{\mathrm{d}z}\log(q^*) = -\gamma \tag{1.7}$$

where γ is defined as

$$\gamma = \frac{L_v}{R_v\,T^2}\frac{\mathrm{d}T}{\mathrm{d}z} - \frac{g}{R\,T} \tag{1.8}$$

By substituting equation 1.7 into equation 1.1 and rearranging, the moist adiabatic lapse rate can be found.

$$\frac{\mathrm{d}T}{\mathrm{d}z} = \frac{g + \frac{q^*\,L_v\,g}{R\,T}}{c_p + \frac{q^*\,L_v^2}{R_v\,T^2}} \tag{1.9}$$

The moist adiabatic lapse rate is a good representation of the lapse rate in the tropical lower free troposphere, but deviations from it are observed in the upper troposphere (*e.g.* Folkins, 2002). Folkins (2002) argues that the deviations arise from a change in the pseudo equivalent potential temperature[1] distribution of air parcels reaching different altitudes, but it is unclear whether other processes, such as radiative effects, also play a role.

1.2.2 Weak temperature gradient approximation

The theory behind the weak temperature gradient approximation is used to explain why temperatures in the tropics show little variation in the horizontal.

The theory of Bretherton and Smolarkiewicz (1989) explains the smallness of horizontal gradients using the notion that gravity wave propagation homogenises buoyancy perturbations. Cloud heating produces a positive buoyancy perturbation everywhere up to the level of neutral buoyancy (which for deep convection, we think of as the base of the TTL) and a negative buoyancy perturbation above that. The cloud heating generates horizontally propagating waves that displace air in the vertical. At altitudes where the cloud buoyancy is positive with respect to the unperturbed atmosphere, the neighbouring air is less buoyant than that inside the cloud and is displaced downwards. Conversely above the level of neutral buoyancy, the cloud buoyancy is negative, so the unperturbed neighbouring air is more buoyant and is therefore displaced upwards. As the wave propagates, it adjusts the atmosphere at increasing distances from the cloud location. By mass continuity, the diverging motion of the wave around the level of neutral buoyancy

[1] Pseudo equivalent potential temperature is a conserved quantity under moist adiabatic expansion, assuming that condensed water is immediately removed. That condensed water is immediately removed is also one of the assumptions used in our derivation of the moist adiabat, where heating of water condensate is neglected. This lapse rate is more accurately referred to as the pseudo-adiabatic lapse rate.

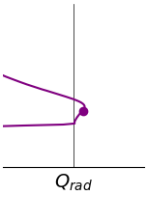

creates horizontal flows away from the cloud into the neighbouring regions as they adjust. The reverse happens near the surface, where the downward motion of the wave increases the air pressure, generating horizontal flows towards the cloud base that can help to sustain convection inside the cloud. The downward motion also produces adiabatic warming, which balances the net radiative cooling there.

As described above, Bretherton and Smolarkiewicz (1989) clarify why both buoyancy and pressure perturbations are eliminated in the tropics. From this, it follows that horizontal gradients in temperature are also small, as temperature is closely tied to those variables (via the ideal gas law).

1.2.3 Tropospheric humidity

Water vapour is a strong greenhouse gas that provides a positive feedback to many different forcings, so it is important to have an accurate picture of how it reacts to changes in environmental conditions, such as global warming. The lifetime of water vapour in the troposphere is relatively short (on the order of 10 days, Zhang et al., 2003), so it reacts quickly to changing conditions. There are theoretical grounds as to why we expect water vapour to change such that the relative humidity of the free troposphere is fixed as a function of temperature. This section aims to explain that theory.

The starting point is the Clausius-Clapeyron relation, which states that the saturation water vapour pressure increases approximately exponentially with temperature at a rate of $\sim 7\%\,\mathrm{K}^{-1}$ for temperatures around 300 K. As this only holds for saturated air and most of the atmosphere is unsaturated, the Clausius-Clapeyron relation alone is not sufficient to explain changes in tropospheric humidity. Mechanisms that contribute to the subsaturation of the atmosphere must be considered, in particular dynamics and condensation.

Thinking about a parcel of air, the water vapour content of it can change by diffusion of water into or out of the parcel from wetter or drier neighbouring parcels respectively, and by condensation or evaporation of water inside the parcel. Condensation occurs whenever the water vapour content of the parcel is greater than the saturation humidity and leads to the formation of clouds or precipitation. If we neglect diffusion, the water vapour content of the parcel is equal to the minimum saturation humidity that the parcel encountered on its journey through the atmosphere. In this conceptual picture, the water vapour content of the parcel is a nonincreasing function of time, with drying events becoming less frequent over time. This view is a bit too simplistic: the drying rate must be balanced by processes which add new water vapour to the parcel. It is thought that the parcels mainly gain new water when they go into the boundary layer, where water vapour concentrations are high and turbulent mixing is strong. Another source of water vapour could be evaporation of precipitation as it falls through dry air. To understand water vapour feedbacks, it is important to understand both changes in the trajectories of air parcels and in the probability of moistening the parcel, and it may also be important to take into account diffusive mixing (which could moisten or dry).

Based on the picture described above, Minschwaner and Dessler (2004) design a simple advection-condensation model, in which saturated air from convective columns detrains and sinks in dry regions. Based on the energy balance between net radiative cooling and adiabatic motion in the dry regions and using observational data of the temperature lapse rate and for the input to the radiative transfer calculations, they calculate the downward mass flux, and then from mass continuity the amount of detrainment from the moist region (*i.e.* the moisture supply). With their advection model, accounting only for downward motion, they can reproduce upper tropospheric humidity values. However, below 10 km their humidity values are drier than observations, leading the authors to conclude that vertical mixing and evaporation play an important role there.

An alternative approach is taken by Romps (2014), who instead of specifying the temperature lapse rate, chooses to specify the entrainment and detrainment rates. As in the study by Minschwaner and Dessler (2004), the tropics are split into two regions, a

saturated convective region and an unsaturated region, with detrainment from the moist to the dry region, but Romps (2014) also includes entrainment from the dry into the moist region. Using this model, Romps (2014) derives both the lapse rate and the relative humidity. Then, under the assumption that entrainment and detrainment rates, normalised by the convective mass flux, are fixed (either constant throughout the whole atmospheric column, or as functions only of temperature), and neglecting the pressure dependence of the saturation mass fraction (the effect of which the study shows to be small), Romps (2014) finds that the relative humidity is a function only of temperature - in other words, it is fixed as a function of temperature.

Relative humidity being fixed as a function of temperature can also be shown to be a solution to the problem as formulated by Minschwaner and Dessler (2004), in combination with the argument of Hartmann and Larson (2002) that as long as relative humidity is approximately fixed as a function of temperature then the clear sky net cooling is approximately fixed as a function of temperature. Minschwaner and Dessler (2004) use the net radiative cooling rates to calculate the downwelling velocity, which is then used to calculate the ratio between detrainment and downward mass flux. Therefore, if we assume that the clear sky net radiative cooling is fixed as a function of temperature, the ratio between detrainment and downward mass flux would be too, which would produce a relative humidity profile fixed as a function of temperature. However, as the starting point is that relative humidity is a function of temperature (to get net radiative cooling rates that are fixed as a function of temperature), this line of argument only shows that fixed relative humidity is a solution, but not that it is a unique solution.

1.2.4 High clouds

Clouds are an important part of the climate system, which play a role in radiative transfer, precipitation, large and small scale atmospheric circulation patterns, and wave generation. Here, we focus only on radiative effects and only on high convectively generated clouds, known as anvil clouds (figure 1.1), which form in the upper troposphere and cause a peak in the cloud area fraction there (figure 1.2). The influence of anvil clouds on shortwave radiative fluxes, as with other types of clouds, depends mainly on the cloud area fraction and the albedo of the underlying surface (or lower clouds). In terms of longwave radiation, low level clouds have little influence on the energy balance, due to their temperature being similar to that of the surface, while high clouds emit at much colder temperatures than the surface below them. In this way anvil clouds act to warm the surface, much like a greenhouse gas. Anvil clouds are also relevant for the tropical tropopause layer (section 1.3.1), with observational data showing that regions of deep convection coincide with colder tropopause temperatures (*e.g.* Johnson and Kriete, 1982; Son et al., 2011; Paulik and Birner, 2012), although the contribution from radiative effects alone is uncertain. Finally, anvil clouds could impact the sensitivity of the tropopause and the surface to increasing CO_2, through changes in their area fraction, optical properties or temperature.

The fixed anvil temperature (FAT) hypothesis argues that anvil clouds should remain at a fixed temperature as the climate warms (Hartmann and Larson, 2002); their reasoning proceeds as follows. Clear sky net radiative cooling is mostly controlled by longwave emission from water vapour, and as water vapour concentrations are approximately a function of temperature (Section 1.2.3), so is clear sky net radiative cooling. In energy balance, changes in clear sky net radiative cooling with height should be balanced by convergence in those regions, and by mass continuity this implies divergence at the same altitude in the convective regions. Divergence is associated with convective detrainment and it is further assumed that cloud cover peaks where detrainment is maximum, leading to the final argument that the peak in cloud cover occurs at a fixed temperature.

The FAT hypothesis is certainly a useful conceptual model, however many subsequent studies (including Kuang and Hartmann, 2007; Zelinka and Hartmann, 2010; Harrop and Hartmann, 2012) showed that although clouds rise with warming in both global climate

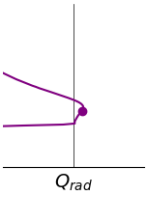

Figure 1.1: Photograph showing an anvil cloud. Downloaded on 10.12.2019 from https://eesa.lbl.gov/new-eesa-research-questions-widely-accepted-anvil-cloud-feedback-on-global-warming/

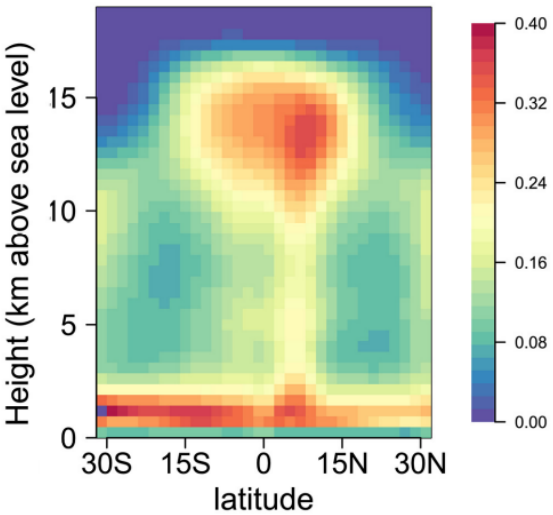

Figure 1.2: Zonally averaged cloud fraction as a function of latitude and altitude. Modified from Seeley et al. (2019a), who used data from colocated spaceborne radar (CloudSat) and lidar (Cloud-Aerosol LIdar with Orthogonal Polarization) instruments following Kay and Gettelman (2009).

models and cloud resolving models, they also undergo a temperature change, albeit smaller than the surface temperature change. Using a cloud resolving model designed specifically to test the FAT hypothesis, forced only by longwave radiative emission from water vapour, Seeley et al. (2019b) find an increase in temperature of anvil clouds by 0.4 K for every 1 K increase in surface temperature in agreement with the previous studies listed above. However, they find a much smaller change in temperature of the lapse rate tropopause (following the World Meteorological Organisation definition: where the temperature lapse rate becomes less than 2 K/km and the average lapse rate between this level and all higher levels within the next 2 km is not larger than 2 K/km) and the radiative tropopause (where clear sky net radiative cooling goes to zero), which suggests that at least the first few assumptions made in the FAT hypothesis hold very well. In another study, Seeley et al. (2019a) argue that detrainment plays little role in determining the anvil cloud peak. Instead, they show the importance of cloud lifetime, which is larger in colder regions as they become saturated more easily, meaning that cloud decay by evaporation occurs more slowly. This implies that one of the assumptions made in the FAT hypothesis - cloud cover peaks where detrainment is maximum - is not a good one, however Seeley et al. (2019a) do not provide an explanation for changes in anvil cloud temperature under warming scenarios.

If high clouds warm at a slower rate than the surface temperature, Zelinka and Hartmann (2010) argue that the increase in longwave cooling of the clouds to space would not be as large as the increase in emitted radiation from the surface. Therefore, Zelinka and Hartmann (2010) expect a positive longwave feedback, which would be stronger in cases where the clouds undergo a smaller warming with respect to surface temperature warming.

1.3 Above the troposphere

1.3.1 The tropical tropopause layer

Traditionally the tropopause has been defined at a single height (generally either at the cold-point or at a certain lapse rate value), but the tropopause is better defined as a layer, which lies between the troposphere and the stratosphere and shares properties of both these regimes. In the tropics, between 30°N and 30°S, this layer is known as the tropical tropopause layer (TTL) and has a vertical extent of several kilometers (Fueglistaler et al., 2009). In the TTL, it is thought that the radiative timescale is shorter than the convective timescale, but that convective transport timescales are shorter than photochemical timescales, such that upflows maintain low ozone mixing ratios in this region (Thuburn and Craig, 2002).

There are many uncertainties in TTL evolution under global warming, with general circulation modelling studies generally predicting a warming of the cold point tropopause, but the magnitude of the trend varies greatly between models. The trends found in CMIP5 models for an RCP 8.5 scenario are in the range $[-0.5,\ 3.6]\,\mathrm{K\,century^{-1}}$, but the same models produced no identifiable trends over the relatively short time period between 1979 to 2006 (Kim et al., 2013). Observational data from 1970 to 2010 show either a cooling or no significant change (Wang et al., 2012). It is perhaps unsurprising that there is disagreement about TTL evolution, as many models still do not accurately represent all processes affecting the current temperature structure of the TTL. Climatological cold point temperatures were found to vary in a range of more than 10 K in a comparison of coupled Chemistry Climate Models (Gettelman et al., 2010), and almost the same range of results was found among the CMIP5 models (Kim et al., 2013).

Radiative heating rates in the TTL are small compared to the rest of the tropical atmosphere, but despite this, they are crucial for determining the temperature structure. Water vapour, CO_2 and ozone have long been considered the most important radiative species (*e.g.*, Manabe and Möller, 1961; Gowan, 1947; Dobson et al., 1946) and Thuburn and Craig (2002) show that all three play a role for the structure of the TTL.

Deep convection is also important for TTL temperatures and observational studies (*e.g.*, Johnson and Kriete, 1982; Son et al., 2011; Paulik and Birner, 2012) provide evidence for

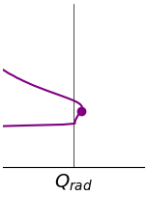

this. Isobars increase in altitude within clouds, due to convective heating, and Holloway and Neelin (2007) propose that the pressure anomaly also extends above the convective heating. They further argue that the horizontal pressure gradients above the cloud top lead to divergence and large scale upward motion, producing adiabatic cooling. Other processes could also contribute to the cooling required to reduce the pressure gradients. The modelling study of Kuang and Bretherton (2004) provides evidence for cooling via overshooting convection (Sherwood and Dessler, 2000), and cloud radiative effects may also have a cooling effect. If either or both of these processes occur and contribute to cooling, the large scale upward motion proposed by Holloway and Neelin (2007) would weaken to maintain the same total cooling (Holloway and Neelin, 2007).

Large scale adiabatic cooling is also produced by the tropical upwelling associated with the Brewer-Dobson circulation (section 1.3.2). Any changes in deep convection and large scale circulation would likely alter the temperature structure of the TTL directly, as well as indirectly by affecting the atmospheric composition, including water vapour and ozone concentrations.

1.3.2 The Brewer-Dobson circulation

The Brewer-Dobson circulation is a large scale circulation pattern, which brings tropospheric air upwards through the TTL into the stratosphere and downwards in the polar regions. The Brewer-Dobson circulation is driven by wave breaking of both planetary scale and smaller scale waves. Under global warming, the upper tropical troposphere warms strongly, increasing the meridional temperature gradient in the midlatitudes. This increases the baroclinicity, a measure of how misaligned the gradients of pressure and density are, which increases baroclinic wave generation. Then, wave propagation out of the troposphere also increases and this leads to an increase in strength of the Brewer-Dobson circulation (*e.g.* Eichelberger and Hartmann, 2005). Indeed, many modelling studies have found a strengthening of the Brewer-Dobson circulation with global warming (*e.g.,* Butchart et al., 2006; Garcia and Randel, 2008), but it is not clear how large any changes would be and Oberländer-Hayn et al. (2016) found no change in tropical upwelling strength when considered with respect to the changing tropopause pressure. An increase in tropical upwelling would provide a larger adiabatic cooling, acting to reduce temperatures in the TTL and tropical lower stratosphere.

1.3.3 Ozone

Ozone is one of the most important radiative species in the atmosphere and is the reason that temperatures increase with height above the tropical tropopause layer. Ozone absorbs shortwave radiation from the Sun, which would otherwise be harmful for life on Earth, and it is speculated that the ozone layer was created around 2×10^9 years ago, allowing life to move from the oceans to the land (Lenton, 2003). In more recent times, anthropogenic emissions of ozone depleting substances (including chlorofluorocarbons) have had a destructive impact on the ozone layer, mostly over the polar regions where their effects were enhanced due to polar stratospheric clouds. The Montreal protocol came into effect in 1989, banning the use of many of these substances and limiting the damage to the ozone layer. However, the ozone layer is also changing due to other processes and in this thesis the focus is on changes in tropical stratospheric ozone under global warming.

The chemical reactions that destroy ozone occur with a rate that depends on temperature. Some reactions occur more rapidly and others more slowly when temperature increases, with the overall effect that a decrease in temperature in the tropical stratosphere leads to an increase in ozone there. As well as a decrease in stratospheric temperature under global warming, stratospheric humidity also changes and also influences ozone (section 1.3.4). Water vapour is broken down in photolysis reactions, forming hydrogen radicals, H and OH. Subsequent reactions produce HO_2 and all three

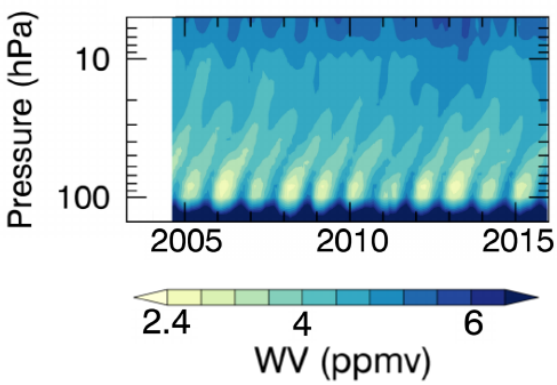

Figure 1.3: Water vapour measurements from Aura Microwave Limb Sounder showing the atmospheric tape recorder. Figure adapted from Davis et al. (2016).

components (H, OH and HO_2) act to destroy ozone.

In the tropical lower stratosphere, the photochemical lifetime of ozone is relatively long, between a few days and a few months, so transport plays an important role. The Brewer-Dobson circulation (section 1.3.2) brings tropospheric air, containing relatively little ozone, into the tropical lower stratosphere, diluting the ozone concentration there. The meridional branches of the Brewer-Dobson circulation carry ozone away from the tropics towards the poles, supplying ozone to the polar regions, where little photochemical production of ozone occurs. An increasing Brewer-Dobson circulation, as expected under global warming, would decrease ozone concentrations in the tropical lower stratosphere, leading to a reduction in absorption of radiation and cooling in this region.

Another factor is that as the troposphere warms it expands upwards in pressure coordinates and more strongly in height coordinates. As tropospheric ozone concentrations are relatively small, we would then expect these low concentrations to expand upwards with the expanding troposphere, meaning that the large gradient in ozone concentration would occur at a higher altitude (and slightly lower pressure) than before. Both the expansion of the troposphere and an increase in the Brewer-Dobson circulation act to decrease the ozone concentration at any specified pressure or altitude of the tropical lower stratosphere.

1.3.4 Stratospheric humidity

The total water vapour amount in the stratosphere is mostly determined by the concentrations in the TTL, as it is this air that is brought up into the tropical lower stratosphere by the Brewer-Dobson circulation (section 1.3.2). Observations over the seasonal cycle support this theory, showing a strong lagged correlation between lower stratospheric water vapour and the mean water vapour mixing ratio at 100 hPa (Mote et al., 1996, and shown in figure 1.3). The lag of the correlation increases with increasing altitude above the TTL, and the signal is known as the atmospheric tape recorder. Fueglistaler and Haynes (2005) find good observational agreement of a trajectory model, in which the water vapour mixing ratio of air entering the stratosphere is determined by the saturation mixing ratio of the coldest point during its ascent. They show that interannual anomalies are more closely related to zonal mean temperature anomalies, than variability in dynamics or the spatial pattern of temperature. Hegglin et al. (2014) also show that observed changes in stratospheric water vapour since the late 1980s can be attributed to changes in TTL temperature, and that in the upper stratosphere a role is also played by chemical reactions involving methane, which is increasing due to an increase in emissions. On the other hand, Dessler et al. (2016) state that while short term variations can be

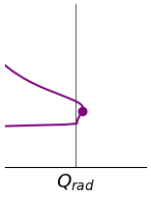

reproduced based on TTL temperatures, this mechanism does not fully explain the long term trends found in modelling studies. They argue that increases in evaporation of convectively lofted ice particles contribute significantly to the projected long term increase in stratospheric water vapour.

1.4 Thesis overview

As part of this thesis, I have co-developed two simple models, a 1D RCE model, konrad (section 2.1), and a simple ozone chemistry model, Agatha (section 2.2). Two advantages of using simple models are the low computational cost, which allows many sensitivity experiments to be performed, and that it is relatively easy to understand the mechanisms underlying the model results. With these models we investigate the importance of CO_2, ozone, large scale upwelling, convection and clouds for the TTL structure. We also study how different factors interact with each other, and how the TTL and surface temperature might evolve with increasing CO_2. This thesis uses the ideas and theory of sections 1.1, 1.2 and 1.3 and builds on the work of many previous studies, some of which are described in the following paragraphs.

A few previous 1D RCE modelling studies have focused on the TTL region, including Thuburn and Craig (2002), who carried out an extensive parameter study, investigating the effects of CO_2 concentration, relative humidity, ozone profile, tropospheric lapse rate and large-scale dynamical cooling. Fu et al. (2018) repeated some of these experiments and additionally studied cloud radiative effects on the TTL. Birner and Charlesworth (2017); Charlesworth (2017); Charlesworth et al. (2019) focused on the relative roles of dynamical cooling due to Brewer-Dobson upwelling and modifications of radiative heating due to changes in the ozone profile. All five of these studies used a model with a fixed surface temperature, so they did not investigate mechanisms linking the tropopause with surface temperature. On the other hand, McElroy et al. (1992) used a model with an interactive surface to study the surface temperature dependence on the ozone profile. However, this study included only three ozone profiles and did not test any other factors.

Charlesworth (2017); Charlesworth et al. (2019) added a new aspect to the other 1D studies of the TTL, by including a simple interactive ozone scheme, using only the Chapman chemistry (pure oxygen chemistry) and reactions with nitrogen oxides. Despite the simple nature of the model, Charlesworth (2017) found reasonable values for the ozone production and destruction rates, justifying their use of this scheme to analyse the structure of the TTL under different conditions. In this work, we have extended the scheme to include HO_x chemistry, allowing us to investigate the importance of ozone in the middle and upper stratosphere for lower stratospheric ozone concentrations (section 3.1.9). With regards to ozone, we also investigate why global climate modelling studies produce such different results regarding how changes in ozone expected from global warming affect surface temperature: Nowack et al. (2014) found a reduction in climate sensitivity to a $4 \times CO_2$ scenario of $\sim 1\,\mathrm{K}$ when including interactive ozone, whereas Dietmüller et al. (2014) found a smaller effect and Marsh et al. (2016) a negligible effect. Experiments with our simple 1D RCE model allow us to at least partially answer this question (sections 3.1.8 and 3.1.9).

There are several other novel aspects of this work, each contributing a small piece towards a greater understanding of the tropical atmosphere. We investigate the link between CO_2 and the TTL, to answer the question of whether CO_2 influences TTL temperatures in a 1D RCE model when the surface temperature is allowed to change (section 3.1.2). We further investigate whether this can be predicted based on the initial temperature tendencies when the forcing is applied (section 3.1.6). Another aspect of our work is the role of convection, which to our knowledge has not previously been studied in a 1D RCE study of the TTL, and here we do this by using two different methods of convective adjustment, each following a few simple assumptions (section 3.1.1). Additionally, we investigate the influence of a high cloud on the TTL structure and surface temperature (section 3.1.7). New compared to the

study of Fu et al. (2018), we prescribe the cloud optical properties and calculate the cloud radiative effect, which adapts to the background climate and cloud altitude, allowing us to investigate the positive longwave feedback of the cloud under a warming scenario (Zelinka and Hartmann, 2010). Similarly to the studies of Thuburn and Craig (2002); Birner and Charlesworth (2017); Charlesworth et al. (2019), we examine the influence of the Brewer-Dobson circulation on the TTL, but unlike those studies we can also investigate its influence on surface temperature (section 3.1.4). Moreover, we perform experiments with upwelling and various CO_2 and ozone concentrations to test whether the combined effect on the TTL and surface temperatures can be approximated by the sum of the effects from the individual perturbations (section 3.1.5).

While most of the work in this thesis and much of the climate community focus on predicting and understanding temperature changes (Jiménez-de-la Cuesta and Mauritsen, 2019; Kluft et al., 2019), other factors are as if not more relevant for policy makers (such as sea level rise, Li et al., 2020). Precipitation is one such factor, of central importance for agriculture (Flach et al., 2020) and flood prediction and management (Stephens and Cloke, 2014; Nobert et al., 2010) and already considered in some studies to inform policy makers regarding greenhouse gas emissions (*e.g.* Roshan et al., 2019). Under warming it is expected that extreme precipitation increases approximately following Clausius-Clapeyron scaling, but that mean precipitation increases at a much slower rate (Trenberth et al., 2003). Various global modeling studies produce results for the mean precipitation in agreement with this (*e.g.* Yang et al., 2003; Andrews and Forster, 2010), with the explanation that precipitation is mostly constrained by radiation in the atmospheric energy balance (O'Gorman et al., 2012). This theory is presented in section 4.1.1 and we aim to use this together with heating rate output from konrad to quantitatively reproduce the increase in mean precipitation under warming in as simple a way as possible (section 4.1.2). In a next step, we consider the tropics as two distinct regions, a saturated moist region of upward motion and a non-saturated region where adiabatic motion balances net radiative cooling. This basic picture allows us to derive the convective mass flux as well as the downwelling and upwelling velocities and area fractions (section 4.1.3) and leads us to question the validity of our conceptual view in the upper troposphere (section 4.2).

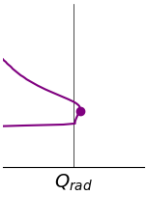

Chapter 2

Simple numerical models

Before we start this chapter, I would like to emphasise the contributions of Lukas Kluft and Ed Charlesworth.

Konrad (section 2.1) has been codeveloped by Lukas and I. Lukas shaped the fundamental design, *i.e.* combining the sub-models, running konrad and writing output files, as well as many of the details, including the treatment of humidity. My main contributions were the development of the methods for the convective adjustment (including designing the relaxed adjustment), the implementation of RRTMG inside konrad through climt (Monteiro et al., 2018) and the initial work of including clouds. Konrad is an open source model, written in python and available on `https://github.com/atmtools/konrad` Parts of the konrad model description have already been published by us in the Journal of Climate (Kluft et al., 2019; Dacie et al., 2019).

The simple ozone model Agatha (section 2.2) was developed by Ed Charlesworth (Charlesworth, 2017; Charlesworth et al., 2019). My work on Agatha has included refactoring, bug fixes, and, following Ed's suggestions, implementing HO_x chemistry. Agatha is also written in python and is available on `https://gitlab.com/simple-stratospheric-chemistry/simotrostra`

2.1 Konrad

Konrad is a one-dimensional radiative-convective equilibrium model (1D RCE), which runs on pressure coordinates with 200 levels and a spacing that increases linearly in logarithmic pressure space to a model top at 0.01 hPa. The surface in the model is a simple slab surface characterised by its heat capacity, but as the heat capacity only affects the temporal evolution of the model, it is not important for the experiments in this thesis, where most of the results are taken from equilibrium states. The results regarding the temporal evolution (section 3.1.6) are also found to be qualitatively similar for a wide range of surface heat capacities.

We use a set-up with fixed relative humidity and take a constant value throughout the troposphere. We choose a relative humidity of 0.40, as this is approximately equal to tropical mean upper tropospheric humidity in ERA5 reanalysis data. Above the cold point tropopause in the stratosphere, we use a fixed water vapour volume mixing ratio set by the temperature and relative humidity at the cold point. Although this profile is unrealistic in several aspects, we choose it for its simplicity and the way it responds to changes in atmospheric temperature. If the troposphere warms and deepens, and the cold point moves upwards to a lower pressure retaining the same temperature, the region with a relative humidity of 0.4 also deepens, in agreement with the theory that relative humidity is fixed as a function of temperature (section 1.2.3). On the other hand, if the cold point cools, the

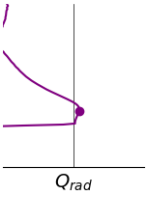

stratospheric humidity decreases, as expected. Unless otherwise specified, all of the runs performed in this thesis use this humidity set-up.

The other trace gas concentrations are those specified in Wing et al. (2018), including a CO_2 concentration of 348 ppmv and an ozone concentration profile given by an analytic approximation to an annual-mean equatorial climatology. For the solar insolation in most of the experiments, we use a tropical mean zenith angle of 42.05° (Wing et al., 2018) and a reduced solar constant of $480\,\mathrm{W\,m^{-2}}$, to avoid unrealistically high temperatures in a model with no meridional heat transport. For the experiments in section 3.1.9, we assume a latitude of 10° and a reduced solar constant of $1147\,\mathrm{W\,m^{-2}}$ and apply a diurnal cycle, so that the insolation changes as a function of time. The RRTMG radiation scheme (Mlawer et al., 1997) is used to calculate the radiative heating rates, which we apply at each timestep to give us the temperature profile T_{rad}, and this is followed by a convective adjustment in the troposphere. Many 1D RCE models use a convective adjustment to restore the tropospheric lapse rate to the moist adiabat (first used in a 1D RCE study by Hummel and Kuhn, 1981a) at each timestep. Our implementation of this is described in section 2.1.1 and in this study we refer to this method as the hard convective adjustment. Here we make comparisons to runs using a different convective adjustment (section 2.1.2), where we have relaxed this constraint. Regardless of the convective adjustment type, the only feedbacks in our model are from the radiation scheme (*e.g.* the Planck feedback), water vapour amount and the lapse rate, as these are the only temperature dependent factors in the model.

2.1.1 Hard convective adjustment

A convective adjustment is performed if the atmosphere is unstable to convection in the troposphere. The adjustment fixes the temperatures according to a specified lapse rate, given in $\mathrm{K\,km^{-1}}$, which is converted to $\mathrm{K\,Pa^{-1}}$ under the assumption of hydrostatic equilibrium.

The change in enthalpy of an atmospheric layer due to a temperature change ΔT_{atm} is proportional to $\rho c_p \,\Delta T_{\mathrm{atm}}\,\mathrm{d}z$, where ρ is the density, c_p is the heat capacity at constant pressure (also assumed to be constant with height) and $\mathrm{d}z$ is the thickness of the layer. This can be rewritten (assuming hydrostatic equilibrium) in pressure coordinates as $-\frac{c_p}{g}\,\Delta T_{\mathrm{atm}}\,\mathrm{d}p$, where g is the gravitational acceleration, assumed to be constant with height. The corresponding energy change of the surface is $\Delta \mathrm{z} \rho_s c_s \,\Delta T_s$, where $\Delta \mathrm{z}$ is the thickness of the surface layer, ρ_s the density and c_s the heat capacity. The surface layer is assumed to be at one temperature (it does not vary with depth). Then, the energy conservation equation required for the convective adjustment is

$$\int_{p_s}^{0} -\frac{c_p}{g}\,\Delta T_{\mathrm{atm}}\,\mathrm{d}p + \Delta \mathrm{z} \rho_s c_s \,\Delta T_s \quad = \quad 0 \tag{2.1}$$

The integral runs over the whole atmosphere, but there is no convective adjustment above a certain pressure level, p_c, called the convective top. The convective temperature change in the atmosphere ΔT_{atm} is a function of pressure and is given by

$$\Delta T_{\mathrm{atm}}(p) \quad = \quad T_{\mathrm{con}}(p) - T_{\mathrm{rad}}(p) \tag{2.2}$$

where T_{rad} is the temperature profile after the radiative heating rates have been applied and T_{con} is the convectively adjusted temperature profile

$$T_{\mathrm{con}}(p) \quad = \quad \begin{cases} T_{con,\ s} - \int_p^{p_s} \gamma_p \,\mathrm{d}p & \text{if } p > p_c \\ T_{\mathrm{rad}}(p) & \text{if } p \leq p_c \end{cases} \tag{2.3}$$

where p_s is the surface pressure and $T_{con,\ s}$ is the convectively adjusted surface temperature and γ_p is the change in temperature of the convective profile with pressure ($\gamma_p > 0$) and comes from the specified lapse rate. In our standard set-up, used throughout this work, the lapse rate is chosen to be the moist adiabatic lapse rate (section 1.2.1). We

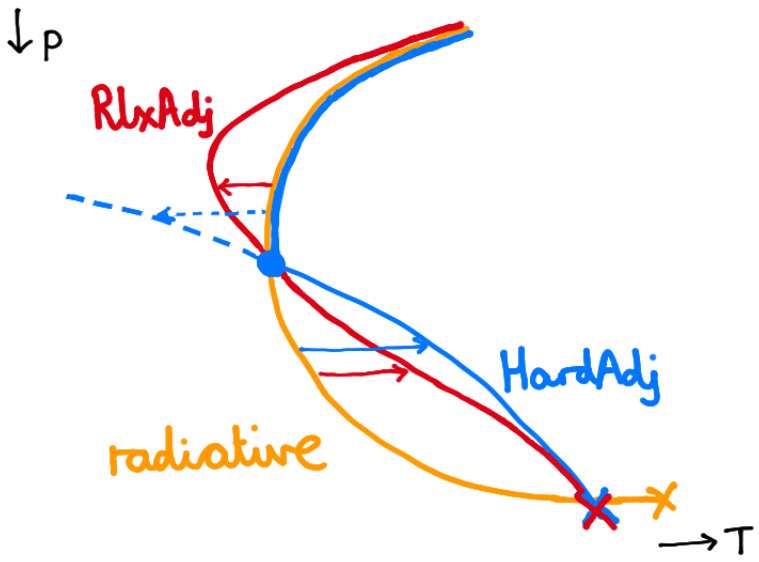

Figure 2.1: Highly exaggerated diagram illustrating the difference between the hard (blue) and relaxed (red) convective adjustment schemes. Not to scale.

assume that convection acts to cool the surface and warm the troposphere and thus do not allow convection to cool the atmosphere. The pressure level p_c is defined as the highest atmospheric level (lowest pressure level) which satisfies $T_{\rm con}(p_c) \geq T_{\rm rad}(p_c)$ and no convective adjustment is applied above this level.

The equations above, or similar equations with a different treatment of the surface, are the same as those used for the convective adjustment of many previous RCE models, including Manabe and Wetherald (1967) and MacKay and Khalil (1991).[1]

2.1.2 Relaxed convection

In the real atmosphere, a gradual transition from radiative-convective equilibrium to radiative equilibrium occurs in the upper troposphere and the TTL when the convective timescale becomes longer than the radiative timescale. Convective events occurs on a range of timescales, with shallow convection acting frequently and quickly over small vertical scales, and with deeper convection requiring more time to develop. Then, the mean convective heating profile can be seen as a combination of the profiles from numerous convective plumes, which extend to a variety of heights. To mimic this, we define a convective temperature increment $\Delta T_{\rm rlx}$ as a function of pressure p, such that convection weakens with height.

$$\begin{aligned} \Delta T_{\rm rlx}(p) &= T_{\rm con}(p) - T_{\rm rad}(p) \\ &= \Delta T_{\rm hard}(p) \times \chi(p) \end{aligned} \tag{2.4}$$

[1]While the equations we are solving are the same as in many previous studies, our computational implementation differs. This enables us to make use of computationally efficient numpy (Oliphant, 2006) functions in our python code, rather than performing a loop of consecutive smaller adjustments as in the energy flux approach taken in previous studies. We start by guessing a surface temperature, $T_{con,\ s}$ and calculate the corresponding convectively adjusted temperature profile according to equation 2.3. Then we test how close this profile is to satisfying energy conservation (equation 2.1). We update our guess surface temperature and repeat the procedure iteratively, until we find a surface temperature and corresponding profile which satisfy equation 2.1.

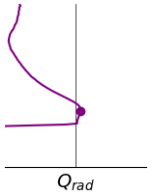

with the subscripts rad and con for the radiatively and convectively adjusted profiles respectively, $\Delta T_{\text{hard}}(p)$ the temperature change for a hard adjustment, and $\chi(p)$ a relaxation factor ($0 \leq \chi(p) \leq 1$). From equations 2.2 and 2.3, we get that

$$\Delta T_{\text{hard}}(p) = T_{\text{con, s}} - \int_{p_s}^{p} \gamma_p \, \mathrm{d}p - T_{\text{rad}}(p) \tag{2.5}$$

We then choose a relaxation factor

$$\chi(p) = 1 - e^{-\frac{t}{\tau(p)}} \tag{2.6}$$

where t is the timestep, and $\tau(p)$ is a convective timescale. Thus, in the relaxed adjustment case for $\tau(p) \neq 0$, our temperature change is smaller than for the hard adjustment in the troposphere. Another difference between the hard and relaxed adjustments, is that the hard adjustment is only applied up to a certain model level, namely the level of neutral buoyancy (where a rising air parcel has the same density as its environment), which is determined by the lapse rate and energy conservation. In contrast, the relaxed adjustment is applied throughout the whole column. $\Delta T_{\text{rlx}}(p)$ and $\Delta T_{\text{hard}}(p)$ are depicted as red and blue horizontal arrows in figure 2.1.

The relaxed adjustment gives us a convective temperature profile of

$$T_{\text{con}}(p) \quad = \quad T_{\text{rad}}(p) \; e^{-\frac{t}{\tau(p)}} + \left(1 - e^{-\frac{t}{\tau(p)}}\right) \left(T_{\text{con, s}} - \int_{p_s}^{p} \gamma_p \, \mathrm{d}p\right) \tag{2.7}$$

which is valid for the whole atmosphere, but it is closely linked to the radiative temperature profile for large $\tau(p)$. As $\tau(p)$ becomes much larger than the radiative timescale, the convection can no longer change the temperature profile and $T_{\text{con}}(p) \simeq T_{\text{rad}}(p)$.

The profile we choose for τ is as follows:

$$\tau(p) \quad = \quad \tau_0 \; e^{\frac{p_0}{p}} \tag{2.8}$$

with p_0 the pressure of the lowest atmospheric level (set as 1000 hPa). τ_0 is set to 1 hour, on the order of the convective adjustment time used in several convection schemes and found to reproduce observations well (*e.g.* Betts and Miller, 1986). As τ increases with height, the influence of convection weakens, thus we may expect other factors (*e.g.* changes in radiative heating due to a shifted ozone profile) to have a larger impact.

Our choice of τ is tuned for our standard model set-up and there is no reason to believe that it is suitable for other climate states. Nevertheless, as there is currently no sound theoretical basis about how the timescale of convection might change, we assume that τ stays fixed with pressure and does not change as we perturb other factors. Regardless of the assumptions about τ, comparisons between the hard and relaxed adjustments allow us to study whether reducing the importance of convection in the upper troposphere in the relaxed adjustment means that other factors have more influence on the TTL. More generally, we can investigate whether the way convection is treated affects the results of any of our experiments.

Around the TTL, the relaxed convective adjustment provides a cooling, which results simply from following the moist adiabatic lapse rate. Thinking about this in terms of a rising air parcel, the parcel follows the moist adiabatic lapse rate and will overshoot its level of neutral buoyancy if it reaches this altitude with enough momentum. Convective cooling of the TTL is not present in the hard adjustment, where the convective adjustment stops abruptly at the level of neutral buoyancy. In a warmer climate, the convective cooling is reduced in the relaxed adjustment with our definition of τ, as the level of neutral buoyancy occurs at a lower pressure where the convective timescale is larger.

Allowing for convective cooling above the level of neutral buoyancy may make the relaxed adjustment seem more realistic than the hard adjustment. However, in the middle

and/or upper troposphere, the relaxed adjustment produces temperatures that decreases more quickly with height than the moist adiabat, whereas observations show deviations from the moist adiabat in the opposite direction (*e.g.* figure 2 of Fueglistaler et al., 2009). In this sense, the relaxed adjustment is less realistic than the hard adjustment, which produces temperature profiles that exactly follow the moist adiabat.

2.1.3 Upwelling

Following Birner and Charlesworth (2017), in some experiments, we include an additional heating rate, which mimics the adiabatic cooling produced by the Brewer-Dobson circulation (section 1.3.2) and is applied everywhere above the convective top. We use the same equation as Birner and Charlesworth (2017) for the dynamical cooling rate:

$$Q = -w_{up}\left(\frac{\partial T}{\partial z} + \frac{\mathrm{g}}{c_p}\right) \tag{2.9}$$

where w_{up} is a prescribed upwelling velocity, T is temperature, z is altitude, g gravity and c_p isobaric heat capacity, with g and c_p approximated as constants.

In experiments that apply an upwelling, energy is constantly being removed due to this stratospheric cooling term, and this is balanced by a non-zero net flux at the top of the atmosphere. In the real atmosphere, this would be compensated for in the extra-tropics. In most of our experiments, we do not apply the upwelling to the gas concentrations, which are treated as before (described in section 2.1); in other words there is no transport. Only in the case where we also use Agatha (sections 2.3 and 3.1.9), is the upwelling used to calculate the upward transport of ozone, as well as to provide adiabatic cooling rates.

2.1.4 A high cloud

In konrad, we do not explicitly include convective mass fluxes or microphysical processes such as ice crystal formation. However, in the normal clear sky set-up, both a latent heat supply and instantaneous precipitation are implicitly assumed, because of the requirements of the moist adiabat and the lack of clouds. For some experiments, we are also interested in the impact of clouds, and specifically of high clouds, as these are the most relevant for the tropopause region. Cloud formation and decay are beyond the scope of konrad, so we instead take a simplistic approach of prescribing a cloud to be seen by the radiation scheme.

The cloud we prescribe has a rectangular shape, such that the cloud area fraction takes a constant value for all model levels inside the cloud. We prescribe the longwave and shortwave optical depths of the cloud, as well as the single scattering albedo and asymmetry parameter, which are important in the shortwave and describe how reflective the cloud is and the direction the radiation is scattered in. The cloud optical properties (parameters mentioned above) are fixed throughout the simulation. This is implemented in the simplest way possible, by fixing the number of model levels that the cloud spans. However, the cloud is not tied to specific model levels, but instead it is coupled to the convective top, such that if the troposphere expands, the cloud shifts upwards in accordance with this.

The radiation scheme, RRTMG, performs two calculations, one in which the radiation sees only the clear sky and the other in which the radiation sees the cloud. A weighted average is calculated for the radiative fluxes and heating rates, taking into account the prescribed cloud area fraction. This method assumes two columns, one with cloud and one without, that do not interact with each other in terms of the radiation (*i.e.* the radiation scattered from the cloud does not enter the clear sky part). This simplification is almost always used in climate models and is generally considered a good approximation as long as the spatial scales are large enough, which is the case for konrad where the aim is to represent the tropical atmosphere.

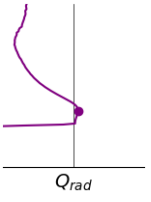

2.1.5 Convective top definition

In previous studies (Thuburn and Craig, 2002; Birner and Charlesworth, 2017), the convective top was defined, for the hard adjustment case, as the highest level to which a convective adjustment was applied. However, this definition suffers from the discrete nature of the model levels, and convective top temperature values depend on the resolution. To resolve this issue, we perform an interpolation, defining the convective top temperature as the temperature corresponding to a convective heating of $0.2\,\mathrm{K\,day^{-1}}$. The value of 0.2 was chosen to be small, so that our convective top is close to the top level of our convective adjustment, where convective heating goes to zero. On the other hand, the chosen value needed to be far enough from zero for the interpolation to completely remove the effect of the zero convective heating level being at a discrete model level. Then, for consistency, the same definition can be used for the relaxed convective adjustment case, where there is no hard transition to radiative equilibrium.

The definition described above is used for all of the analysis that was published in Dacie et al. (2019). However, when clouds are included, we find a reduction in the magnitude of the upper tropospheric net radiative cooling rates and thus a reduction in the upper tropospheric convective heating rates. Moreover, both the net radiative cooling and the convective heating profiles are not smooth in the upper troposphere where the cloud is located, so performing a linear interpolation between two model levels would be unlikely to help reduce noise associated with the discretisation of the model levels. Therefore, we choose to revert to the definition of Thuburn and Craig (2002); Birner and Charlesworth (2017) for the analysis in section 3.1.7.

2.2 Agatha

Agatha calculates changes in ozone due to chemistry in a column of the atmosphere. The only chemistry considered is that of pure oxygen, NO_x and HO_x and only the most important reactions are considered. If used iteratively (to calculate ozone profiles rather than only to calculate ozone tendencies corresponding to specified ozone profiles), Agatha should be used in combination with a transport model, as for example described in section 2.3.

2.2.1 Ozone source

The odd oxygen source term, comprised of stable and excited atomic oxygen and ozone ($\mathrm{O}_x = \mathrm{O} + \mathrm{O}^* + \mathrm{O}_3$), is based on the following photolysis reactions.

$$J2 : \mathrm{O}_2 + h\nu\,(\lambda < 242\,\mathrm{nm}) \rightarrow \mathrm{O} + \mathrm{O} \tag{2.10}$$

$$J2^* : \mathrm{O}_2 + h\nu\,(\lambda < 175\,\mathrm{nm}) \rightarrow \mathrm{O} + \mathrm{O}^* \tag{2.11}$$

These are the only two reactions that create odd oxygen, other reactions either convert between one type of odd oxygen and another, or act to destroy odd oxygen. We then make the assumption that O_x is approximately equal to O_3 below the mesosphere, so a source of O_x is a source of O_3. This gives an ozone source term equal to $2\,(J2 + J2^*)\,[\mathrm{O}_2]$, where $J2$ and $J2^*$ are the rates for the above reactions and square brackets indicate concentration in this case of diatomic oxygen.

2.2.2 Odd oxygen partitioning

To calculate the odd oxygen tendencies, the model requires an ozone profile as input, along with temperature, pressure and height profiles and a specified zenith angle. When running the model iteratively, we use the odd oxygen tendencies to update the ozone profile.

We do not use the tendencies to update the concentration of atomic oxygen directly, but instead we calculate the concentration of atomic oxygen from that of ozone. This partitioning is based on the following reactions:

$$J3 : \mathrm{O_3} + h\nu\,(\lambda < 1180\,\mathrm{nm}) \rightarrow \mathrm{O_2} + \mathrm{O} \tag{2.12}$$

$$J3^* : \mathrm{O_3} + h\nu\,(\lambda < 411\,\mathrm{nm}) \rightarrow \mathrm{O_2} + \mathrm{O}^* \tag{2.13}$$

$$k2 : \mathrm{O_2} + \mathrm{O} + M \rightarrow \mathrm{O_3} + M \tag{2.14}$$

$$k4 : \mathrm{O}^* + M \rightarrow \mathrm{O} + M \tag{2.15}$$

where $J3$, $J3^*$, $k2$ and $k4$ indicate rates and M is any inert molecule. Because the chemical timescales are short, we can assume that O and O^* are in a steady state. The excited and stable atomic oxygen concentrations are given by:

$$[\mathrm{O}^*] = \frac{J3^*\ [\mathrm{O_3}]}{k4\ [M]} \tag{2.16}$$

$$[\mathrm{O}] = \frac{J3\ [\mathrm{O_3}] + k4\ [\mathrm{O}^*][M]}{k2\ [\mathrm{O_2}][M]} \tag{2.17}$$

and combining these gives

$$[\mathrm{O}] = \frac{(J3 + J3^*)\ [\mathrm{O_3}]}{k2\ [\mathrm{O_2}][M]} \tag{2.18}$$

At nighttime we assume that there is no atomic oxygen, as there are no photons available for the photodissociation of ozone and atomic oxygen quickly undergoes recombination reactions.

2.2.3 Photolysis rates

Both the ozone source term and odd oxygen partitioning (which is used in the O_x, NO_x and HO_x sink terms) involve photolysis reactions. The two photolysis rate coefficients we are interested in are

$$J_{\mathrm{O_2}} = J2 + J2^* \tag{2.19}$$

$$J_{\mathrm{O_3}} = J3 + J3^* \tag{2.20}$$

The photolysis rate coefficients are calculated for each model level by multiplying the absorption cross-section by the amount of radiation reaching that level and integrating in wavelength space. For both $J_{\mathrm{O_2}}$ and $J_{\mathrm{O_3}}$, we assume a quantum efficiency of 1.

The calculation of $J_{\mathrm{O_3}}$ is relatively simple, because we can ignore the small dependence of the absorption cross-section on temperature and pressure. Then, we only need to take into account the wavelength dependence of the absorption cross-section, as well as the flux of photons of each wavelength through the atmosphere. The flux of photons of a certain wavelength reaching a certain depth depends on the incoming irradiance (which depends on zenith angle) and the transmissivity of the atmosphere above. Flux at wavelengths relevant

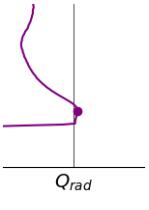

for J_{O_3} is only absorbed in the photolysis reactions with ozone, so the transmissivity $Tr_{O_3}(z)$ depends only on the amount of ozone $[O_3]$ and the absorption cross-section $\sigma(\lambda)$.

$$J_{O_3}(p) = \int Tr_{O_3}(p)\ F_{TOA}(\lambda)\ \sigma(\lambda)\ d\lambda \tag{2.21}$$

where $F_{TOA}(\lambda)$ is the flux of photons as a function of wavelength λ at the top of the atmosphere and

$$Tr_{O_3}(z) = \exp\left(-\sigma(\lambda)N_{O_3}(z)\right) \tag{2.22}$$

where $N_{O_3}(z)$ is the slant column O_3 above z:

$$N_{O_3}(z) = \int_z^{TOA} \frac{[O_3]}{\cos\theta} dz \tag{2.23}$$

where θ is the zenith angle and $[O_3]$ is the density of ozone molecules at height z. In equation 2.21 pressure is used as the vertical coordinate, while in equations 2.22 and 2.23, height is used. When these equations are implemented in the model, the integrals are approximated by summations and the summations are applied over the model levels, each of which has an associated pressure and height value.

For the calculation of J_{O_2}, we consider two wavelength ranges separately, the Schumann-Runge bands between 175 and 205 mm and the Herzberg continuum between 205 and 245mm. The contribution to J_{O_2} from the Schumann-Runge bands we will denote as J_{srb} and that from the Herzberg continuum as J_{hz}.

To calculate J_{hz}, we need to consider the pressure dependence of the oxygen absorption cross-section, which is approximately linear (Yoshino et al. 1988). In addition, when calculating the flux of photons of a certain wavelength reaching a certain depth in the atmosphere, we need to consider both absorption due to the photolysis reactions with O_2 and absorption by ozone.

$$J_{hz}(p) = \int Tr(p)\ F_{TOA}(\lambda)\ \sigma_{O_2}(\lambda, p)\ d\lambda \tag{2.24}$$

where

$$\sigma_{O_2}(\lambda, p) = \sigma_{O_2,0}(\lambda) + p\frac{d\sigma_{O_2}}{dp}(\lambda) \tag{2.25}$$

and

$$Tr(z) = \exp\left(-\sigma_{O_3}(\lambda)N_{O_3}\right)\ \exp\left(-\int_z^{TOA} \sigma_{O_2}(\lambda, p)\ \frac{[O_2]}{\cos\theta}\ dz\right) \tag{2.26}$$

For both J_{O_3} and J_{hz}, the integrals can be reasonably approximated by summations in the model. However, for J_{srb}, the absorption cross-sections are highly dependent on wavelength such that a very high spectral resolution would be required. To avoid this, we use the parameterisation of Minschwaner et al. (1993).

$$J_{srb}(p) = \sum_{i=1}^{15} F_{TOA,i}\ \Delta\lambda_i\ Tr_{O_3,i}\ \sum_{j=1}^{6} \sigma_{i,j} \exp(-\sigma_{i,j}N_{O_2})W_j \tag{2.27}$$

where N_{O_2} is the slant column diatomic oxygen above the pressure level p, and W_j is a weighting factor. For each of 15 wavelength intervals $\Delta\lambda_i$, the solar flux and ozone transmissivity are represented by mean values, $F_{TOA,i}$ and $Tr_{O_3,i}$. The wavelength interval is then split into 6 subintervals according to the value of the oxygen cross-section. Each of

these subintervals is represented by its median cross-section $\sigma_{i,j}$ and a weighting factor W_j for its width.

The data for the parameterisation of J_{srb} can be obtained by contacting Minschwaner. The sources for data for the non-parameterised part are WMO Report No 16: Atmospheric Ozone (1985) for wavelength and top-of-atmosphere flux data and JPL Evaluation 18 (Chemical Kinetics and Photochemical Data for Use in Atmospheric Studies) for cross-section data and as a reference for the quantum yield, which we always take as 1.

2.2.4 Odd oxygen recombination

Odd oxygen can be removed from the atmosphere by the reaction

$$k3 : \mathrm{O_3} + \mathrm{O} \rightarrow 2\mathrm{O_2} \tag{2.28}$$

There are also other reactions between odd oxygen species, but these are of second order importance and are neglected here.

2.2.5 Sink from nitrogen oxide family

The NO_x family partitioning chemistry is based on:

$$b3 : \mathrm{NO_2} + \mathrm{O} \rightarrow \mathrm{NO} + \mathrm{O_2} \tag{2.29}$$

$$b4 : \mathrm{NO} + \mathrm{O_3} \rightarrow \mathrm{NO_2} + \mathrm{O_2} \tag{2.30}$$

Assuming steady state, then

$$\frac{[\mathrm{NO}]}{[\mathrm{NO_2}]} = \frac{b3\ [\mathrm{O}]}{b4\ [\mathrm{O_3}]} \tag{2.31}$$

The loss of O_x due to NO_x is:

$$b4\ [\mathrm{NO}][\mathrm{O_3}] + b3\ [\mathrm{NO_2}][\mathrm{O}] \tag{2.32}$$

We do not include the photolysis reaction of $\mathrm{NO_2}$ to NO, which produces odd oxygen:

$$J_{\mathrm{NO_2}} : \mathrm{NO_2} + h\nu\,(\lambda < 405\,\mathrm{nm}) \rightarrow \mathrm{NO} + \mathrm{O} \tag{2.33}$$

Excluding this means that NO levels are lower during daytime, but at high altitudes they're already dominant (NO_x = NO) during daytime, so this is really just an effect at lower altitudes where O concentrations are in any case low.

2.2.6 Sink from hydrogen oxide family

The following reactions involving members of the HO_x family are included, both in the partitioning of HO_x into OH and $\mathrm{HO_2}$ and for the destruction of odd oxygen.

$$a5 : \mathrm{OH} + \mathrm{O} \rightarrow \mathrm{O_2} + \mathrm{H} \tag{2.34}$$

$$a7 : \mathrm{HO_2} + \mathrm{O} \rightarrow \mathrm{O_2} + \mathrm{OH} \tag{2.35}$$

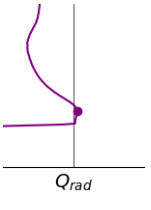

$$a6 : \mathrm{OH} + \mathrm{O_3} \rightarrow \mathrm{O_2} + \mathrm{HO_2} \tag{2.36}$$

$$a6b : \mathrm{HO_2} + \mathrm{O_3} \rightarrow 2\mathrm{O_2} + \mathrm{OH} \tag{2.37}$$

The first two are important in the upper stratosphere, while the third and forth are important in the middle and lower stratosphere respectively.

These reactions convert one member of the OH to HO_2 and vice versa, but do not actually create or destroy HO_x. HO_x is created via photolysis reactions, mainly from H_2O. The lifetime of HO_x in the stratosphere is around 20 minutes (figure 5.27 of Brasseur and Solomon (2005)), so during nighttime there is very little HO_x. For simplicity, we do not include the photolysis reactions that create HO_x, but simply specify a HO_x profile. At night, we assume there is no HO_x and during the day we take the mean daytime profile, calculated as twice the diurnal profile of $OH + HO_2$. For the partitioning, we make the assumption that OH and HO_2 are in chemical equilibrium, which is reasonable as their lifetimes are short (on the order of seconds).

The rate coefficients, $a5$, $a7$, $a6$ and $a6b$ are from the JPL Evaluation 18.

Other reactions (e.g., including CO and NO) are neglected, and we also neglect atomic hydrogen, which destroys ozone and would affect the HO_x partitioning ($HO_x = OH + HO_2 + H$). H only becomes important in the upper stratosphere and mesosphere.

2.3 Agatha and konrad

For simplicity and consistency, when konrad and Agatha are run together, they both use the same vertical grid (as described in section 2.1) and the same timestep of 15 minutes, together with a diurnal cycle of insolation. [2] Konrad provides the temperature profile and time (zenith angle) as input for Agatha and Agatha provides the ozone profile as input for konrad. However, this is the only exchange between the models, so for example the amount of radiation absorbed in the photolysis reactions in Agatha does not affect the heating rates in konrad. This may seem inconsistent, but it is the standard approach in most chemistry climate models, as Agatha requires a higher spectral resolution for some wavelength ranges than konrad, where an increased resolution would be computationally costly. Another example is that the HO_x profile in Agatha is independent of the stratospheric water vapour amount in konrad, which increases as the cold point warms. Likewise we do not consider methane or N_2O emissions, both of which would also enhance ozone destruction in the stratosphere (via the production of HO_x and NO_x respectively).

Another difficulty of using Agatha is the need to include an ozone transport term and this is one of the main contributors to the ozone profile in the lower stratosphere. In combination with konrad, we only consider vertical motion, under the assumption that horizontal mixing of air is negligible. Large scale horizontal transport out of the tropics towards mid latitudes can be neglected as it does not change the mixing ratio of ozone; it only affects the total amount of air, which is compensated for by the upward transport. Thus, we only consider the large scale upwelling, but as described in section 1.3.2, it is not clear exactly how the Brewer-Dobson circulation responds to global warming (or other forcings). In section 3.1.9, we keep the upwelling velocity fixed and therefore underestimate the change in lower stratospheric

[2] It would be more computationally efficient to run konrad using a reduced temporal resolution, but keeping the high temporal resolution for Agatha. This is because RRTMG, used by konrad, is much more computationally expensive than Agatha, and moreover the mean radiative heating rates can be accurately calculated using a constant insolation and the diurnal mean ozone profile (as in most experiments in this thesis). On the other hand, a diurnal cycle of radiation is required for Agatha to accurately reproduce the mean ozone profile, but diurnal variations in temperature have a relatively small impact and could be neglected. If further experiments were to be done, it would be advisable to combine Agatha and konrad in such a way that diurnal mean profiles and values are used for konrad, while a higher temporal resolution and diurnal cycle of insolation are used for Agatha.

ozone. Similar to the upwelling induced cooling term (equation 2.9), the transport tendency is calculated as

$$\frac{\partial \mathrm{O}_3}{\partial t} = -w_{up} \frac{\partial \mathrm{O}_3}{\partial z} \tag{2.38}$$

where t is time, w_{up} is a prescribed upwelling velocity, O_3 is the ozone concentration (volume mixing ratio) and z is altitude. For most experiments, to be physically consistent, we choose an upwelling velocity that is the same for both the adiabatic cooling term and the ozone transport term.

Finally, when using Agatha iteratively, we not only need to consider ozone transport, but also the tropospheric concentration of ozone (as Agatha does not model tropospheric chemistry). As such, we set a minimum ozone concentration of 40 ppbv, following Charlesworth (2017) and in accordance with observed values.

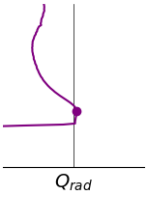

Chapter 3

Changing the atmosphere

Sections 3.1.2 to 3.1.6 as well as most of sections 3.1.1, 3.1.8 and 3.2 have been published in the Journal of Climate (Dacie et al., 2019). I would like to thank my coauthors and the reviewers of that publication for their assistance and insights, which helped strengthen this work.

This chapter contains the experiments we performed with konrad and Agatha, investigating the influence of various factors on the TTL and surface climate, as well as how those factors interact with each other.

3.1 Idealised experiments

3.1.1 Comparison of convective adjustment methods

Here we briefly compare how our relaxed convective adjustment (section 2.1.2) compares to the well known hard adjustment (section 2.1.1) when no other perturbations are applied. The relaxed convective adjustment gives rise to a cooling around the TTL (see the top row of figure 3.1), as expected from following the moist adiabatic lapse rate. In our standard set-up, our choice of $\tau(p)$ (equation 2.8) produces an equilibrium cold point temperature of 200.1 K, 1.2 K colder than that for the hard adjustment and a surface temperature of 297.7 K, 0.2 K colder than the hard adjustment. The slight decrease in surface temperature arises due to the decrease in humidity in the stratosphere, TTL and upper troposphere (associated with the decrease in temperatures there) and the corresponding reduction in the greenhouse effect.

With our definition of τ (equation 2.8), the convective cooling above the level of neutral buoyancy is larger when that level occurs at larger pressures. Under warming, the level of neutral buoyancy occurs at a lower pressure where the convective timescale is larger, leading to very little convective cooling and an unrealistic temperature lapse rate in the upper troposphere (as shown in the bottom panels of figure 3.1, where the surface temperature is so high that also the mid troposphere is badly represented). As emphasised in section 2.1.2, with the relaxed adjustment we are not aiming to perfectly reproduce tropical temperature profiles under all scenarios, but rather to provide a comparison to the hard adjustment, allowing us to investigate the influence of convection in the experiments in the rest of this chapter.

3.1.2 Increasing carbon dioxide

In this section, we study the effect of changing the CO_2 concentration on the TTL. Standard runs are performed with 348 ppmv CO_2 (the standard value for the proposed RCEMIP, Wing et al., 2018) and in these sensitivity experiments we use values in the range [0.25, 4] times this amount.

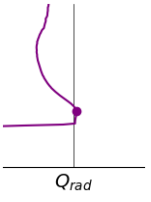

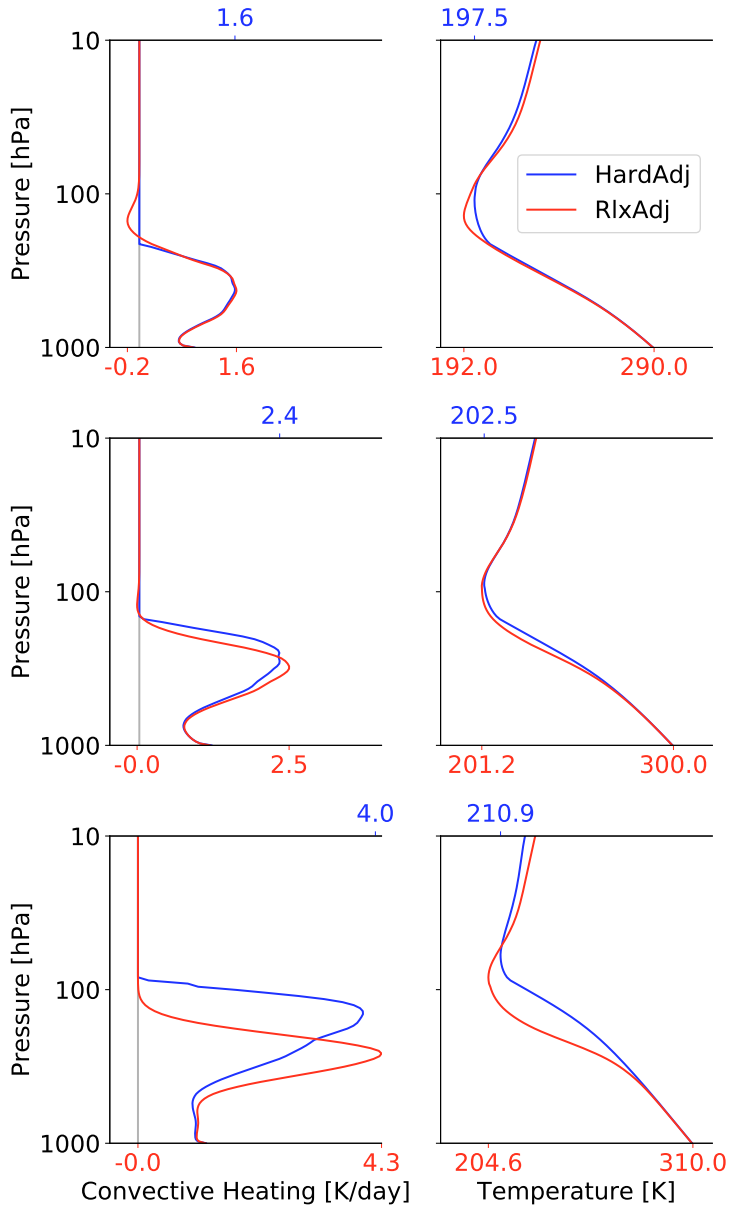

Figure 3.1: Convective heating rate and temperature profiles for the hard (blue) and relaxed (red) convective adjustments with surface temperatures fixed at 290 K (top row), 300 K (middle row) and 310 K (bottom row). Surface and cold point temperatures are indicated, as are minimum and maximum convective heating rates.

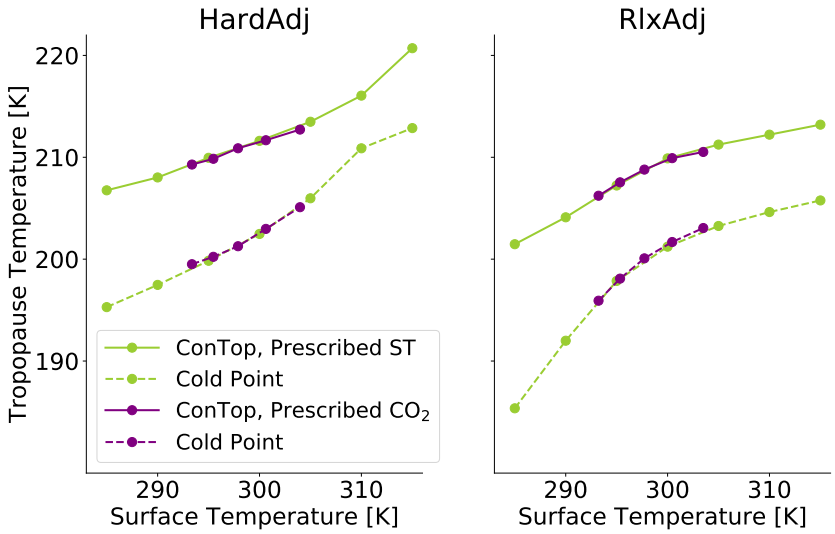

Figure 3.2: Temperature of the convective top (solid) and the cold point (dashed) plotted against the surface temperature. Changes in TTL temperature and structure due to CO_2 changes (dark purple) are very similar to those found when simply fixing the surface temperature at higher values (pale green).

Performing runs with a fixed surface temperature we see little change in the temperature, height or shape of the TTL (not shown), in agreement with Thuburn and Craig (2002) and Fu et al. (2018), who used a hard convective adjustment to a lapse rate of $6.5\,\mathrm{K\,km^{-1}}$. This is the case for both our hard convective adjustment and our relaxed adjustment.

In contrast, if we allow the surface temperature to change, an increase in CO_2 concentration produces an increase in temperature and height of both the convective top (as shown by Kluft et al., 2019) and the cold point. We perform additional experiments with a fixed CO_2 concentration and a fixed surface temperature and use a different surface temperature for each run. We see a very similar response of TTL temperatures to increasing surface temperature as to increasing CO_2 concentration (figure 3.2). This suggests that at equilibrium TTL temperatures are intrinsically linked to surface and tropospheric temperatures. For other scenarios, such as when a Brewer-Dobson-like dynamical cooling term is applied, an increase in CO_2 has a different effect on TTL temperatures than an equivalent increase in surface temperature (section 3.1.5).

In the relaxed convective adjustment case, the upper troposphere and TTL is colder than in the hard adjustment case, as discussed in section 2.1. Additionally, the changes in cold point temperature with surface temperature change are larger in the relaxed adjustment case for temperatures in the range $[285,\ 300]\,\mathrm{K}$. A warming climate produces a rising TTL, and as the TTL rises, convective cooling becomes weaker, (compare the negative convective heating values in the upper left and middle left panels of figure 3.1), leading to a stronger warming of the TTL compared to the hard adjustment case. This effect is not so strong for the convective top, due to its definition at a fixed convective heating rate (section 2.1.5). Conversely, for higher surface temperatures, $[300,\ 315]\,\mathrm{K}$, the changes in convective top and cold point temperature are smaller in the relaxed than the hard adjustment case. In this temperature range, the longwave cooling is stronger and the troposphere is deeper, so with further increases in surface temperature the convective warming becomes less and less effective at balancing the net radiative cooling in the upper troposphere. This causes the temperature profiles to deviate strongly from the moist adiabat (lower two rows of figure

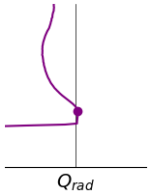

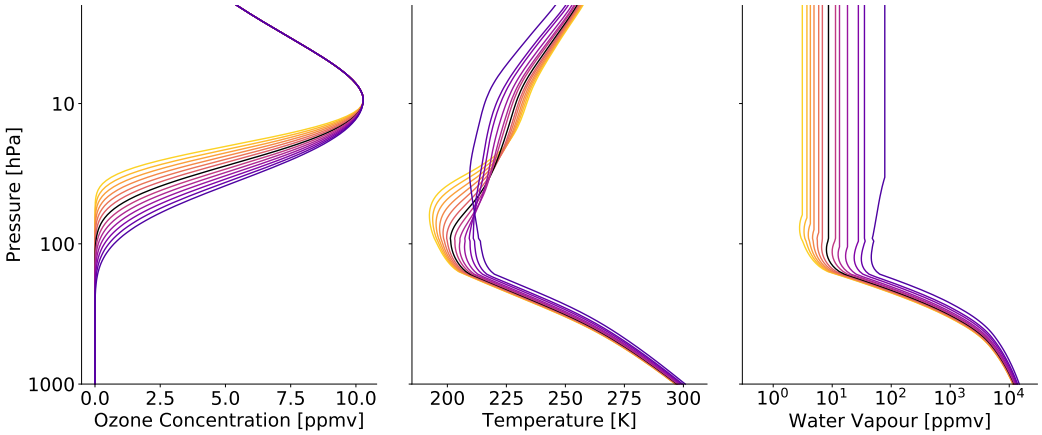

Figure 3.3: Artificial changes to the ozone concentration profile (left) and the corresponding changes to the temperature and water vapour profiles for the hard convective adjustment case. The black lines indicate the standard profiles, and the yellow correspond to an upward shift in the ozone profile, as might be expected under global warming.

3.1), with radiation acting to cool the upper troposphere. This results in a cooler TTL than if convection were very efficient (adjusting strictly to the moist adiabatic lapse rate as in the hard adjustment case). We conclude that the assumptions relating to the convective adjustment strongly influence the structure of the TTL and its response to warming.

3.1.3 Ozone profile changes

In this set of experiments, we prescribe a variety of idealised ozone profiles, which have been shifted with respect to our standard profile from Wing et al. (2018) (figure 3.3). An upward shifted profile could be expected under global warming as the troposphere expands, and this effect would be enhanced if the Brewer-Dobson circulation strengthens, bringing more ozone-poor air upwards. We apply a range of perturbations to the ozone profile, some of which are much larger than what might be expected in a $4 \times CO_2$ scenario (see section 3.1.8), to improve our understanding. We also consider the opposite cases, in which the ozone profile is shifted downwards, unrealistically allowing ozone rich air into the upper troposphere. The temperature and humidity profiles which result from shifting the ozone profile are also shown in figure 3.3. These experiments are similar to the runs of Birner and Charlesworth (2017), Thuburn and Craig (2002) and McElroy et al. (1992) and indeed our results are similar to theirs for the TTL. Both the convective top and the cold point increase in height and decrease in temperature when the ozone profile is shifted upwards, due to a reduction of radiative heating in this region (approximately in the range $[200,\ 10]$ hPa). The TTL changes are almost the same for the runs with fixed surface temperature (not shown) and those with variable surface temperature. Qualitatively similar results were found for the hard and relaxed convective adjustment cases.

We also investigate the effect that shifting the ozone profile has on the surface temperature (figure 3.4) and find that a downward shifted ozone profile is associated with an increase in surface temperature and an upward shifted profile with a somewhat smaller decrease. Our surface temperature changes are larger than those of McElroy et al. (1992), which is somewhat surprising given the similarities in the model set-up and the additional lapse rate feedback in our model which acts to weaken the surface temperature response.

We expected that the solar insolation may play a role in the strength of the response to changes in the ozone profile, so we test this in runs with an applied constant heat sink at the surface such that the reference climate remains approximately constant. With a stronger

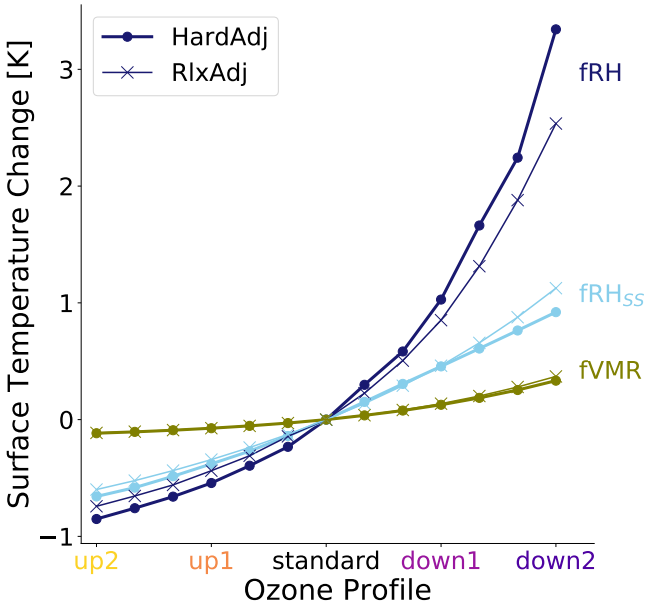

Figure 3.4: Surface temperature changes corresponding to artificially shifted ozone profiles, with negative surface temperature changes on the left corresponding to an upward shift (yellow in figure 3.3) and positive temperature changes on the right to a downward shift (purple in figure 3.3). Dots and crosses correspond to experiments with the hard convective adjustment (HardAdj) and the relaxed adjustment (RlxAdj) respectively. The different colours of the lines and markers are for the different treatment of water vapour. The standard treatment, with fixed relative humidity in the troposphere and stratospheric humidity set by the cold point, is indicated by fRH. Runs with fixed relative humidity in the troposphere but a constant specified stratospheric water vapour mixing ratio are labeled as fRH$_{SS}$. Runs with a fixed water vapour volume mixing ratio at each pressure level throughout the column are labeled as fVMR.

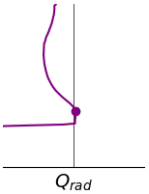

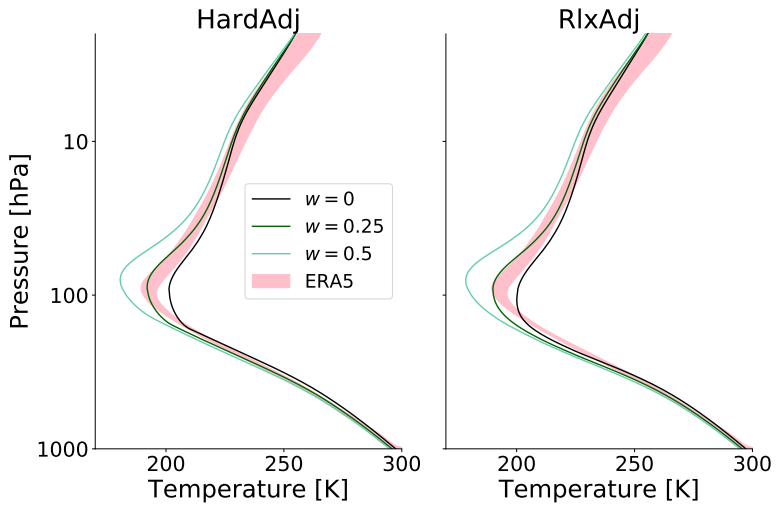

Figure 3.5: Temperature profiles for runs with different stratospheric upwelling velocities. The standard set-up with no upwelling is shown in black and runs with upwelling velocities of 0.25 and 0.5 mm s^{-1} are shown in dark and light green respectively. Pink shading shows ERA5 reanalysis data within one standard deviation of the mean tropical temperature profile.

insolation, shortwave heating increases, especially around the stratopause. However, we find little difference in the tropopause and surface/tropospheric temperature response to ozone, suggesting that ozone induced changes occur through longwave heating changes.

In our model, we find that the surface temperature changes due to the radiative effects of ozone alone are small (fVMR in figure 3.4), but that these are amplified by the water vapour response by a factor between 4.8 and 7.9 for the upward shifted profiles and up to 10.0 for the downward shifted profiles (compare fRH and fVMR in figure 3.4). Cooling of TTL temperatures due to an upward shift in the ozone profile (discussed above) leads to a reduction in water vapour content of the air in this region (figure 3.3). This acts to both reduce the greenhouse effect and to destabilise the TTL and upper troposphere, leading to increased convection, both of which produce surface cooling. Tropospheric temperatures also cool and this causes a reduction in tropospheric water vapour, which further reduces the surface temperature.

3.1.4 Upwelling

Birner and Charlesworth (2017) found that their RCE model overestimated TTL temperatures by up to $\sim$ 15 K when no dynamical stratospheric cooling was applied (see for example their figure 3). With a cooling term corresponding to an upwelling velocity of 0.5 mm s^{-1} everywhere above the convective top, mimicking the Brewer-Dobson circulation, they found temperatures much closer to those observed (their figure 11). Following the implementation of Birner and Charlesworth (2017) (described in section 2.1.3), We repeat their experiments with two different upwelling velocities: 0.25 mm s^{-1}, which is close to estimates of upwelling velocities from reanalysis (Abalos et al., 2015) between $\sim$100 hPa and 30 hPa, and a stronger value of 0.5 mm s^{-1}. Additionally, we study how the upwelling affects surface temperature.

As shown in figure 3.5 and found by Birner and Charlesworth (2017), including a dynamical cooling term reduces TTL temperatures, and makes the cold point sharper. Although the cooling is applied everywhere above the convective top, it mainly affects the TTL region and lower stratosphere, as above radiative heating is very efficient at

		Cold Point		ConTop		Surface	
$w = 0.25$	fRH	-9.3	-10.1	-6.0	-5.4	-1.5	-1.5
	fVMR	-10.1	-10.3	-3.8	-4.0	-0.3	-0.3
$w = 0.5$	fRH	-20.7	-21.7	-11.2	-9.6	-2.5	-2.5
	fVMR	-19.2	-20.2	-6.6	-6.9	-0.4	-0.5

Table 3.1: Temperature changes [K] associated with different upwelling velocities [mm s^{-1}], compared to the case with no upwelling. Values for the hard adjustment are given in blue, and those for the relaxed adjustment in red font. Results are shown for both runs with fixed tropospheric relative humidity (fRH) and runs with fixed water vapour mixing ratio (fVMR).

maintaining the atmosphere near radiative equilibrium.

Larger upwelling velocities also act to cool the modeled tropical surface and troposphere, and as for ozone profile effects on the surface (section 3.1.3), these changes occur mainly through changes in water vapour content (table 3.1). The applied upwelling acts to lift the TTL, as well as to cool it. While a cooling of the TTL would be associated with a cooler troposphere and surface (due to their connection via the specified lapse rate), a higher TTL leads to a warmer troposphere and surface (following the same reasoning). For the fVMR cases studied here, the two factors almost cancel and the surface temperature changes little. When water vapour is allowed to vary, a cooling of the TTL (and therefore also troposphere and surface) would be associated with a drying of the whole atmospheric column. On the other hand, a lifting of the cold point to a lower pressure leads to an increase in stratospheric water vapour, as the conversion from relative humidity (fixed at 0.4) depends on pressure. This leads to a slight warming of the cold point in the fRH case compared to the fVMR case. For the convective top and surface temperatures, the decrease in tropospheric humidity has a larger affect than the increase in stratospheric humidity, leading to a much larger cooling for fRH than fVMR.

To summarise, there are two main competing factors affecting the surface temperature in the fRH case: a warming due to an increase in altitude of the TTL and the requirement to follow the moist adiabatic lapse rate in the troposphere, and a cooling due to the decrease in temperature of TTL and the associated reduction in water vapour content.

3.1.5 Combined effects

It is also of interest to study combined cases, for example an increase in CO_2 together with an upward shifted ozone profile. One might naively assume that the total effect would be the sum of the individual effects, and if this were the case we could say that the factors act independently of each other. In this section, we investigate whether and under which conditions such a summation provides a good prediction for the combined effect.

Figure 3.6 shows the combined effect of a change in CO_2 concentration and a shifted ozone profile. The predicted trends (dashed), calculated by summation of the temperature changes found in section 3.1.2 and 3.1.3, are close to the temperature changes for runs where both factors are changed simultaneously (coloured solid lines) in some parts of the parameter space. Similar results are found for the interaction between CO_2 and ozone also for cases with applied stratospheric upwelling velocities of 0.25 and 0.5 mm s^{-1} (not shown). However, there are some extreme cases (seen in all three upwelling scenarios), where the effects of ozone and CO_2 cannot be considered independent. One such example is the cold point temperature for a strongly downward shifted ozone profile and an increase in CO_2 in both the hard and relaxed adjustment cases (figure 3.6(a)). The cooler stratosphere associated with an increase in CO_2 leads to a less distinct TTL region, and when the ozone profile is simultaneously shifted downwards, the resultant warming beneath the cold point causes it to jump to a significantly higher altitude.

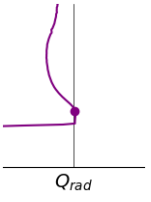

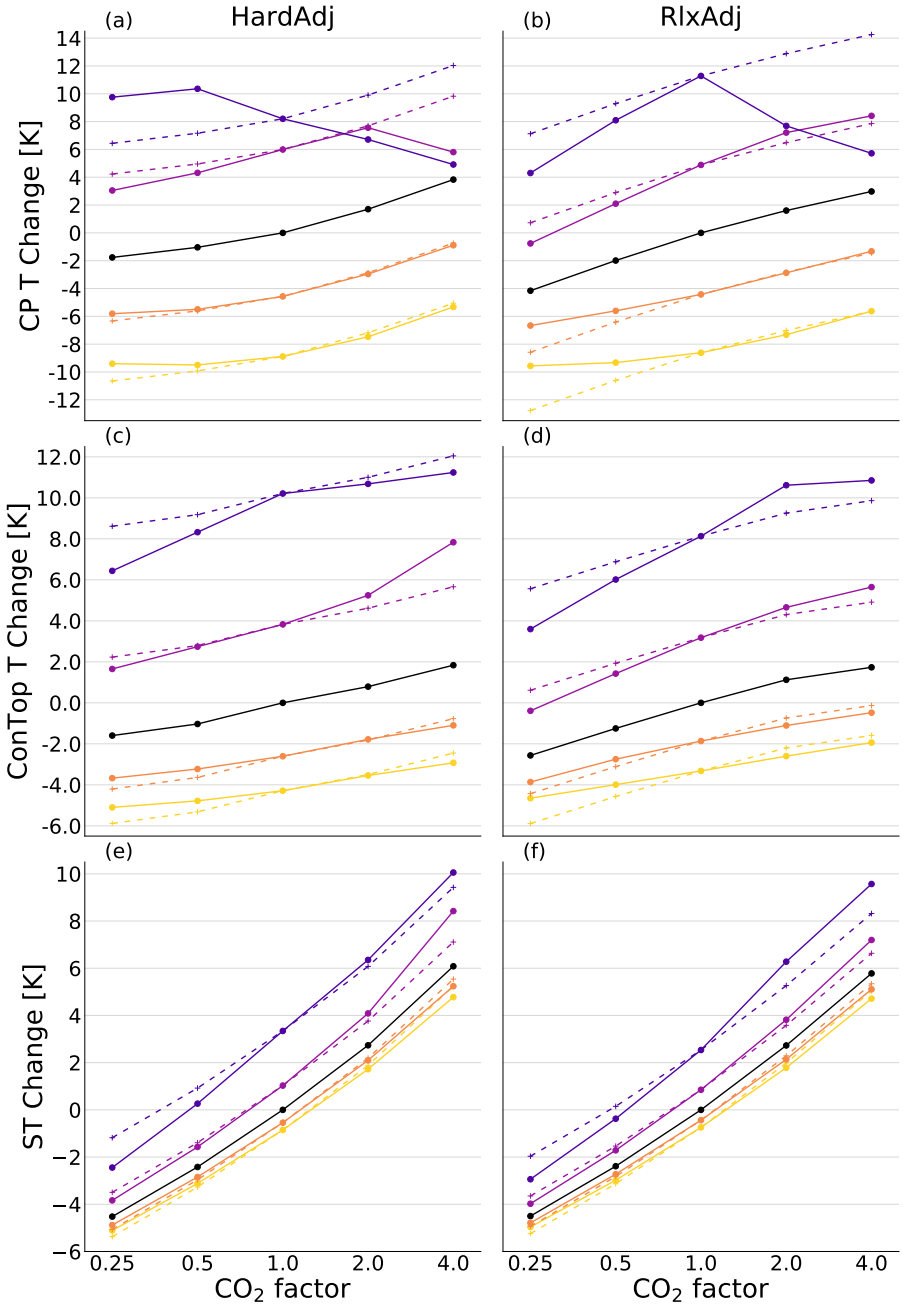

Figure 3.6: Cold point (top row), convective top (middle row) and surface (bottom row) temperature changes with increasing CO_2 and different ozone profiles. The ozone profile used is indicated by the color, with black representing the standard profile, pink and purple representing downward shifted profiles (those indicated as down1 and down2 in figure 3.4) and orange and yellow representing upward shifted profiles (up1 and up2 respectively). Results for the set-up with the hard convective adjustment are shown on the left, and those with the relaxed convective adjustment on the right. Dashed lines and crosses show the predicted behaviour assuming additivity and solid lines and dots show the actual behaviour.

	Cold Point		ConTop		Surface	
$w = 0$	1.7	1.6	0.8	1.1	2.7	2.7
$w = 0.25$	3.6	3.4	1.4	1.2	2.8	2.6
$w = 0.5$	4.9	4.0	1.8	0.9	2.7	2.5

Table 3.2: Temperature changes [K] associated with a doubling of CO_2 (696 ppmv compared to 348 ppmv) for different upwelling velocities [mm s^{-1}]. Values for the hard adjustment are given in blue, and those for the relaxed adjustment in red font.

	Cold Point		ConTop		Surface	
$w = 0$	-4.6	-4.4	-2.6	-1.9	-0.5	-0.4
$w = 0.25$	-7.0	-6.4	-2.4	-1.8	-0.3	-0.3
$w = 0.5$	-8.4	-8.6	-2.3	-1.6	-0.1	-0.1

Table 3.3: Temperature changes [K] associated with an upward shift of the ozone profile (up1 from figure 3.4) for different upwelling velocities [mm s^{-1}]. Values for the hard adjustment are given in blue, and those for the relaxed adjustment in red.

There are also notable differences in convective top temperature trends for the relaxed adjustment case, namely that the sensitivity to ozone depends on CO_2 concentration (the solid lines in figure 3.6(d) diverge with increasing CO_2). For a larger CO_2 concentration, the convective top is at a lower pressure (higher altitude), where the ozone changes are more significant than at higher pressures where ozone concentrations are always low.

The assumption of additivity is quite good for the surface temperature (bottom panels of figure 3.6), where the predicted behaviour (dashed) closely matches the actual behaviour (solid). In other words, the effect of CO_2 on surface temperature is nearly independent of the prescribed ozone profile.

Likewise, we find that surface temperature changes due to changes in CO_2 concentration are almost independent of the applied stratospheric dynamical cooling term (table 3.2). Conversely, the upwelling term significantly alters cold point temperature trends with changing CO_2 concentration or shifting the ozone profile (tables 3.2 and 3.3). The warming of the cold point corresponding to a doubling of CO_2 increases for larger upwelling velocities, and there are two main processes contributing to this. One can be explained through an alteration of the relationship between surface temperature and TTL temperature when an upwelling is applied. To balance an increase in upwelling longwave radiation from below, a colder tropopause layer must undergo a larger increase in temperature than a tropopause layer which is initially warmer. The other is related to the calculation of the cooling term associated with the upwelling, which depends on the temperature gradient. By cooling the stratosphere, CO_2 reduces the temperature gradient particularly in the lower stratosphere and this reduces the adiabatic cooling term there (equation 2.9). Reduction in this cooling term produces an apparent warming just above the cold point, which then leads to an additional warming of the cold point through radiative transfer. For these cases, there is an influence of CO_2 induced stratospheric cooling on the cold point temperature, unlike in the case with no upwelling where the cold point temperature is found to depend almost exclusively on surface temperature (figure 3.2).

The cold point sensitivity to an upward shift in the ozone profile increases under stronger upwelling velocities (table 3.3). The upwelling lofts the cold point, bringing it closer to the large ozone gradient, where larger changes in ozone concentration occur when a vertical shift to the profile is applied. A second contribution comes from the increase in longwave heating by ozone at colder temperatures, so any changes in ozone concentration have a larger impact. However, the colder TTL produced when an upwelling is applied contains less water vapour, so changes in the ozone profile are associated with relatively small changes in water vapour concentration. As most of the ozone effect on the surface is through water

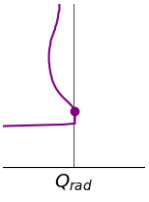

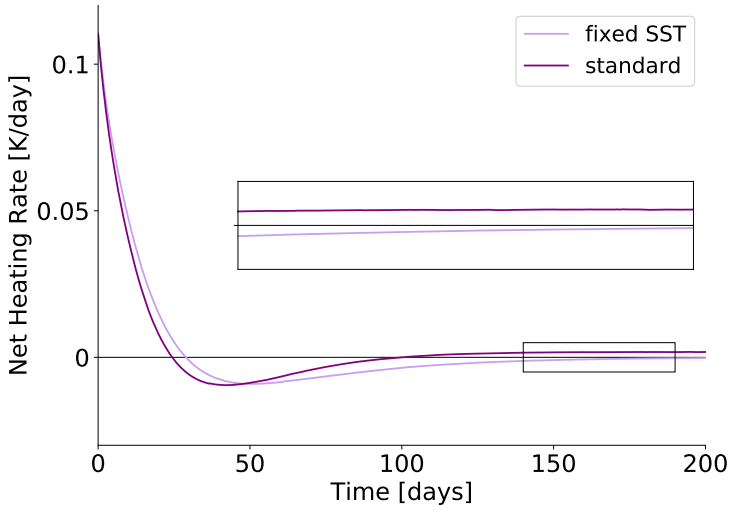

Figure 3.7: Net radiative heating rates at the cold point after a $4 \times CO_2$ perturbation and their evolution with time for two different model set-ups.

vapour changes (figure 3.4), the surface sensitivity to ozone decreases for cases with strong upwelling velocities.

In summary, ozone and CO_2 act almost independently of each other for some parts of the parameter space tested, but in other parts, the assumption of additivity is a bad one. Likewise, using a different upwelling velocity in the model affects the response of the column atmosphere to changes in our prescribed ozone and CO_2 concentrations.

3.1.6 Temporal evolution of the cold point

In this section, we investigate how the system evolves over time and how initial responses relate to equilibrium states. When considering a local temperature response to an instantaneous forcing (*e.g.* a CO_2 perturbation), it is important to keep in mind that the entire column can adjust and therefore that the local temperature response at a later time cannot necessarily be inferred from the initial heating rate at that location. If the temperature initially responds by warming, one might assume that it continues warming, albeit at a slower rate, until equilibrium is reached. Likewise, if it cools, one might assume that it continues cooling until equilibrium is reached. By making such an assumption, the column response is considered of little or no importance for the local response. This proves reasonable for the surface in our 1D model, which, after a positive radiative forcing is applied, warms slowly and with a rate of warming that decreases towards zero as the forcing decreases towards zero. Here we investigate whether such an assumption is also appropriate for the tropopause, by studying the specific case of cold point evolution under an instantaneous CO_2 perturbation.

Two sets of experiments are used, one with the standard set-up, hard convective adjustment and CO_2 prescribed at 0.25, 0.5, 2 or 4 times our standard concentration (348 ppmv), and another set where we fix the surface temperature and the absolute humidity. In the second set of experiments, the only variable that can change is temperature and this is fixed in the troposphere due to the fixed surface temperature and our hard convective adjustment. The runs are initialised using the equilibrium state of the standard $1 \times CO_2$ run. Figure 3.7 shows the evolution of the net radiative heating rate at the cold point for the $4 \times CO_2$ runs. In all these experiments, the net radiative heating

rate translates directly into a subsequent change in temperature of the cold point, as there is no upwelling and also no convection affecting the temperature at this altitude.

With increased CO_2, we find a net positive heating rate at the cold point for the first $\sim$ 30 model days. This is in agreement with the results of Lin et al. (2017), who calculated radiative heating rates for a single tropical mean temperature profile under a variety of CO_2 concentrations. However, as the temperature profile evolves and the stratosphere cools, the heating rate anomaly at the cold point decreases, becoming negative, before increasing again towards zero as the simulation reaches equilibrium. As the stratosphere cools, the net radiative forcing on the tropopause decreases and the initial positive temperature perturbation reduces. With decreased CO_2 the opposite evolution is found (not shown), namely an initial cooling and a subsequent warming as the stratosphere warms.

Both sets of experiments show a similar evolution during the first approximately 100 model days, suggesting that changes in TTL and stratospheric temperatures are responsible for the early evolution, while changes in humidity or surface and tropospheric temperatures have little influence. The initial warming and subsequent cooling approximately cancel and the cold point temperature after approximately 100 days is almost the same as the initial cold point temperature. This contradicts the assumption that an initial warming leads to a warmer temperature at any later time in the evolution compared to the initial state.

Differences between the two sets of experiments only occur during the later evolution (zoom box of figure 3.7), where in the fixed surface temperature case, the net heating rate at the cold point quickly reaches zero, but when the surface temperature is allowed to change, the cold point warms slowly as the surface warms, until both the surface and the cold point eventually reach equilibrium (not shown). The relationship between surface temperature and tropopause temperature found in section 3.1.2 only holds after the initial adjustment period, while during the initial adjustment time the influence of the stratosphere must be taken into account.

3.1.7 A high cloud

In these experiments we include a high cloud, as described in section 2.1.4. We first discuss the influence of the cloud on the TTL and surface compared to the clear sky case. The cloud produces a positive atmospheric cloud radiative effect (defined as the difference between all sky and clear sky net radiative heating rates) in the upper troposphere of the same order of magnitude as that found in the observational study of Fu et al. (2018). This leads to a warming of the convective top, that is approximately the same regardless of whether the surface is allowed to warm or kept fixed (table 3.4). When the surface is allowed to warm, the greenhouse effect of the cloud leads to a surface warming of around 3 K. Tropospheric temperatures are strongly tied to the surface by the moist adiabat, particularly in the hard convective adjustment case, so changes in the convective top temperature occur either with a change in surface temperature or with a change in pressure of the convective top. When the surface temperature is fixed, the warming of the convective top is associated with an increase in pressure of the convective top, equivalent to a decrease in altitude of around 1 km. However, when the surface temperature is allowed to warm, the cloud produces surface and tropospheric warming and tropospheric expansion, causing the convective top to rise slightly as well as warm. This leads to an upward shift and warming of the cold point, which is not seen in the fixed surface temperature case.

Trends in convective top temperature with surface temperature are much noisier in the cloudy case than the clear sky case, as even at equilibrium the convective top and cloud location oscillate between discrete model levels, but despite this we can still identify trends. As for the clear sky case (figure 3.2), when no upwelling is applied, the changes in cloudy convective top and cold point temperature per degree of surface warming in runs with increased CO_2 concentrations are approximately equivalent to those trends found from experiments with a range of prescribed surface temperature and no change in CO_2

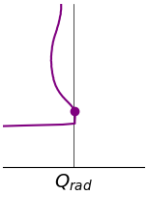

	Cold Point		ConTop		Surface	
standard	1.6	2.1	9.9	8.4	3.1	3.4
fixed ST	-0.2	0.1	9.4	7.5		

Table 3.4: Temperature changes [K] after the addition of a high cloud compared to clear sky equilibrium. Values for the hard adjustment are given in blue, and those for the relaxed adjustment in red.

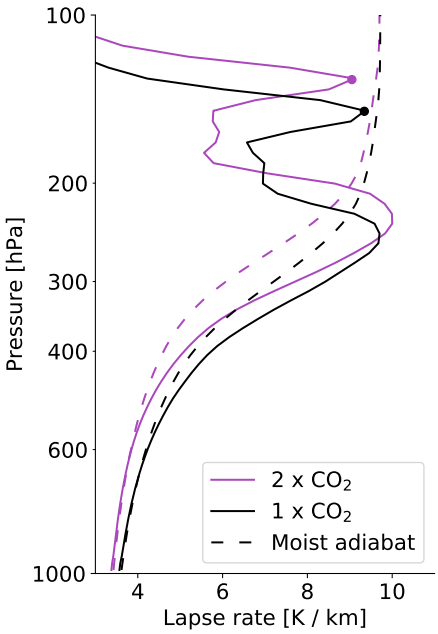

Figure 3.8: Profiles of the temperature lapse rate for the 1 and $2 \times CO_2$ relaxed convective adjustment cases (solid lines, black and purple respectively). Dots indicate the convective top. For comparison, the moist adiabat is shown for each case (dashed).

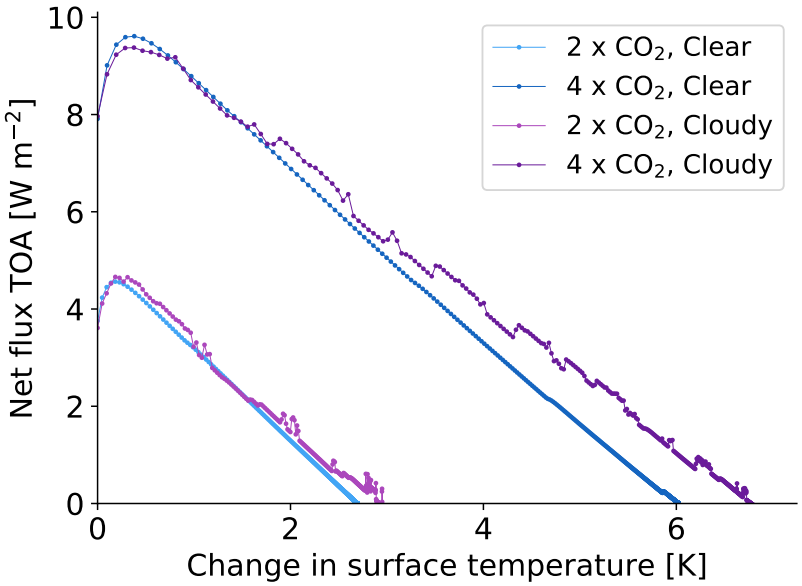

Figure 3.9: A Gregory plot showing the evolution of the surface temperature with the net radiative flux at the top of the atmosphere (TOA) in the instantaneous 2 and $4 \times CO_2$ experiments with and without cloud for the hard convective adjustment and with no upwelling.

concentration. In other words the direct radiative effect of CO_2 does not significantly impact the cloud radiative effect. On the other hand, with surface warming, the cloud radiative effect increases, as the difference between surface temperature and cloud temperature increases. However, this has little effect on the convective top temperature trends in the hard adjustment case, as the convective heating also increases with surface warming, so the convective top is not able to shift further downwards relative to the clear sky case. This, combined with the strong tie between surface temperature and the rest of the troposphere via the lapse rate, means that the convective top temperature trend with surface warming in the cloudy case is approximately the same as for the clear sky case. However, in the relaxed adjustment case, as the troposphere expands with surface warming, the convective heating cannot increase as much as the cloud radiative effect, due to our specification that the convective timescale is longer at lower pressures (equation 2.8). Thus, the convective heating cannot push the convective top upwards as far, so the convective top warms more with surface warming when clouds are present than in the clear sky case.

In the relaxed convective adjustment case, the temperature profile is allowed to deviate from the moist adiabat in the upper troposphere, and the increased radiative heating due to the cloud impacts this. Below the convective top at around 200 hPa, where the cloud is situated, the lapse rate is weaker (in other words the atmosphere is more stable) than the moist adiabat (figure 3.8). This is possible in konrad only because the lapse rate below the cloud, at around 300 hPa is larger than the moist adiabat, such that (by the constraints of the relaxed convective adjustment, section 2.1.2, and the definition of the convective top) upper tropospheric temperatures are not warmer than those found simply by following the moist adiabat upwards from the surface. The same occurs in the clear sky case when the relaxed convective adjustment is used, namely the lapse rate is first larger than the moist adiabat and then smaller than the moist adiabat just below the convective top, but this is much less pronounced than in the cloudy case. Despite the unrealistic implementation of

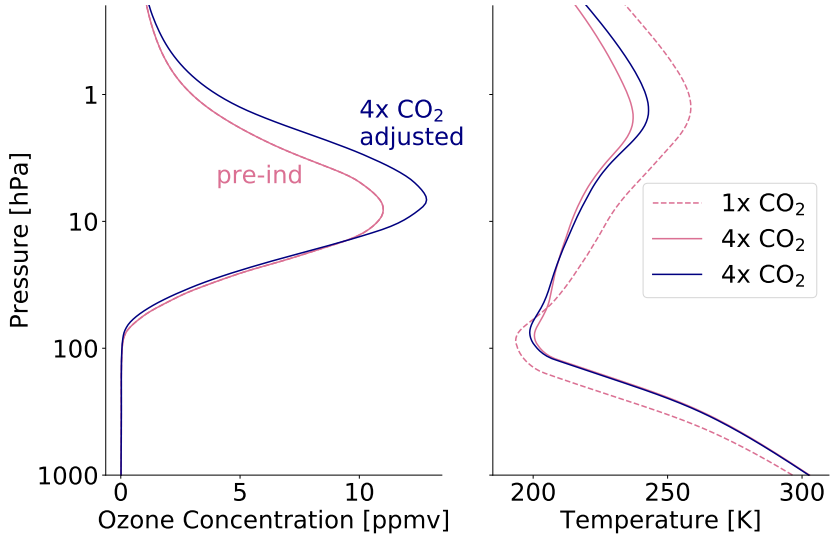

Figure 3.10: Temperature profiles (right) from our 1D RCE when using the ozone profiles (left) from Marsh et al. (2016). The dashed pink temperature profile is from that found for the run with $1 \times CO_2$ and the pre-industrial ozone profile (pink, left panel). The solid pink and blue temperature profiles are from runs with $4 \times CO_2$ and the ozone profiles of corresponding colours.

convection and clouds in konrad, this result suggests that radiative effects from high clouds could affect the lapse rate in the upper troposphere such that it is weaker than the moist adiabat.

Finally, we find an increase in surface temperature sensitivity to increasing CO_2 when including cloud, for both the hard and relaxed convective adjustment cases. There is little change in forcing (figure 3.9), presumably due to the cancellation of an increase in forcing due to a warmer background state and larger temperature difference between the surface and upper levels (Huang et al., 2016) and a decrease in forcing due to masking effects of the cloud. Instead, the increase in climate sensitivity comes from a positive cloud feedback (indicated by the difference in slopes between the clear sky and cloudy cases of figure 3.9), in agreement with Zelinka and Hartmann (2010) and explained in section 1.2.4.

3.1.8 Ozone from Chemistry Climate Models

Here we use the tropical mean ozone profiles from the interactive chemistry pre-industrial or reference (367 ppmv CO_2) runs and $4 \times CO_2$ runs of Marsh et al. (2016), Dietmüller et al. (2014) and Nowack et al. (2014) and investigate the differences between the effect of interactive ozone in the three studies and the influence of our model set-up. The two ozone profiles of Marsh et al. (2016) are shown in the left panel of figure 3.10, labeled as pre-ind and $4 \times CO_2$ adjusted respectively. A large increase in ozone concentration is apparent in the upper stratosphere, due to CO_2 induced cooling, but this is not expected to have much impact on tropospheric and TTL temperatures, as the absolute ozone concentrations are small here. In the lower stratosphere, a small upward shift in the ozone profile can be seen (figure 3.11), similar to the idealised ozone profiles of section 3.1.3.

The right panel of figure 3.10 shows the equilibrium temperature profiles produced in our model using the hard convective adjustment and an upwelling velocity of $0.25\,\mathrm{mm\,s^{-1}}$. In this case, the cold point temperature increase when increasing the CO_2 by a factor of 4 and changing the ozone profile from the pre-industrial to the adjusted profile is 5.2 K

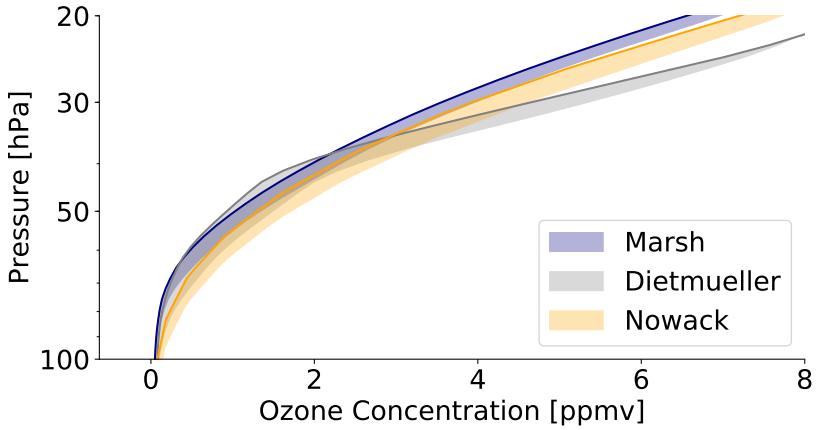

Figure 3.11: Tropical mean lower stratospheric ozone profiles from the coupled chemistry climate models of Marsh et al. (2016), Dietmüller et al. (2014) and Nowack et al. (2014). The solid lines indicate the profiles in the $4 \times CO_2$ scenarios, and the shading shows the change from the $1 \times CO_2$ runs.

	Marsh		Dietmueller		Nowack	
$w = 0.25$	6.3	-0.3	6.5	-0.4	6.6	-0.6
$w = 0$	6.3	-0.4	6.5	-0.6	7.1	-1.1
Manabe RH	4.3	-0.2	4.3	-0.2	4.3	-0.3
a high cloud	7.3	-0.4	7.8	-1.0	8.0	-1.1

Table 3.5: Change in surface temperature [K] under a $4 \times CO_2$ scenario (left) and the change in this [K] when using an ozone profile from a $4 \times CO_2$ simulation compared to the climatology ozone profile (right). Ozone profiles are from the coupled chemistry climate models of Marsh et al. (2016), Dietmüller et al. (2014) and Nowack et al. (2014). Results are shown for three different configurations of our 1D model. The first row includes an upwelling velocity of $0.25\,\mathrm{mm\,s^{-1}}$ and our standard humidity profile. The second row neglects the upwelling and the third both neglects upwelling and uses the relative humidity profile from Manabe and Wetherald (1967) and Kluft et al. (2019). The final row contains the same set-up as the first row, but also includes the high cloud from section 3.1.7.

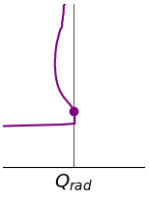

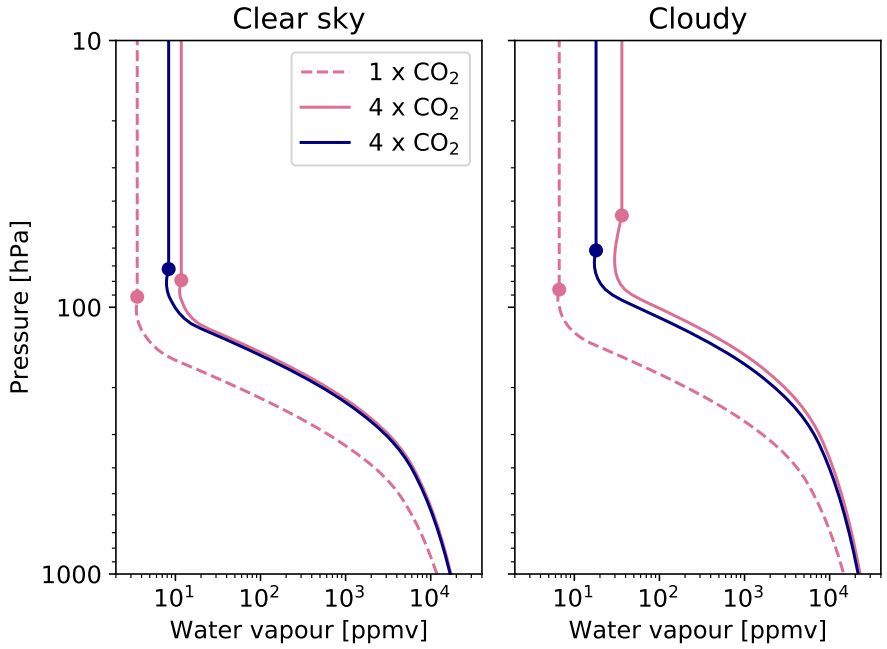

Figure 3.12: Humidity profiles for the clear sky and cloudy experiments using the climatology and $4 \times CO_2$ ozone profiles from Dietmüller et al. (2014). The dashed pink profiles are those from the $1 \times CO_2$ experiments, while the solid line profiles are from the $4 \times CO_2$ runs; pink with the climatology ozone and blue with the adjusted ozone profile. Dots indicate the location of the cold point.

compared with 7.0 K when keeping the pre-industrial ozone profile. We find corresponding surface temperature changes of about 6.0 K and 6.3 K, and it follows that the adjusted ozone profile produces a decrease in surface temperature of 0.3 K compared to the pre-industrial profile. Performing the same analysis with ozone profiles from Dietmüller et al. (2014) and Nowack et al. (2014) gives decreases in surface temperature of 0.4 and 0.6 K respectively. The differing results suggest that some, but not all, of the discrepancy between the global modelling studies (Marsh et al., 2016; Dietmüller et al., 2014; Nowack et al., 2014) can be explained by differences in their ozone profiles (figure 3.11). However, from this study it is not possible to tell whether these differences arise due to the ozone schemes, the model top (relatively low in Dietmüller et al., 2014) or the background state, including temperature profile and circulation, of the global climate models.

The results stated above come from experiments with upper tropospheric relative humidity and TTL temperatures of the $1 \times CO_2$ state in approximate agreement with ERA5 reanalysis data (figure 3.5). However, it is clear that many processes are missing from our model and that several of our model assumptions are overly simplistic. Changing some of these assumptions to ones that have been used in previous 1D RCE studies drastically affects our results (table 3.5). Changing the humidity profile has a large impact on the climate sensitivity itself and a more detailed study of this can be found in Kluft et al. (2019). Humidity is also the main modulating factor for the influence of ozone on surface temperature, with both stratospheric and tropospheric humidity playing a role in amplifying the response to ozone (as shown in section 3.1.3). Using the tropospheric relative humidity profile from Manabe and Wetherald (1967) produces an upper troposphere that is drier than observed, and therefore the impact of ozone on the surface temperature is reduced. On the other hand, neglecting upwelling produces a TTL that is warm and moist, as does the inclusion of a high cloud, and both produce a larger impact

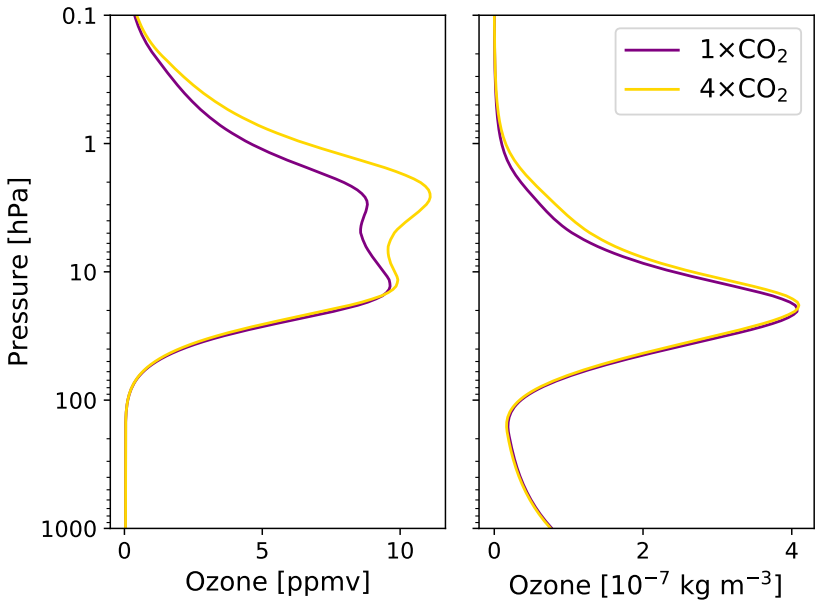

Figure 3.13: Tropical diurnal mean ozone profiles produced by Agatha for 1 and $4\times$ CO_2 scenarios in konrad.

of ozone than in the clear sky case with upwelling (table 3.5). In some extreme cases, when the ozone profile is fixed to the climatology and a CO_2 forcing is applied, warming of the TTL (which is already warm due to cloud or lack of upwelling) produces an upward jump of the cold point to a lower pressure (figure 3.12). The pressure dependence of the saturation humidity means that for only a small change in cold point temperature the stratosphere moistens strongly, and the resultant increase of the greenhouse effect and subsequent tropospheric moistening lead to a higher climate sensitivity. Using the $4 \times CO_2$ adjusted ozone profile leads to a relatively small upward shift of the cold point along with a cooling compared to the fixed ozone case thereby reducing the increase in TTL and stratospheric water vapour and reducing the climate sensitivity. It is essential that temperature and humidity (particularly in the upper troposphere and lower stratosphere) are well represented in order to obtain reasonable results regarding the influence of changes in ozone.

3.1.9 Ozone from Agatha

To investigate how the ozone profile reacts to atmospheric changes, we use konrad in combination with Agatha such that the temperature profile reacts to changes in ozone concentration and the ozone concentration profile reacts to changing temperatures. We use our simple set-up to investigate how the ozone profile changes with increasing upwelling velocity and independently with increasing CO_2 concentration. For the case of increasing CO_2 we also investigate how ozone impacts surface temperature, and how this compares to the results found in section 3.1.8.

The total column ozone and the vertical structure of the ozone profiles produced by Agatha are comparable to observed values, although there is a second peak in ozone concentration in ppmv between around 2 and 3 hPa, that we speculate may be related to missing chlorine chemistry in Agatha. The total column ozone concentration is 269 Dobson units in the standard setup with $1\times$ CO_2 and an upwelling velocity of $0.25\,\mathrm{mm\,s^{-1}}$. The region of the ozone profile of most interest in this work is the lower stratosphere, as

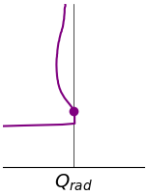

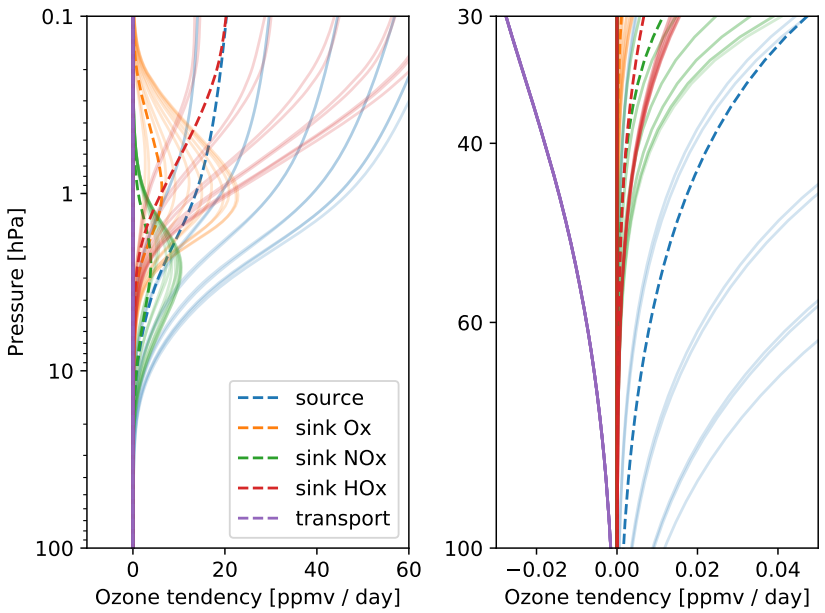

Figure 3.14: Ozone tendency profiles from Agatha for the $1\times CO_2$ scenario in konrad. The source and transport terms are defined as positive contributions to the total ozone tendency, while the sink terms are by definition negative contributions. Pale lines are at different times of day, and daily mean values are shown as dashed lines. The transport term shows very little diurnal variation.

this is the part that has the largest effect on TTL temperatures. The ozone concentrations in this region are mostly determined by the ozone source term, which varies strongly over the diurnal cycle, and the transport term (right panel of figure 3.14).

As expected, increasing the upwelling velocity decreases ozone concentrations in the lower stratosphere, with absolute changes in upwelling velocity having a larger impact when the upwelling is small than when it is large (figure 3.15). The increase in magnitude of the transport term (equation 2.38) leads to a reduction of ozone, which increases the transmittance of photons through the column, leading to an increase in magnitude of the source term (sections 2.2.1 and 2.2.3) and allowing the system to reach a new equilibrium. The changes in ozone are mostly associated with the increase in ozone transport and not the different temperature profiles associated with changes in the adiabatic cooling term (equation 2.9). This is because it is mostly the temperature in the TTL and lower stratosphere that is affected by the adiabatic cooling term (figure 3.5) and the ozone terms of most importance there; the transport and source terms, have no direct dependence on temperature. This is confirmed by further experiments (not shown), with a fixed upwelling velocity of $0.25\,\mathrm{mm\,s^{-1}}$ for the adiabatic cooling term and upwelling velocities of 0, 0.25 and $0.5\,\mathrm{mm\,s^{-1}}$ for the ozone transport term.

It is clear that transport plays an important role for lower stratospheric ozone, but it is uncertain how much the large scale upwelling will change with warming (section 1.3.2), so in the following experiments we keep the upwelling velocity fixed to $0.25\,\mathrm{mm\,s^{-1}}$. Nevertheless, under an increasing CO_2 scenario, Agatha qualitatively reproduces the expected behaviour, showing an increase in ozone in the middle and upper stratosphere as these regions cool, and an upward shift in terms of pressure coordinates of the ozone profile in the lower stratosphere (figure 3.13). As the upwelling velocity is fixed, any changes in the transport term come from changes in the ozone concentrations, *i.e.* if there were no change in the ozone concentrations from the other terms, there would be no change in the transport term.

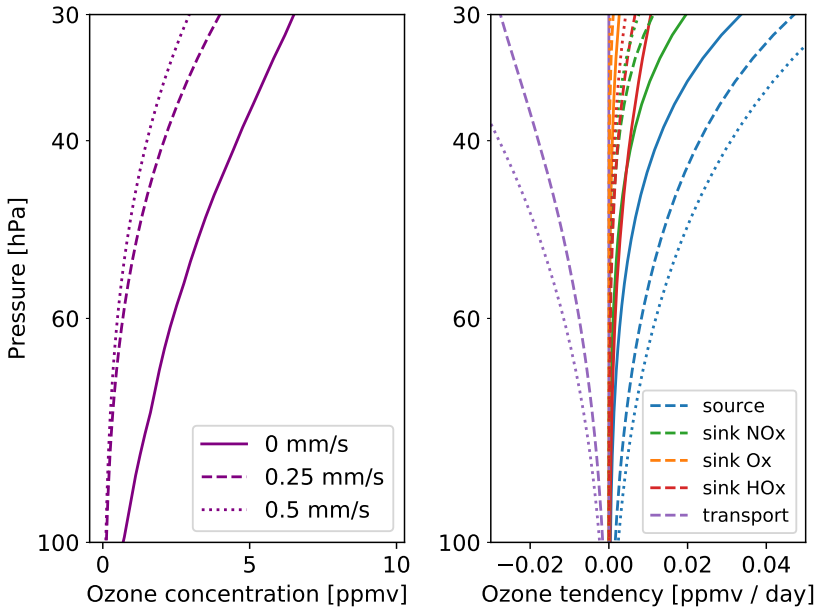

Figure 3.15: Lower stratospheric ozone profiles (left) and diurnal mean ozone tendencies (right) from Agatha with different upwelling velocities.

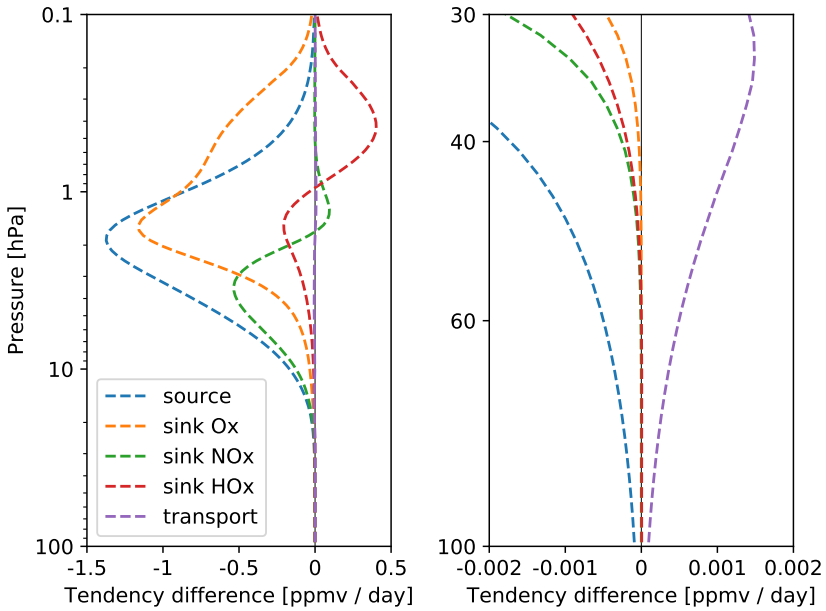

Figure 3.16: Differences in daily mean ozone tendencies from Agatha between the $4\times CO_2$ and $1\times CO_2$ runs in konrad.

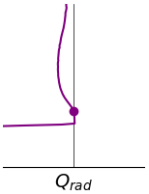

Therefore, the main contributing factor for the decrease in ozone concentrations between 100 and 30 hPa under the $4\times CO_2$ scenario is a reduction in the source term on timescales much longer than a day (as ozone has a long lifetime in the lower stratosphere, as illustrated by the constancy of the transport term over the diurnal cycle, figure 3.14). The source term has no explicit temperature dependence (sections 2.2.1 and 2.2.3), but does depend on the incoming radiative flux, which in turn depends on the overlying ozone column. A decrease in destruction of ozone by NO_x, O_x and HO_x occurs in the upper stratosphere (between 1 and 10 hPa, left panel of figure 3.16) when it cools, leading to an increase in ozone there (figure 3.13), which reduces the transmittance of solar irradiance to the lower stratosphere and thus reduces the source term there. In this set-up, not considering an increase in the upwelling velocity, Agatha provides a lower bound on tropical lower stratospheric ozone changes.

Indeed, the change in lower stratospheric ozone under the $4\times CO_2$ scenario with fixed upwelling velocity is smaller than that produced by the CCMs of section 3.1.8 (figure 3.17), as circulation changes in these models likely make the largest contribution to the loss of lower stratospheric ozone. As we would expect, this leads to a smaller impact of Agatha on surface temperature than the CCM ozone profiles, with Agatha acting to decrease surface temperature sensitivity to a $4\times CO_2$ perturbation by 0.1 K compared to 0.3 - 0.6 K for the CCM ozone profiles.[1]

The impact of including interactive ozone either from a CCM or Agatha depends on what it is being compared to. If we fix the RCEMIP ozone profile (Wing et al., 2018, and used in our standard konrad runs, section 2.1) with height instead of pressure, we find a relatively large impact on surface temperature sensitivity to quadrupling CO_2, namely an increase in sensitivity by 0.9 K. This is in qualitative agreement with the study of (Hardiman et al., 2019), who show that keeping the ozone profile fixed with height increases climate sensitivity compared to redistributing the ozone such that the ozone concentrations around the tropopause remain fixed as the troposphere expands. Thus, the importance of including interactive ozone and the decrease in climate sensitivity associated with it appear much larger in a comparison with an ozone profile fixed with height, than in a comparison with an ozone profile fixed with pressure or to simulations in which the ozone is redistributed around the tropopause. Pressure is a more suitable vertical coordinate for fixing ozone, because under warming the troposphere does not expand as much in pressure coordinates as it does in height coordinates. This is responsible for at least part of the larger apparent impact of interactive ozone on climate sensitivity found by Nowack et al. (2014) using a non-hydrostatic model running on height coordinates, than by Dietmüller et al. (2014); Marsh et al. (2016) whose ozone profiles in the non-interactive run were fixed with pressure.

To conclude, we expect that the transport term is the most important for TTL and lower stratospheric ozone concentrations. On the other hand, we show that middle and upper stratospheric ozone concentrations do have an impact on the source term in the TTL and lower stratosphere. For estimating climate sensitivity, it would likely be sufficient to use a high top model (one that extends into the upper stratosphere) with a simplistic ozone scheme, such as Agatha, including only the most important reactions, and together with a realistic representation of the circulation for the transport. Depending on the topic of interest and accuracy required, fixing the ozone profile may be sufficient, but in that case we recommend to fix it using pressure coordinates rather than height coordinates.

3.2 Conclusions

Using konrad, we find that several factors influence the structure of the TTL in our 1D model, with an increase in CO_2 and the addition of a high cloud acting to warm it,

[1] The values stated here are for the konrad set-up with the standard humidity treatment, an upwelling velocity of $0.25\,\mathrm{mm\,s^{-1}}$ and clear sky. The results are not strictly comparable due to the different treatment of insolation in the experiments with Agatha (section 2.1), however, we know that the treatment of insolation does not have a big impact on the surface temperature response to ozone (section 3.1.3).

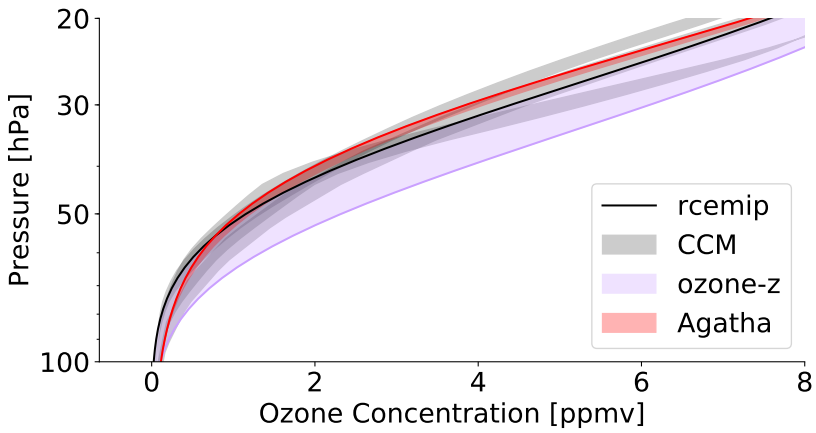

Figure 3.17: Tropical mean lower stratospheric ozone profiles from Agatha (red) compared to the coupled chemistry climate models of Marsh et al. (2016), Dietmüller et al. (2014) and Nowack et al. (2014) (shaded gray), the RCEMIP profile (solid black) and the RCEMIP profile when fixed with height (purple). The solid red and purple lines indicate the profiles from the $4 \times CO_2$ scenarios and the shading shows the change from the $1 \times CO_2$ runs.

although the impact of both of these factors depends on whether or not the surface temperature is allowed to respond. This suggests an upward influence of the surface and tropospheric temperatures on the TTL temperature and structure. On the other hand, an upward shift in the ozone profile acts to cool the TTL, as does an applied stratospheric dynamical cooling and a convective adjustment that takes into account cooling aloft, and all of these act independently of changes in surface temperature. In addition, we investigate the interplay of different factors, and find that the choice of upwelling velocity and convective adjustment treatment both affect how changes in the gas concentrations affect TTL temperatures. Further, the ability to accurately predict the combined effect of CO_2 and ozone from their individual effects depends on the convective adjustment method. Even in our relatively simple model set-up, we show that a number of factors play a significant role for the TTL and that they interact in a complicated way, which may help to explain disagreements in global model predictions of TTL evolution. Moreover, the temporal response of the TTL depends on processes occurring on different timescales, creating additional complications to predicting TTL evolution under realistic forcing conditions, when the stratosphere is not equilibrated.

Studying surface temperature response to CO_2 in our model, we find that including a high cloud and making alterations to the humidity profile have a large effect (table 3.5 and Kluft et al., 2019), while the type of convective adjustment and strength of upwelling velocity having relatively little impact. On the other hand, the type of convective adjustment and strength of upwelling play a role when studying surface temperature response to a shift in the ozone profile. Water vapour feedbacks have a strong effect here, and when no upwelling is applied, they amplify the surface temperature response to a shift in the ozone profile by a factor between 4.8 and 10.0, depending on the method of convective adjustment and the size of the ozone shift. When considering ozone profile changes that might be expected from a $4 \times CO_2$ scenario (from the CCMs of Marsh et al., 2016; Dietmüller et al., 2014; Nowack et al., 2014), we find a surface temperature decrease between $\sim$ 0.3 and 0.6 K, compared to an increase in temperature from the quadrupling of CO_2 of $>$ 6 K. Using our simple ozone model Agatha produces smaller decreases in surface temperature, as the changes in lower stratospheric ozone are smaller than those from the CCMs, due to the use of a fixed upwelling velocity in Agatha. However, even without a change in the upwelling transport

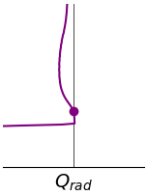

term, a decrease in ozone is found in the lower stratosphere under a warming scenario, due to changes in ozone occurring above this.

Chapter 4

A conceptual model of precipitation and circulation

4.1 Derivations

Energetic constraints on mean precipitation have been discussed extensively in the scientific community, for example by Mitchell et al. (1987); Trenberth et al. (2003); O'Gorman et al. (2012) among others. Using their insight, in section 4.1.1 we describe a simple energy balance model and use black body radiation to predict precipitation changes under warming. The simple model provides some ideas for the later derivations using heating rate profiles output from konrad. Although konrad does not explicitly include precipitation, condensation is implied by the convective adjustment and the assumptions of the moist adiabat. In section 4.1.2 we derive the precipitation rate predicted by konrad and furthermore we infer the circulation changes associated with this (section 4.1.3). Finally we apply our model to scenarios with increased CO_2 concentrations (section 4.2).

4.1.1 The simplest model

If we take the energy balance equation for the whole atmosphere, we have

$$\frac{\partial \mathrm{U}}{\partial t} = Q_{rad} + \mathrm{LH} + \mathrm{SH} \tag{4.1}$$

where $\frac{\partial \mathrm{U}}{\partial t}$ is the change in energy stored in the atmosphere over time, Q_{rad} is net radiative cooling, LH is latent heating and SH is sensible heating. At equilibrium, $\frac{\partial \mathrm{U}}{\partial t} \to 0$. Further, we assume that sensible heating is much smaller than latent heating, and therefore that SH can be neglected, giving a balance between radiation and latent heating.[1]

Considering conservation of water in the atmosphere,

$$\frac{\partial W}{\partial t} = -\mathrm{P} + \mathrm{E} \tag{4.2}$$

where P is precipitation, E is evaporation and $\frac{\partial W}{\partial t}$ is the change in water content stored in the atmosphere over time, which again tends to zero in the mean at equilibrium. This gives a balance between evaporation and precipitation.

[1] Takahashi (2009) also uses this balance between latent heating and radiation, but for the atmosphere above cloud base. In this case it is more reasonable to neglect sensible heating, which mainly affects the boundary layer, and indeed O'Gorman et al. (2012) show that their conceptual model is in better agreement with GCMs than assuming that radiation and latent heating balance in the whole atmospheric column. In section 4.1.2, we use the heating rates from konrad, and konrad does not represent the boundary layer (the temperature profile follows the moist adiabatic lapse rate directly from the surface), so we do not distinguish between the whole atmospheric column and that of the free atmosphere. Then for simplicity, we neglect sensible heating.

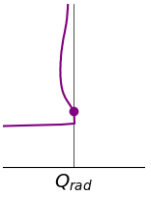

Using the relationship between evaporation and latent heating ($\mathrm{LH} = -L_v\,\mathrm{E}$), the balance at equilibrium between radiation and precipitation can be derived:

$$\mathrm{P} = \frac{Q_{rad}}{L_v} \tag{4.3}$$

where L_v is the latent heat of vaporisation of water.

To understand how precipitation will change in a warming climate, we can consider how radiative heating will change. The simplest model for longwave radiation is that of a black body, whose rate of energy emission (j) depends on temperature to the power of four.

$$j = \sigma T^4 \tag{4.4}$$

According to the theorem of equipartition of energy, internal energy is proportional to temperature, so the rate of change of energy j can be related to a rate of change of temperature i.e. a cooling rate:

$$Q_{rad} \propto T^4 \tag{4.5}$$

We calculate the fractional change in longwave radiative cooling for an increase in temperature of one degree, as

$$\frac{1}{Q_{rad}}\frac{\partial Q_{rad}}{\partial T} = \frac{4}{T} \tag{4.6}$$

and from this we estimate the fractional change in precipitation for an increase in temperature of one degree. For a temperature of 300 K, we get a change in longwave radiative cooling of $1.33\,\%\,\mathrm{K}^{-1}$ and an estimated increase in precipitation of $1.33\,\%\,\mathrm{K}^{-1}$. If we instead take an effective emission temperature of 255 K, longwave radiative cooling and precipitation are predicted to increase by $1.57\,\%\,\mathrm{K}^{-1}$.

4.1.2 Precipitation

Arguably a bad assumption in the simple model of section 4.1.1 is that for the radiation. For the rest of this study, we use konrad to provide convective heating rate profiles, from which we make inferences about precipitation changes. Our method follows the advice of Sobel and Bretherton (2000) who argue that conceptual models for precipitation should derive vertical velocity from temperature profiles rather than the other way round. In our case we derive precipitation and in section 4.1.3 vertical velocity from convective heating rate profiles from konrad, which have been constrained by the requirement that the temperature profile follows the moist adiabatic lapse rate. Konrad was designed to represent the tropical atmosphere, so while in the simple model of section 4.1.1 we were discussing the global mean state, here we need to make the additional assumption that transport of water in the atmosphere from the tropics to mid or high latitudes is negligible. We further assume mass conservation in the tropical troposphere, neglecting the relatively small net tropical upwelling, which brings mass into the stratosphere (section 1.3.2).

A starting point for the derivation is the convective heating rate profile, one of the output variables from konrad, which can be thought of as the term that has to balance the net radiative cooling in the troposphere. We assume that in the mean the convective heating comes from latent heat as water vapour condenses and we ignore the contribution from sensible heating. Then we can calculate the amount of condensation per unit of height of an atmospheric column of unit area, C, that must take place to produce the convective heating profile from konrad.

$$\mathrm{C} = \frac{Q\,\rho\,c_p}{L_v} \tag{4.7}$$

where Q is the convective heating rate profile from konrad in units of K/day, ρ is the air density, L_v is the latent heat of vaporisation of water and c_p is the isobaric mass heat capacity, which we take to be that of dry air (neglecting the enthalpy change of water

vapour). To calculate the precipitation, we integrate the condensation rate profile over the height of the column.

Note that this method is equivalent to the atmospheric energy budget given in Jeevanjee and Romps (2018). In konrad, the convective adjustment must satisfy enthalpy balance between the surface and atmosphere (equation 2.1). Therefore, our derivation of precipitation is equivalent to studying the surface energy and water budgets, ignoring sensible heating, such that radiative heating is balanced by evaporative cooling and evaporation is balanced by precipitation.

4.1.3 Circulation changes

Konrad is typically used to represent the mean state (temporally and/or spatially), but we assume it also provides a reasonable representation of any local area in the tropics, in accordance with the weak temperature gradient approximation (section 1.2.2). We imagine that the tropics are split into two distinct regions, a saturated moist region dominated by convective updrafts and a region with downwelling. It is the saturated upwelling region that provides the water vapour for the condensation rate profile we calculated in section 4.1.2.

As the saturated air moves upward, the water vapour it contains must condense out as it rises and cools. Knowing how much water vapour condenses, we can calculate the rate at which the saturated air must move upwards *i.e.* the upward mass flux. From mass conservation, neglecting net tropical upwelling, we assume that the upward mass flux must equal the downward mass flux. The equation for the condensation rate in this form is as follows.

$$\begin{aligned} \mathrm{C} &= -w_{up}\, A_{up}\, \frac{\partial \rho_v^*}{\partial z} \\ &= -w_{down}\, A_{down}\, \frac{\partial \rho_v^*}{\partial z} \end{aligned} \tag{4.8}$$

where w_{up} and w_{down} are the upwelling and downwelling velocities, A_{up} and A_{down} the upwelling and downwelling area fractions and $\frac{\partial \rho_v^*}{\partial z}$ the change of water vapour mass density with height in the saturated upwelling region. In equation 4.8 we have also implicitly assumed that the density of air is the same in the upwelling and downwelling, in accordance with the weak temperature gradient hypothesis (section 1.2.2).

At this point we need to make another assumption and there are two possibilities for this, which we discuss separately.

In one case we assume that the area fractions remain constant regardless of the scenario. The specific values we assume are irrelevant to the qualitative discussion of results in section 4.2. Fixing the area fraction allows us to calculate the downwelling and upwelling velocities directly from equation 4.8.

In the second case, we avoid making an assumption about the area fractions and how they might change under warming. Instead we consider the downwelling region and assume that it has the same convective heating rate as the tropical mean. In reality, this is not the case, as downwelling regions are drier than upwelling regions, allowing more radiation to escape to space, which changes the energy balance. This would lead to a systematic error, that would not affect the qualitative trends discussed in section 4.2, unless large changes in the spatial distribution of relative humidity occur under warming (not possible to investigate with konrad). In the downwelling regions, the term that balances radiative cooling (the convective heating rate in konrad) comes from adiabatic warming as air sinks and is compressed;

$$Q = w_{down} \left(\frac{\partial T}{\partial z} + \frac{g}{c_p} \right) \tag{4.9}$$

From a simple rearrangement of equation 4.9 and by specifying the convective heating rate (to that output from konrad), we can find the downwelling velocity, w_{down}. Then, we can infer the area fraction of the downwelling region, by rearranging equation 4.8. This also

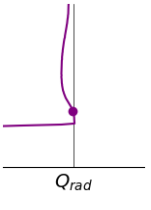

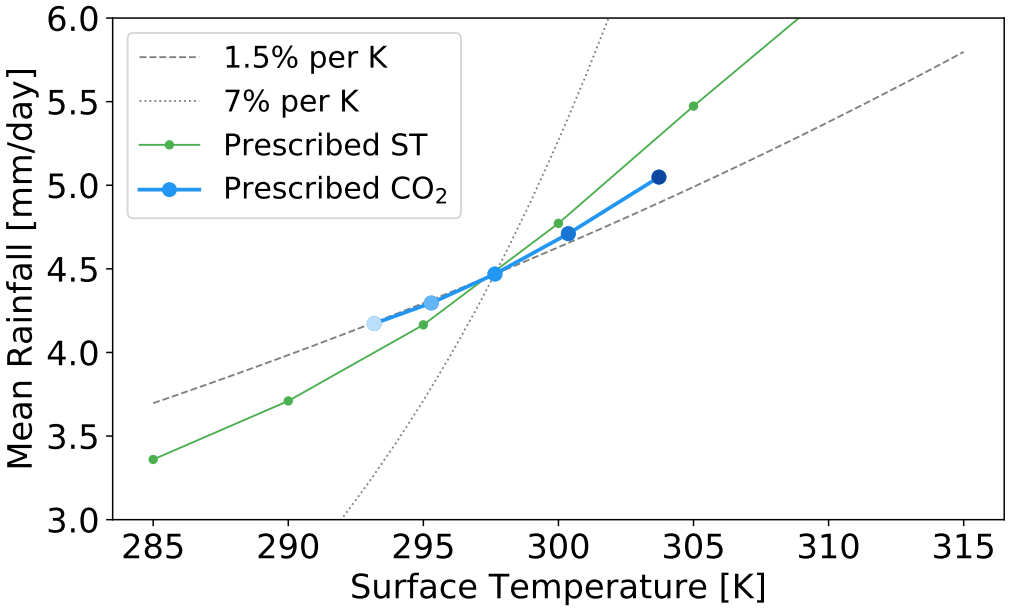

Figure 4.1: Mean rainfall derived from konrad output from experiments with different CO_2 concentrations (blue) and different prescribed surface temperatures (green). For reference, the dashed line shows the slope estimated from the simplest model of section 4.1.1, while the dotted line approximates Clausius-Clapeyron scaling.

gives us the area fraction of the upwelling region (one minus that of the downwelling region) and from this and the mass flux[2], we get the upwelling velocity. In section 4.2, we refer to results derived using this approach as the homogeneous radiation case.

4.2 Increasing carbon dioxide

With an increase in surface temperature we find an increase in precipitation between 2.0 and 2.7 % K^{-1} for surface temperatures between 285 and 310 K (green line in figure 4.1), with the largest increases occurring for surface temperatures close to 300 K. These results come from konrad runs with a prescribed surface temperature and no change in atmospheric constituents (except water vapour which increases to maintain a fixed relative humidity in the troposphere). If we instead use an interactive surface temperature and increase CO_2, we find a smaller increase in precipitation per Kelvin of surface temperature warming (between 1.4 and 2.0 % K^{-1}, blue line in figure 4.1). This agrees with many previous studies in which the effect on precipitation of an increase in temperature and an increase in CO_2 have been considered separately (*e.g.* Allen and Ingram, 2002; Yang et al., 2003; Romps, 2020) and the explanation is as follows.

CO_2 traps outgoing longwave radiation in the troposphere, making longwave cooling of the lower troposphere less efficient. If there was no change in surface temperature, at equilibrium a reduction in longwave cooling would enforce a reduction in convective heating, which in turn would lead to a reduction in condensation rate (equation 4.7) and a decrease in mean precipitation. With an increase in temperature, the expansion of the troposphere leads to an increase in precipitation (Jeevanjee and Romps, 2018). When the troposphere expands,

[2]When we discuss the mass flux in this chapter, we are referring to the density normalised mass flux, defined as vertical velocity multiplied by area fraction, $w\,A$.

longwave cooling occurs over a larger depth, which leads to convective heating (required to balance net radiative cooling at equilibrium) and therefore condensation to occur over a larger depth. The mean precipitation rate, given by the integral of the condensation rate, increases. The direct radiative impact of an increase in CO_2 is a decrease in precipitation, but at equilibrium the effect of the increased surface temperature is larger than the direct radiative effect of CO_2.

Associated with the warming and increase in precipitation, the convective mass flux decreases, in agreement with Held and Soden (2006). The warmer atmosphere contains more water vapour and more water vapour condenses per unit mass of rising air, leading to the decrease in convective mass flux ($w_{up}\,A_{up}$ from equation 4.8). Under the fixed area assumption, this decrease is actualised by decreases in the upwelling and downwelling velocities. Under the homogeneous radiation assumption, the downwelling velocity calculated from adiabatic warming (equation 4.9) also decreases with warming throughout most of the troposphere (when plotted against pressure as in figure 4.2), as the temperature lapse rate becomes less negative with warming. The decrease in downwelling velocity alone does not cause a sufficient decrease in the downward mass flux, so the downwelling area fraction also decreases with warming. As such, the upwelling area fraction must increase ($A_{up} + A_{down} = 1$) and the combination of an increased upwelling area fraction and a decrease in mass flux implies a much decreased upwelling velocity (particularly in terms of fractional decrease).

We further investigate whether the velocities and area fractions are simply functions of temperature, *i.e.* whether the curves of figure 4.2 collapse on top of each other if temperature is used as the vertical coordinate instead of pressure (figure 4.3). Under the fixed area assumption (not shown), we find a slight increase in downwelling and upwelling velocities with increasing surface temperature, because the net radiative cooling rates[3] and thus condensation rates are larger in these experiments. Under the homogeneous radiation assumption, we also find a small increase in downwelling velocity at temperatures between approximately 280 and 240 K in experiments with larger surface temperature. This is clearer in the experiments with fixed CO_2 concentration and prescribed surface temperature, where the surface temperature range is larger (figure 4.4). There are also differences in the downwelling area fraction, because as well as depending on temperature, the downwelling area fraction has an approximately linear dependence on pressure (shown by substituting C from equation 4.7 and w_{down} from equation 4.9 into equation 4.8 and using the ideal gas law to write density as a function of pressure). Following from this, the upwelling area fraction increases and in order to satisfy mass conservation a slight decrease in upwelling velocity occurs, in contrast to the results obtained under the fixed area assumption.

The methodoloy performs poorly in the upper troposphere, where the convective heating and thus condensation rates are large, but the atmosphere there is cold and contains very little water vapour. It follows (equation 4.8) that the downwelling mass flux ($w_{down}\,A_{down}$) must be large, which leads to large vertical velocities particularly under the fixed area assumption. In the homogeneous radiation case, it is clear that the values of the mass flux are unrealistic, as dividing the downwelling mass flux by the downwelling velocity required for adiabatic warming (equation 4.9), produces an area fraction larger than one. This is impossible in the real world, suggesting that at least one of our assumptions does not hold

[3]It is often argued that radiative cooling rates are approximately a function of temperature (*e.g.* Hartmann and Larson, 2002), but this is a poor approximation. The longwave radiative cooling or heating of an atmospheric layer depends on the difference between the emission and the absorption of longwave radiation within that layer. Assuming each particle emits more when it is hotter and the relationship is linear, then the contribution of the emission to the radiative cooling rate depends only on temperature. However, the amount of longwave absorption depends on the amount of emission from neighbouring layers, which in turn depends on their density. At lower pressures the density is reduced, so longwave absorption within a layer decreases and the radiative cooling increases, or equivalently radiative heating decreases. Another factor is the assumption that the amount of emission from a particle is linearly proportional to its temperature and some studies (*e.g.* Seeley et al., 2019b) argue that this is a weak assumption

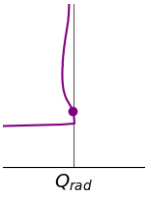

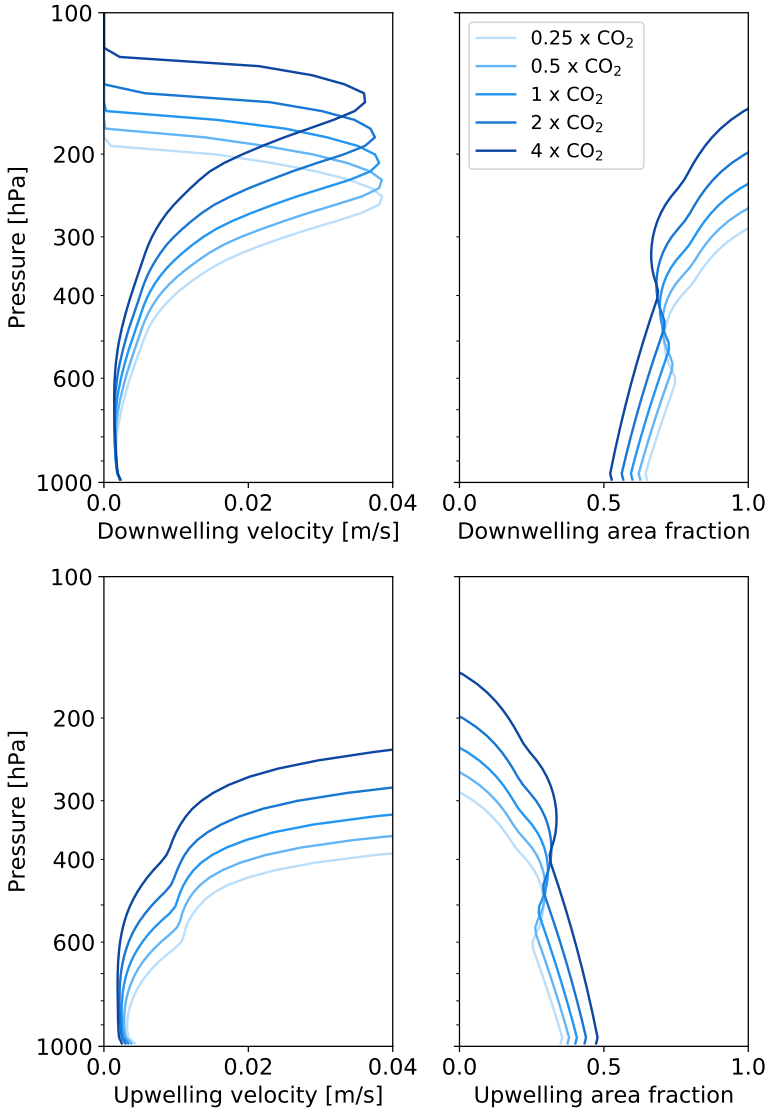

Figure 4.2: Downwelling and upwelling velocities and area fractions as inferred from konrad output assuming homogeneous radiation for equilibrium states of experiments with varying CO_2 concentrations.

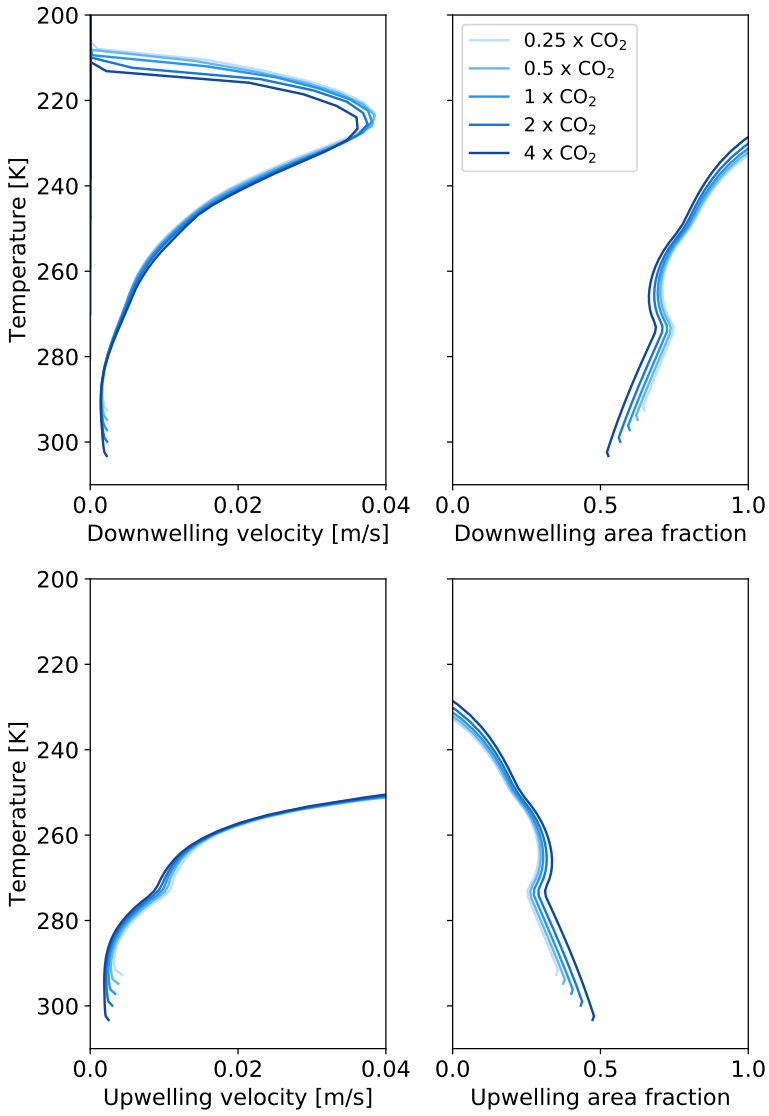

Figure 4.3: As figure 4.2, but with temperature as the vertical coordinate.

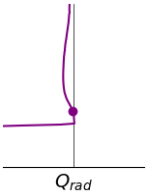

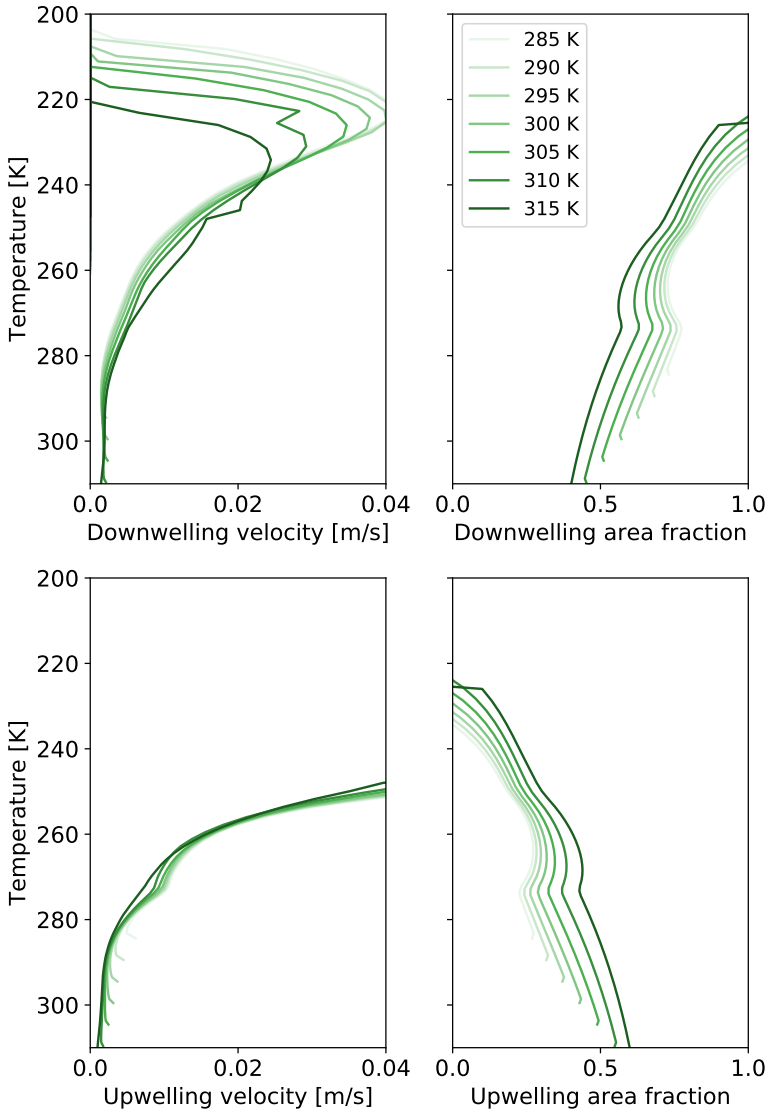

Figure 4.4: As figure 4.3, but using output from konrad experiments with fixed CO_2 concentration and a range of prescribed surface temperatures.

in the upper troposphere. The unrealistically large mass flux values can be attributed to the smallness of $\frac{\partial \rho_v^*}{\partial z}$ in the upper troposphere. Perhaps parts of the real upper troposphere are supersaturated or the air parcels that are upwelling have a higher temperature than average, such that more water vapour is available for condensation at upper levels. Probably it is too simplistic to split the atmosphere into two distinct regimes, each with mean properties, ignoring any variability within the regimes.

4.3 Conclusions

Using a simple approach and 1D model output, we are able to derive the tropical mean precipitation and circulation and how they change under different climate scenarios. Because we use the convective heating rate output from konrad, rather than net radiative cooling profiles, it would also be possible to study transient periods during which the atmosphere is not in radiative-convective equilibrium. We find that the direct radiative impact of CO_2 is a decrease in mean precipitation, but the warming it induces gives rise to an overall increase in precipitation between 1.4 and 2.0 %/K. This suggests that the continual increase in atmospheric carbon dioxide in the real world is suppressing the increase in mean precipitation that will occur in the long term, in agreement with global modeling studies (*e.g.* Yang et al., 2003; Andrews and Forster, 2010; Fläschner et al., 2016) and the 3D RCE study of Romps (2020). Further, using our simplistic approach we find a decrease in convective mass flux in a warming climate, in agreement with the theory and global modeling results presented by Held and Soden (2006). Associated with this, under our homogeneous radiation assumption, we find a decrease in downwelling area, which has implications for convective aggregation and how it may change with climate change.

The methodology performs poorly in the upper troposphere, which would likely be better represented by rare strong convective events (air parcels in the positive tail of the equivalent potential temperature distribution, Folkins, 2002) rather than mean ones.

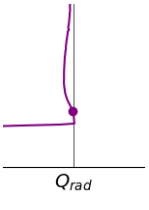

Chapter 5

Summary and outlook

We have contributed to the development of two simple numerical models, a 1D RCE model (konrad, section 2.1) and a stratospheric ozone chemistry model (Agatha, section 2.2), and we have created an analytical model to derive mean precipitation and circulation from the output of konrad (section 4).

A parameter study was performed using konrad to quantify the effects of various factors on the TTL and surface temperatures (section 3.1). In agreement with other studies (*e.g.* Thuburn and Craig, 2002; Birner and Charlesworth, 2017; Fu et al., 2018; Kuang and Bretherton, 2004), we find the TTL to be a sensitive region, with CO_2, ozone, water vapour, convection, cloud and upwelling all playing a role. In addition, we investigate how the different factors interact with each other and for example find that a downward shifted ozone profile causes an upward jump and apparent cooling of the cold point under increasing CO_2 concentrations. We also study the temporal evolution of TTL temperature after an instantaneously increased CO_2 concentration, which evolves from a strong initial warming (in agreement with Lin et al., 2017) that subsequently decreases and then increases again as the surface temperature and troposphere warm. We show that under increased CO_2 concentrations the equilibrium TTL temperature is strongly linked to surface temperature (explaining the lack of dependence of the TTL temperature on CO_2 in the fixed surface temperature model of Thuburn and Craig, 2002), but note that the relationship is altered when a dynamical upwelling is applied. With regards to the surface, we find that its temperature is mainly sensitive to CO_2, humidity and cloud, with the choice of method of convective adjustment and stratospheric upwelling velocity having little effect. In our simple set-up, we show that the importance of changes in the ozone profile on the surface temperature depends largely on the representation of humidity and cloud in the upper troposphere, as suggested by the 3D studies of Hardiman et al. (2019) and Nowack et al. (2014) respectively. As in other studies (*e.g.* Jiang et al., 2007), we highlight the importance of the Brewer-Dobson circulation for changes in the ozone profile under a warming scenario.

An obvious future use of Agatha would be to include the scheme in a 3D model with an accurate representation of the Brewer-Dobson circulation to quantify the importance of the different terms to the ozone profile. When including Agatha in a 3D model, it would also be of interest to look in more detail at the interaction of ozone and convection and in particular deep convective events which bring ozone-poor air directly into the TTL. Another interesting next step would be to include the photolysis of H_2O to form HO_x, allowing Agatha to be coupled to konrad or another model via humidity as well as temperature.

We touch on the transient evolution of TTL temperature and mean precipitation under a $4 \times CO_2$ scenario (sections 3.1.6 and 4.2), both of which undergo an initial decrease before increasing as surface temperature increases. This complicates predictions for the real world, where the forcing is not instantaneous. It may be of interest to run konrad with the historical forcing and/or other forcing scenarios, such as the representative concentration pathway

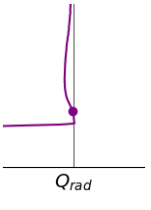

(RCP) scenarios.

Our conceptual model for mean precipitation and circulation produces results in agreement with previous studies, i.e. an increase in precipitation with warming less than that associated with the Clausius-Clapeyron relation and an associated slow down of the mean circulation Held and Soden (*e.g.* 2006), but the upper troposphere is not well represented. In particular, the mass flux values are unrealistic in the upper troposphere due to the lack of water vapour there. This could be accounted for by considering the upwelling air parcels to have a broad distribution of pseudo equivalent potential temperature (as in Folkins, 2002), with parcels that reach high into the upper troposphere being warmer and moister than average. Modelling how this distribution may change under different climate scenarios would be an important step, but an initial approach could be to keep the distribution fixed about a changing mean value.

The conceptual model of section 4 could also be extended by incorporating it into konrad. For example, the derivative of the mass flux with height could be used to infer detrainment from the moist saturated region into the downwelling region and through this the humidity profile could be calculated (following Minschwaner and Dessler, 2004). These humidity profiles could then be used as input to konrad to calculate the convective heating rate profile for the derivation of the mass flux. This would avoid the simplification used by Romps (2014) of specifying the detrainment rates to calculate humidity profiles and would build on the work of Minschwaner and Dessler (2004) by taking into account changes in the areas of the upwelling and downwelling regions. However, as in Minschwaner and Dessler (2004), this method would require the lapse rate to be specified in konrad and the currently specified moist adiabat does not provide an accurate picture of the upper troposphere. As suggested above, if we model the upwelling air parcels with a broad distribution of temperatures (Folkins, 2002), a more realistic lapse rate could be calculated and used within konrad. A further extension along similar lines, could be to infer cloud amounts, rather than assuming that condensates precipitate immediately. However, this would require a microphysics scheme to determine the cloud particle lifetimes, which should depend on evaporative drying (Seeley et al., 2019a).

All of the above suggestions for future studies make the model(s) more complicated in some way. This study has shown the benefits of keeping things simple, namely a greater understanding of the included processes, which can then be applied to more complex models or real world scenarios.

Abbreviations and Symbols

Abbreviations

1D	One Dimensional
3D	Three Dimensional
CCM	Chemistry Climate Model
CMIP5	Coupled Model Intercomparison Project phase 5
ECS	Equilibrium Climate Sensitivity
ERA5	the fifth generation of atmospheric reanalyses of the global climate provided by the European Centre for Medium-Range Weather Forecasts
FAT hypothesis	Fixed Anvil Temperature hypothesis
fRH	fixed Relative Humidity
fVMR	fixed water vapour Volume Mixing Ratio
JPL	Jet Propulsion Laboratory (California Institute of Technology)
RCE	Radiative Convective Equilibrium
RCEMIP	Radiative Convective Equilibrium Model Intercomparison Project
RCP 8.5	Representative Concentration Pathway business as usual scenario (radiative forcing of $8.5\,\mathrm{W\,m^{-2}}$ in the year 2100)
RRTMG	Rapid Radiative Transfer Model for Global climate models
TTL	Tropical Tropopause Layer
WMO	World Meteorological Organisation

Physical symbols

A_{down}	downwelling area
A_{up}	upwelling area
C	condensation
c_p	heat capacity of air at constant pressure
c_s	heat capacity of the surface layer
E	evaporation
g	Earth's gravity
j	black body radiant emittance
LH	latent heating
L_v	Latent heat of vapourisation
m	mass of air
m_v^*	mass of water vapour at saturation
P	precipitation
p	pressure
p_0	pressure of the lowest atmospheric model level

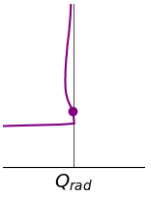

p_c	pressure at the convective top
p_s	pressure at the surface
p_v^*	partial pressure due to water vapour at saturation
Q	cooling or heating rate
Q_{rad}	net radiative cooling rate
q^*	saturation water vapour mass fraction
R	specific gas constant of air
R_v	specific gas constant of water vapour
SH	sensible heating
T	temperature
T_{con}	temperature after the convective adjustment has been applied
$T_{\text{con, } s}$	temperature of the surface after the convective adjustment has been applied
T_{rad}	temperature after the radiative heating rates have been applied
t	time
U	energy stored in the atmosphere
W	water content stored in the atmosphere
w_{down}	downwelling velocity
w_{up}	upwelling velocity
z	height
γ_p	pressure lapse rate
ΔT_{atm}	change in temperature of the atmosphere
ΔT_{hard}	change in temperature due to the hard convective adjustment
ΔT_{rlx}	change in temperature due to the relaxed convective adjustment
ΔT_s	change in temperature of the surface
ρ	density of air
ρ_s	density of the surface layer
ρ_v^*	density of water vapour at saturation
σ	Stefan–Boltzmann constant for black body radiation
τ	timescale for the relaxed convective adjustment
τ_0	timescale for the relaxed convective adjustment at the lowest atmospheric model level
$\chi(p)$	pressure dependent relaxation factor

Photochemical symbols

a	chemical reaction rate for a reaction including a member of the hydrogen oxide family
b	chemical reaction rate for a reaction including a member of the nitrogen oxide family
CO	carbon monoxide
F_{TOA}	flux of photons at the top of the atmosphere
HO_2	hydrogen dioxide
HO_x	the hydrogen oxide family
$h\nu$	a photon
J	photolysis reaction rate
k	chemical reaction rate for a reaction between oxygen species
M	an inert molecule

NO	nitric oxide
NO_2	nitrogen dioxide
NO_x	the nitrogen oxide family
$N(z)$	number of molecules in the slant column above height z
O	atomic oxygen in its ground state
O^*	excited atomic oxygen
O_2	diatomic oxygen
O_3	ozone
O_x	the odd oxygen family
OH	hydroxide
Tr	transmissivity
W_j	weighting factors used in the parameterisation of Minschwaner et al. (1993) (section 2.2)
$\Delta\lambda$	wavelength interval
θ	zenith angle
λ	wavelength of light
σ	absorption cross-section

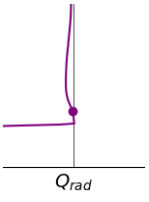

List of Figures

List of Tables

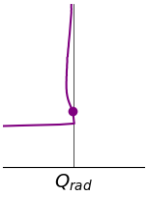

Bibliography

Abalos, M., B. Legras, F. Ploeger, and W. J. Randel, 2015: Evaluating the advective brewer-dobson circulation in three reanalyses for the period 1979–2012. *Journal of Geophysical Research: Atmospheres*, **120 (15)**, 7534–7554.

Allen, M. R., and W. J. Ingram, 2002: Constraints on future changes in climate and the hydrologic cycle. *Nature*, **419 (6903)**, 228–232.

Andrews, T., and P. M. Forster, 2010: The transient response of global-mean precipitation to increasing carbon dioxide levels. *Environmental Research Letters*, **5 (2)**, 025 212, doi: 10.1088/1748-9326/5/2/025212.

Becker, T., B. Stevens, and C. Hohenegger, 2017: Imprint of the convective parameterization and sea-surface temperature on large-scale convective self-aggregation. *Journal of Advances in Modeling Earth Systems*, **9 (2)**, 1488–1505.

Betts, A., and M. Miller, 1986: A new convective adjustment scheme. part ii: Single column tests using gate wave, bomex, atex and arctic air-mass data sets. *Quarterly Journal of the Royal Meteorological Society*, **112 (473)**, 693–709.

Birner, T., and E. J. Charlesworth, 2017: On the relative importance of radiative and dynamical heating for tropical tropopause temperatures. *Journal of Geophysical Research: Atmospheres*, **122 (13)**, 6782–6797, doi:10.1002/2016JD026445, URL http://dx.doi.org/10.1002/2016JD026445, 2016JD026445.

Brasseur, G., and S. Solomon, 2005: *Aeronomy of the Middle Atmosphere: Chemistry and Physics of the Stratosphere and Mesosphere*. Atmospheric and Oceanographic Sciences Library, Springer Netherlands, URL https://books.google.de/books?id=HoV1VNFJwVwC.

Bretherton, C. S., and P. K. Smolarkiewicz, 1989: Gravity waves, compensating subsidence and detrainment around cumulus clouds. *Journal of the atmospheric sciences*, **46 (6)**, 740–759.

Butchart, N., and Coauthors, 2006: Simulations of anthropogenic change in the strength of the brewer–dobson circulation. *Climate Dynamics*, **27 (7-8)**, 727–741.

Chae, J. H., and S. C. Sherwood, 2007: Annual temperature cycle of the tropical tropopause: A simple model study. *Journal of Geophysical Research Atmospheres*, **112 (19)**, 1–10, doi:10.1029/2006JD007956.

Charlesworth, E. J., 2017: Transport-radiation feedbacks of ozone in the tropical tropopause layer. M.S. thesis, Department of Atmospheric Science, Colorado State University, URL https://dspace.library.colostate.edu/handle/10217/181353.

Charlesworth, E. J., T. Birner, and J. R. Albers, 2019: Ozone transport-radiation feedbacks in the tropical tropopause layer. *Geophysical Research Letters*, **46 (23)**, 14 195–14 202, doi:10.1029/2019GL084679.

Cronin, T. W., K. A. Emanuel, and P. Molnar, 2015: Island precipitation enhancement and the diurnal cycle in radiative-convective equilibrium. *Quarterly Journal of the Royal Meteorological Society*, **141 (689)**, 1017–1034.

Dacie, S., and Coauthors, 2019: A 1d rce study of factors affecting the tropical tropopause layer and surface climate. *Journal of Climate*, **32 (20)**, 6769–6782.

Davis, S. M., and Coauthors, 2016: The stratospheric water and ozone satellite homogenized (swoosh) database: A long-term database for climate studies. *Earth system science data*, **8 (2)**, 461.

Dessler, A., and Coauthors, 2016: Transport of ice into the stratosphere and the humidification of the stratosphere over the 21st century. *Geophysical research letters*, **43 (5)**, 2323–2329.

Dietmüller, S., M. Ponater, and R. Sausen, 2014: Interactive ozone induces a negative feedback in CO2-driven climate change simulations. *Journal of Geophysical Research: Atmospheres*, **119 (4)**, 1796–1805.

Dobson, G. M. B., A. Brewer, and B. Cwilong, 1946: Bakerian lecture: Meteorology of the lower stratosphere. *Proc. R. Soc. Lond. A*, **185 (1001)**, 144–175.

Eichelberger, S. J., and D. L. Hartmann, 2005: Changes in the strength of the brewer-dobson circulation in a simple agcm. *Geophysical Research Letters*, **32 (15)**, doi:10.1029/2005GL022924, URL https://agupubs.onlinelibrary.wiley.com/doi/abs/10.1029/2005GL022924, https://agupubs.onlinelibrary.wiley.com/doi/pdf/10.1029/2005GL022924.

Flach, R., R. Skalskỳ, C. Folberth, J. Balkovič, K. Jantke, and U. A. Schneider, 2020: Water productivity and footprint of major brazilian rainfed crops–a spatially explicit analysis of crop management scenarios. *Agricultural Water Management*, **233**, 105 996.

Fläschner, D., T. Mauritsen, and B. Stevens, 2016: Understanding the intermodel spread in global-mean hydrological sensitivity. *Journal of Climate*, **29 (2)**, 801–817.

Folkins, I., 2002: Origin of lapse rate changes in the upper tropical troposphere. *Journal of the atmospheric sciences*, **59 (5)**, 992–1005.

Forster, P., 2017: In Retrospect: Half a century of robust climate models. *Nature*, **545 (7654)**, 296–297, doi:10.1038/545296a, URL http://www.nature.com/doifinder/10.1038/545296a.

Fu, Q., M. Smith, and Q. Yang, 2018: The impact of cloud radiative effects on the tropical tropopause layer temperatures. *Atmosphere*, **9 (10)**, 377.

Fueglistaler, S., A. Dessler, T. Dunkerton, I. Folkins, Q. Fu, and P. W. Mote, 2009: Tropical tropopause layer. *Reviews of Geophysics*, **47 (1)**.

Fueglistaler, S., and P. Haynes, 2005: Control of interannual and longer-term variability of stratospheric water vapor. *Journal of Geophysical Research: Atmospheres*, **110 (D24)**.

Garcia, R. R., and W. J. Randel, 2008: Acceleration of the brewer–dobson circulation due to increases in greenhouse gases. *Journal of the Atmospheric Sciences*, **65 (8)**, 2731–2739.

Gettelman, A., and Coauthors, 2010: Multimodel assessment of the upper troposphere and lower stratosphere: Tropics and global trends. *Journal of Geophysical Research: Atmospheres*, **115 (D3)**, n/a–n/a, doi:10.1029/2009JD013638, URL http://dx.doi.org/10.1029/2009JD013638, d00M08.

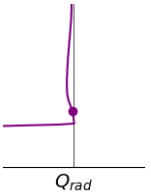

Gowan, E., 1947: Ozonosphere temperatures under radiation equilibrium. *Proc. R. Soc. Lond. A*, **190 (1021)**, 219–226.

Hardiman, S. C., and Coauthors, 2019: The impact of prescribed ozone in climate projections run with hadgem3-gc3.1. *Journal of Advances in Modeling Earth Systems*, **11 (11)**, 3443–3453, doi:10.1029/2019MS001714, URL https://agupubs.onlinelibrary.wiley.com/doi/abs/10.1029/2019MS001714, https://agupubs.onlinelibrary.wiley.com/doi/pdf/10.1029/2019MS001714.

Harrop, B. E., and D. L. Hartmann, 2012: Testing the role of radiation in determining tropical cloud-top temperature. *Journal of Climate*, **25 (17)**, 5731–5747.

Hartmann, D. L., and K. Larson, 2002: An important constraint on tropical cloud-climate feedback. *Geophysical Research Letters*, **29 (20)**, 12–1.

Hegglin, M., and Coauthors, 2014: Vertical structure of stratospheric water vapour trends derived from merged satellite data. *Nature Geoscience*, **7 (10)**, 768.

Held, I. M., and B. J. Soden, 2006: Robust responses of the hydrological cycle to global warming. *Journal of climate*, **19 (21)**, 5686–5699.

Holloway, C. E., and J. D. Neelin, 2007: The convective cold top and quasi equilibrium. *Journal of the atmospheric sciences*, **64 (5)**, 1467–1487.

Huang, Y., X. Tan, and Y. Xia, 2016: Inhomogeneous radiative forcing of homogeneous greenhouse gases. *Journal of Geophysical Research: Atmospheres*, **121 (6)**, 2780–2789.

Hummel, J., and W. Kuhn, 1981a: Comparison of radiative-convective models with constant and pressure-dependent lapse rates. *Tellus*, **33 (3)**, 254–261.

Hummel, J. R., and W. R. Kuhn, 1981b: An atmospheric radiative-convective model with interactive water vapor transport and cloud development. *Tellus*, **33 (4)**, 372–381.

Hummel, J. R., and W. R. Kuhn, 1981c: Comparison of radiative-convective models with constant and pressure-dependent lapse rates. *Tellus*, **33 (1979)**, 154–261, doi:10.3402/tellusa.v33i3.10713.

Jeevanjee, N., and D. M. Romps, 2018: Mean precipitation change from a deepening troposphere. *Proceedings of the National Academy of Sciences*, **115 (45)**, 11 465–11 470.

Jiang, X., S. J. Eichelberger, D. L. Hartmann, R. Shia, and Y. L. Yung, 2007: Influence of doubled co2 on ozone via changes in the brewer–dobson circulation. *Journal of the Atmospheric Sciences*, **64 (7)**, 2751–2755, doi:10.1175/JAS3969.1, URL https://doi.org/10.1175/JAS3969.1, https://doi.org/10.1175/JAS3969.1.

Jiménez-de-la Cuesta, D., and T. Mauritsen, 2019: Emergent constraints on Earth's transient and equilibrium response to doubled CO2 from post-1970s global warming. *Nature Geoscience*, **12 (11)**, 902–905, doi:https://doi.org/10.1038/s41561-019-0463-y.

Johnson, R. H., and D. C. Kriete, 1982: Thermodynamic and circulation characteristics, of winter monsoon tropical mesoscale convection. *Monthly Weather Review*, **110 (12)**, 1898–1911.

Kay, J. E., and A. Gettelman, 2009: Cloud influence on and response to seasonal arctic sea ice loss. *Journal of Geophysical Research: Atmospheres*, **114 (D18)**.

Kim, J., K. M. Grise, and S.-W. Son, 2013: Thermal characteristics of the cold-point tropopause region in CMIP5 models. *Journal of Geophysical Research: Atmospheres*, **118 (16)**, 8827–8841, doi:10.1002/jgrd.50649, URL http://dx.doi.org/10.1002/jgrd.50649.

Kluft, L., S. Dacie, S. A. Buehler, H. Schmidt, and B. Stevens, 2019: Re-examining the first climate models: Climate sensitivity of a modern radiative–convective equilibrium model. *Journal of Climate*, **32 (23)**, 8111–8125.

Kuang, Z., and C. S. Bretherton, 2004: Convective Influence on the Heat Balance of the Tropical Tropopause Layer: A Cloud-Resolving Model Study. *Journal of the Atmospheric Sciences*, **61 (23)**, 2919–2927, doi:10.1175/JAS-3306.1.

Kuang, Z., and D. L. Hartmann, 2007: Testing the fixed anvil temperature hypothesis in a cloud-resolving model. *Journal of Climate*, **20 (10)**, 2051–2057.

Lenton, T. M., 2003: 3 - the coupled evolution of life and atmospheric oxygen. *Evolution on Planet Earth*, L. J. Rothschild, and A. M. Lister, Eds., Academic Press, London, 35 – 53, doi:https://doi.org/10.1016/B978-012598655-7/50030-6, URL http://www.sciencedirect.com/science/article/pii/B9780125986557500306.

Li, C., H. Held, S. Hokamp, and J. Marotzke, 2020: Optimal temperature overshoot profile found by limiting global sea level rise as a lower-cost climate target. *Science Advances*, **6 (2)**, doi:10.1126/sciadv.aaw9490, URL https://advances.sciencemag.org/content/6/2/eaaw9490, https://advances.sciencemag.org/content/6/2/eaaw9490.full.pdf.

Lin, P., D. Paynter, Y. Ming, and V. Ramaswamy, 2017: Changes of the tropical tropopause layer under global warming. *Journal of Climate*, **30 (4)**, 1245–1258.

MacKay, R. M., and M. A. K. Khalil, 1991: Theory and development of a one dimensional time dependent radiative convective climate model. *Chemosphere*, **22 (3)**, 383–417, doi:10.1016/0045-6535(91)90326-9, URL http://www.sciencedirect.com/science/article/pii/0045653591903269.

Manabe, S., and F. Möller, 1961: *On the radiative equilibrium and heat balance of the atmosphere*. Monthly Weather Review.

Manabe, S., and R. F. Strickler, 1964: Thermal Equilibrium of the Atmosphere with a Convective Adjustment. URL http://journals.ametsoc.org/doi/abs/10.1175/1520-0469{%}281964{%}29021{%}3C0361{%}3ATEOTAW{%}3E2.0.CO{%}3B2, 361–385 pp., doi:10.1175/1520-0469(1964)021⟨0361:TEOTAW⟩2.0.CO;2.

Manabe, S., and R. T. Wetherald, 1967: Thermal Equilibrium of the Atmosphere with a Given Distribution of Relative Humidity. *Journal of the Atmospheric Sciences*, **24 (3)**, 241–259, doi:10.1175/1520-0469(1967)024⟨0241:TEOTAW⟩2.0.CO;2, URL http://journals.ametsoc.org/doi/abs/10.1175/1520-0469{%}281967{%}29024{%}3C0241{%}3ATEOTAW{%}3E2.0.CO{%}3B2.

Marsh, D. R., J.-F. Lamarque, A. J. Conley, and L. M. Polvani, 2016: Stratospheric ozone chemistry feedbacks are not critical for the determination of climate sensitivity in CESM1(WACCM). *Geophysical Research Letters*, **43 (8)**, 3928–3934, doi:10.1002/2016GL068344, URL http://dx.doi.org/10.1002/2016GL068344, 2016GL068344.

McElroy, M. B., R. J. Salawitch, and K. Minschwaner, 1992: The changing stratosphere. *Planetary and Space Science*, **40**, 373–401, doi:10.1016/0032-0633(92)90070-5.

Minschwaner, K., and A. E. Dessler, 2004: Water vapor feedback in the tropical upper troposphere: Model results and observations. *Journal of Climate*, **17 (6)**, 1272–1282.

Minschwaner, K., R. J. Salawitch, and M. B. McElroy, 1993: Absorption of solar radiation by o2: Implications for o3 and lifetimes of n2o, cfcl3, and cf2cl2. *Journal of Geophysical Research: Atmospheres*, **98 (D6)**, 10 543–10 561, doi:10.1029/93JD00223, URL https://agupubs.onlinelibrary.wiley.com/doi/abs/10.1029/93JD00223, https://agupubs.onlinelibrary.wiley.com/doi/pdf/10.1029/93JD00223.

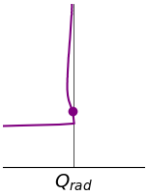

Mitchell, J., C. Wilson, and W. Cunnington, 1987: On co2 climate sensitivity and model dependence of results. *Quarterly Journal of the Royal Meteorological Society*, **113 (475)**, 293–322.

Mlawer, E. J., S. J. Taubman, P. D. Brown, M. J. Iacono, and S. A. Clough, 1997: Radiative transfer for inhomogeneous atmospheres: RRTM, a validated correlated-k model for the longwave. *Journal of Geophysical Research: Atmospheres*, **102 (D14)**, 16 663–16 682.

Monteiro, J. M., J. McGibbon, and R. Caballero, 2018: sympl (v. 0.4. 0) and climt (v. 0.15. 3)–towards a flexible framework for building model hierarchies in python. *Geoscientific Model Development*, **11 (9)**, 3781–3794.

Mote, P. W., and Coauthors, 1996: An atmospheric tape recorder: The imprint of tropical tropopause temperatures on stratospheric water vapor. *Journal of Geophysical Research: Atmospheres*, **101 (D2)**, 3989–4006.

Müller, S. K., E. Manzini, M. Giorgetta, K. Sato, and T. Nasuno, 2018: Convectively generated gravity waves in high resolution models of tropical dynamics. *Journal of Advances in Modeling Earth Systems*, **10 (10)**, 2564–2588.

Nobert, S., D. Demeritt, and H. Cloke, 2010: Informing operational flood management with ensemble predictions: lessons from sweden. *Journal of Flood Risk Management*, **3 (1)**, 72–79.

Nowack, P. J., A. N. Luke, A. C. Maycock, P. Braesicke, J. M. Gregory, M. M. Joshi, A. Osprey, and J. A. Pyle, 2014: A large ozone-circulation feedback and its implications for global warming assessments. *Nature Climate Change*, **5**, 41, doi:http://dx.doi.org/10.1038/nclimate245110.1038/nclimate2451, URL https://www.nature.com/articles/nclimate2451#supplementary-information.

Oberländer-Hayn, S., and Coauthors, 2016: Is the brewer-dobson circulation increasing or moving upward? *Geophysical Research Letters*, **43 (4)**, 1772–1779, doi:10.1002/2015GL067545, URL http://dx.doi.org/10.1002/2015GL067545, 2015GL067545.

Oliphant, T. E., 2006: *A guide to NumPy*, Vol. 1. Trelgol Publishing USA.

O'Gorman, P. A., R. P. Allan, M. P. Byrne, and M. Previdi, 2012: Energetic constraints on precipitation under climate change. *Surveys in geophysics*, **33 (3-4)**, 585–608.

Paulik, L. C., and T. Birner, 2012: Quantifying the deep convective temperature signal within the tropical tropopause layer (TTL). *Atmospheric Chemistry and Physics*, **12 (24)**, 12 183–12 195.

Romps, D. M., 2014: An analytical model for tropical relative humidity. *Journal of Climate*, **27 (19)**, 7432–7449.

Romps, D. M., 2020: Climate sensitivity and the direct effect of carbon dioxide in a limited-area cloud-resolving model. *Journal of Climate*, **(2020)**.

Roshan, E., M. M. Khabbazan, and H. Held, 2019: Cost-Risk Trade-Off of Mitigation and Solar Geoengineering: Considering Regional Disparities Under Probabilistic Climate Sensitivity. *Environmental and Resource Economics*, **72 (1)**, 263–279, doi:https://doi.org/10.1007/s10640-018-0261-9.

Satoh, M., and Y.-Y. Hayashi, 1992: Simple Cumulus Models in One-Dimensional Radiative Convective Equilibrium Problems. URL http://journals.ametsoc.org/doi/abs/10.1175/1520-0469{%}281992{%}29049{%}3C1202{%}3ASCMIOD{%}3E2.0.CO{%}3B2{#}.VuFKnh6zre0.mendeley, 1202–1220 pp., doi:10.1175/1520-0469(1992)049⟨1202:SCMIOD⟩2.0.CO;2.

Seeley, J. T., N. Jeevanjee, W. Langhans, and D. M. Romps, 2019a: Formation of tropical anvil clouds by slow evaporation. *Geophysical Research Letters*, **46 (1)**, 492–501.

Seeley, J. T., N. Jeevanjee, and D. M. Romps, 2019b: Fat or fitt: Are anvil clouds or the tropopause temperature invariant? *Geophysical Research Letters*, **46 (3)**, 1842–1850.

Sherwood, S. C., and A. E. Dessler, 2000: On the control of stratospheric humidity. *Geophysical Research Letters*, **27 (16)**, 2513–2516, doi:10.1029/2000GL011438, URL http://dx.doi.org/10.1029/2000GL011438.

Sobel, A. H., and C. S. Bretherton, 2000: Modeling tropical precipitation in a single column. *Journal of climate*, **13 (24)**, 4378–4392.

Son, S.-W., N. F. Tandon, and L. M. Polvani, 2011: The fine-scale structure of the global tropopause derived from COSMIC GPS radio occultation measurements. *Journal of Geophysical Research: Atmospheres*, **116 (D20)**, n/a–n/a, doi:10.1029/2011JD016030, URL http://dx.doi.org/10.1029/2011JD016030, d20113.

Stephens, E., and H. Cloke, 2014: Improving flood forecasts for better flood preparedness in the uk (and beyond). *The Geographical Journal*, **180 (4)**, 310–316, doi:10.1111/geoj.12103, URL https://rgs-ibg.onlinelibrary.wiley.com/doi/abs/10.1111/geoj.12103, https://rgs-ibg.onlinelibrary.wiley.com/doi/pdf/10.1111/geoj.12103.

Takahashi, K., 2009: Radiative constraints on the hydrological cycle in an idealized radiative–convective equilibrium model. *Journal of the atmospheric sciences*, **66 (1)**, 77–91.

Thuburn, J., and G. Craig, 2002: On the temperature structure of the tropical substratosphere. *Journal of Geophysical Research: ...*, **107**, 1–10, doi:10.1029/2001JD000448, URL http://onlinelibrary.wiley.com/doi/10.1029/2001JD000448/full.

Trenberth, K. E., A. Dai, R. M. Rasmussen, and D. B. Parsons, 2003: The changing character of precipitation. *Bulletin of the American Meteorological Society*, **84 (9)**, 1205–1218, doi:10.1175/BAMS-84-9-1205, URL https://doi.org/10.1175/BAMS-84-9-1205, https://doi.org/10.1175/BAMS-84-9-1205.

Wang, J. S., D. J. Seidel, and M. Free, 2012: How well do we know recent climate trends at the tropical tropopause? *Journal of Geophysical Research Atmospheres*, **117 (9)**, 1–10, doi:10.1029/2012JD017444.

Warren, R. A., M. S. Singh, and C. Jakob, 2020: Simulations of radiative–convective–dynamical equilibrium. *Journal of Advances in Modeling Earth Systems*, **n/a (n/a)**, e2019MS001734, doi:10.1029/2019MS001734, URL https://agupubs.onlinelibrary.wiley.com/doi/abs/10.1029/2019MS001734, e2019MS001734 2019MS001734, https://agupubs.onlinelibrary.wiley.com/doi/pdf/10.1029/2019MS001734.

Wing, A. A., K. A. Reed, M. Satoh, B. Stevens, S. Bony, and T. Ohno, 2018: Radiative-convective equilibrium model intercomparison project. *Geoscientific Model Development*, **11 (2)**, 793–813.

Yang, F., A. Kumar, M. E. Schlesinger, and W. Wang, 2003: Intensity of hydrological cycles in warmer climates. *Journal of Climate*, **16 (14)**, 2419–2423, doi:10.1175/2779.1, URL https://doi.org/10.1175/2779.1, https://doi.org/10.1175/2779.1.

Zelinka, M. D., and D. L. Hartmann, 2010: Why is longwave cloud feedback positive? *Journal of Geophysical Research Atmospheres*, **115 (16)**, 1–16, doi:10.1029/2010JD013817.

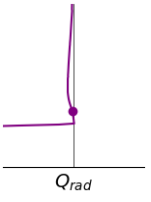

Zhang, C., B. E. Mapes, and B. J. Soden, 2003: Bimodality in tropical water vapour. *Quarterly Journal of the Royal Meteorological Society*, **129 (594)**, 2847–2866, doi:10.1256/qj.02.166, URL https://rmets.onlinelibrary.wiley.com/doi/abs/10.1256/qj.02.166, https://rmets.onlinelibrary.wiley.com/doi/pdf/10.1256/qj.02.166.

Versicherung an Eides statt
Declaration of oath

Hiermit versichere ich an Eides statt, dass ich die vorliegende Dissertation mit dem Titel: "Using simple models to understand changes in the tropical mean atmosphere under warming" selbstständig verfasst und keine anderen als die angegebenen Hilfsmittel – insbesondere keine im Quellenverzeichnis nicht benannten Internet-Quellen – benutzt habe. Alle Stellen, die wörtlich oder sinngemäß aus Veröffentlichungen entnommen wurden, sind als solche kenntlich gemacht. Ich versichere weiterhin, dass ich die Dissertation oder Teile davon vorher weder im In- noch im Ausland in einem anderen Prüfungsverfahren eingereicht habe und die eingereichte schriftliche Fassung der auf dem elektronischen Speichermedium entspricht.

Sally Dacie, Hamburg 2020

Hinweis / Reference

Die gesamten Veröffentlichungen in der Publikationsreihe des MPI-M
„Berichte zur Erdsystemforschung / Reports on Earth System Science“,
ISSN 1614-1199

sind über die Internetseiten des Max-Planck-Instituts für Meteorologie erhältlich:
http://www.mpimet.mpg.de/wissenschaft/publikationen.html

All the publications in the series of the MPI -M
„Berichte zur Erdsystemforschung / Reports on Earth System Science“,
ISSN 1614-1199

are available on the website of the Max Planck Institute for Meteorology:
http://www.mpimet.mpg.de/wissenschaft/publikationen.html